

ASSESSING THE MECHANICAL RESPONSE OF PAVEMENTS DURING AND AFTER FLOODING

BY

MOHAMED HAMDALLAH ELSHAER

Bachelor of Science in Civil Engineering, El Shorouk Academy, 2007

Master of Science in Civil Engineering, Cairo University, 2011

DISSERTATION

Submitted to the University of New Hampshire

in Partial Fulfillment of

the Requirement for the Degree of

Doctor of Philosophy

in

Civil Engineering

May, 2017

ProQuest Number: 10280594

All rights reserved

INFORMATION TO ALL USERS

The quality of this reproduction is dependent upon the quality of the copy submitted.

In the unlikely event that the author did not send a complete manuscript and there are missing pages, these will be noted. Also, if material had to be removed, a note will indicate the deletion.



ProQuest 10280594

Published by ProQuest LLC (2017). Copyright of the Dissertation is held by the Author.

All rights reserved.

This work is protected against unauthorized copying under Title 17, United States Code
Microform Edition © ProQuest LLC.

ProQuest LLC.
789 East Eisenhower Parkway
P.O. Box 1346
Ann Arbor, MI 48106 – 1346

This dissertation has been examined and approved in partial fulfillment of the requirements for the degree of Doctor of Philosophy in Civil Engineering by:

Dissertation Director, Jo Sias Daniel, Professor
of Civil Engineering

Majid Ghayoomi, Assistant Professor of Civil
Engineering

Eshan V. Dave, Assistant Professor of Civil
Engineering

Rajib B. Mallick, Professor, Worcester
Polytechnic Institute

Leslie Myers McCarthy, Associate Professor,
Villanova University

On April 10, 2017

Original approval signatures are on file with the University of New Hampshire Graduate School.

DEDICATION

This dissertation is dedicated to my parents, my sister and my brother.

ACKNOWLEDGEMENTS

First and foremost, I would like to thank god for providing me the blessings to complete this work. You have given me the power to believe in my passion and pursue my dreams. I could never have done this without the faith I have in you.

I would like to express my deepest appreciation to my advisors, Dr. Jo Sias Daniel and Dr. Majid Ghayoomi, for the excellent guidance, caring, patience, motivation, enthusiasm, immense knowledge, generosity and providing me with an excellent atmosphere for doing research. You have been tremendous mentors for me and without your guidance and persistent help this dissertation would not have been possible. Thank you for selection me as a student of yours.

Besides my advisors, I would like to thank the rest of my dissertation committee, Dr. Eshan Dave, Dr. Rajib Mallick, and Dr. Leslie McCarthy, for their encouragement, significant feedback and for working with me during this process. To Dr. Eshan Dave, you have been an excellent friend, mentor and a great inspiration for me. It is wonderful to have a person like you.

I am grateful to Dr. Mohamed Abdel-Raheem for being a friend and for his motivation and support throughout my entire life and my Ph.D. Journey. Many thanks to my research mates, Dr. David Mensching, Dr. Yaning Qiao, Chris Jacques, Jayne Knott, Mirkat Oshone, Chris DeCarlo, Reyhaneh Rahbar-Rastegar, Rasool Nemati, Katie Haslett, Morteza Mirshekari, Pegah Jarast-Shamsabadi, Seyed Amin Borghei, Kimberly Perkins and Eric Caron. In one way or another, you all provided guidance and friendship,

and I wish you all the best. I would like to thank Karim Naji, who as a good friend, was always willing to help and give his best suggestions.

Finally, I would also like to thank my parents, my sister and my brother for their wise counsel and sympathetic ear. Words cannot express how thankful I am to my parents for all the sacrifices that you've made on my behalf. Your prayer for me was what sustained me thus far. You are always there for me.

TABLE OF CONTENTS

| | |
|--|-------------|
| DEDICATION | III |
| ACKNOWLEDGEMENTS | IV |
| LIST OF TABLES | XI |
| LIST OF FIGURES | XIII |
| ABSTRACT | XVII |
| CHAPTER 1: INTRODUCTION | 1 |
| 1.1 Statement of Problem | 1 |
| 1.2 Objectives..... | 3 |
| 1.3 Structure of Dissertation | 4 |
| CHAPTER 2: IMPACT OF PAVEMENT LAYER PROPERTIES ON STRUCTURAL PERFORMANCE OF INUNDATED PAVEMENTS | 8 |
| 2.1 Introduction..... | 8 |
| 2.2 Methods and Data | 11 |
| 2.2.1 Pavement Evaluation: Mechanistic Approach..... | 14 |
| 2.2.2 Pavement Evaluation: AASHTO Empirical Approach | 16 |
| 2.3 Results and Discussion | 20 |
| 2.3.1 Mechanistic Approach: Layer Elastic Analysis | 20 |
| 2.3.2 AASHTO Empirical Approach Results Discussion | 30 |
| 2.4 Summary and Conclusions | 36 |

| | | |
|---|--|-----------|
| 2.5 | Acknowledgement | 38 |
| | | |
| CHAPTER 3: METHODOLOGY TO EVALUATE PERFORMANCE OF PAVEMENT STRUCTURE USING SOIL MOISTURE PROFILE | | 39 |
| 3.1 | Introduction..... | 39 |
| 3.2 | Background..... | 41 |
| 3.2.1 | Resilience Modulus Models for Unsaturated Subgrade Soils ... | 41 |
| 3.2.2 | In Situ Pavement Response Evaluation | 44 |
| 3.2.3 | Long Term Pavement Performance (LTPP) Program..... | 45 |
| 3.2.4 | Layered Elastic Analysis (LEA) of Pavements..... | 46 |
| 3.3 | Procedures | 48 |
| 3.3.1 | LTPP Sites Selection..... | 48 |
| 3.3.2 | Methodologies to Estimate a Moisture-Dependent Resilient Modulus from Field Data..... | 51 |
| 3.3.3 | Asphalt Modulus Correction..... | 56 |
| 3.3.4 | Linear Elastic Analysis (LEA) Method | 56 |
| 3.4 | Results and Discussions | 57 |
| 3.4.1 | Interpretation of the Results from the Selected LTPP Sections | 57 |
| 3.4.2 | Effect of Asphalt Concrete Modulus on the Deflection Prediction | 66 |
| 3.5 | Conclusion | 67 |
| 3.6 | Acknowledgement | 69 |

**CHAPTER 4: IMPACT OF SUBSURFACE WATER ON THE STRUCTURAL
CAPACITY OF INUNDATED FLEXIBLE PAVEMENTS 70**

4.1 Introduction..... 70

4.2 Background..... 72

4.3 Pavement Sections and Procedures 76

 4.3.1 Pavement Section Characterizations 76

 4.3.2 Subsurface Water Level and Water Pressure Distribution 79

 4.3.3 SWCC and Degree of Saturation..... 80

 4.3.4 Resilient Modulus, Mr 81

 4.3.5 Linear Elastic Analysis (LEA)82

4.4 Results and Discussion83

 4.4.1 Maximum Surface Deflection83

 4.4.2 Horizontal Tensile Strain at the Bottom of Asphalt Layer..... 85

 4.4.3 Vertical Compressive Strain at the Top of Subgrade Layer87

 4.4.4 Structural Capacity of Pavements89

 4.4.5 Influence Depths.....90

4.5 Conclusions..... 92

4.6 Acknowledgement 93

**CHAPTER 5: ASSESSING THE IMPACT OF RESILIENT MODULUS
PREDICTIVE MODELS OF UNBOUND MATERIALS ON THE
PAVEMENT DEFLECTION RESPONSE 94**

5.1 Introduction..... 94

5.2 Background..... 96

5.2.1 Resilient Modulus Models for Unbound Materials 96

5.2.2 Long Term Pavement Performance (LTPP) Program..... 103

5.2.3 Layered Elastic Analysis (LEA) of Pavements..... 104

5.3 Pavement Sections..... 104

5.3.1 Analysis Procedures 106

5.4 Results and Discussions 115

5.5 Summary and Conclusions..... 123

5.6 Acknowledgements..... 125

**CHAPTER 6: BEARING CAPACITY ANALYSIS OF PAVEMENT
STRUCTURES FOR SHORT TERM FLOODING EVENTS 126**

6.1 Introduction..... 126

6.2 Materials and Methods..... 128

6.2.1 Material Characterization 128

6.2.2 Bearing Capacity Calculation Procedure..... 134

6.3 Results and Discussions 137

6.4 Summary and Conclusions..... 140

| | | |
|-----|---|------------|
| 6.5 | Acknowledgements..... | 142 |
| | CHAPTER 7: SUMMARY AND CONCLUSIONS | 143 |
| | CHAPTER 8: REFERENCES | 149 |

LIST OF TABLES

| | |
|--|-----|
| Table 2.1. Subgrade Soil Properties from Selected LTPP Sites | 12 |
| Table 2.2. Pavement Material Types and Material Properties..... | 13 |
| Table 2.3. Truck, Axle and Tire Types | 14 |
| Table 2.4. Combinations of Material Types and Parameters | 16 |
| Table 2.5. Layer Coefficient and Drainage Coefficient for the AASHTO Method | 17 |
| Table 2.6. AASHTO Input Parameters | 18 |
| Table 2.7. ANOVA Testing for the Horizontal and Vertical Strain Values and Ratios for Low Volume Cross Sections (p-Value)..... | 21 |
| Table 2.8. ANOVA Testing for the Horizontal and Vertical Strain Values and Ratios for Interstate Cross Sections at Single Axle Single Tire Loading Type (p-Value) | 21 |
| Table 2.9. Tukey-Kramer HSD Testing for the Ratio of Horizontal Strain for Low Volume Cross Sections (p-Value) | 23 |
| Table 3.1. Employed LTPP Data | 46 |
| Table 3.2. Selected LTPP Sites and Subgrade Soil Characterizations | 49 |
| Table 3.3. Regression Parameters of Equation 3.2 | 52 |
| Table 3.4. Input Parameters and Source of Information..... | 57 |
| Table 4.1. Unbound Materials Properties..... | 78 |
| Table 4.2. Regression Parameters of Equation 4.1 | 81 |
| Table 4.3. Axle and Tire Types | 83 |
| Table 4.4. Influence Depth from Top of Subgrade Surface in Meter..... | 91 |
| Table 5.1. Selected LTPP Sites and Subgrade Soil Characterizations | 105 |
| Table 6.1. Pavement Cross Sections and Material Properties..... | 129 |
| Table 6.2. Properties of the Selected Soils | 130 |

Table 6.3. Regression Parameters of Equation 6.19 134

LIST OF FIGURES

| | |
|--|----|
| Figure 2.1. Typical Cross Section for a) Low-Volume Road b) Interstate Highway..... | 11 |
| Figure 2.2. Ratio of Saturated to Optimum Moisture Condition for Horizontal Tensile Strain and Vertical Compressive Strain Under Full Bond and Full Slip Interlayer Conditions for Low Volume Roads. | 21 |
| Figure 2.3. Ratio of Saturated to Optimum Moisture Condition for Horizontal Tensile Strain and Vertical Compressive Strain Under Different Truck Loading Types for All Low Volume Cross Sections | 24 |
| Figure 2.4. Ratio of Saturated to Optimum Moisture Condition for Horizontal and Vertical Strain Under Different Traffic Loading Types for (a) 75 mm AC, 150 mm Base (b) 125 mm AC, 255 mm Base Cross Section Under Different Base Course and Subgrade Material Types..... | 24 |
| Figure 2.5. (a) Horizontal Strain (b) Vertical Strain at Optimum Moisture Content Under Different Base Course and Subgrade Material Types Under Single Loading Type on Low Volume Cross Sections | 27 |
| Figure 2.6. (a) Horizontal Strain (b) Vertical Strain at Optimum Moisture Content Under Different Base Course and Subgrade Material Types Under Single Loading Type on Interstate Cross Sections..... | 28 |
| Figure 2.7. Ratio of Saturated to Optimum Moisture Condition for Horizontal Strains for (a) Low-Volume Sections (b) Interstate Sections Under Different Base Course and Subgrade Material Types Under Single Loading Type | 29 |
| Figure 2.8. Ratio of Saturated to Optimum Moisture Condition for Vertical Strains for (a) Low-Volume Sections (b) Interstate Sections Under Different Base Course and | |

| | |
|---|----|
| Subgrade Material Types Under Single Loading Type | 30 |
| Figure 2.9. Structural Number (SN) for (a) Low-Volume Sections (b) Interstate Sections Under Different Base Course Types..... | 31 |
| Figure 2.10. Number of ESALs for (a) Low-Volume Sections (b) Interstate Sections Under Optimum Moisture Content Condition | 32 |
| Figure 2.11. Ratio of Saturated to Optimum Moisture Condition for the Structural Number (SN) for (a) Low Volume Sections (b) Interstate Sections Under Different Base Course Types | 33 |
| Figure 2.12. Change in ESALs Versus Change in Subgrade Resilient Modulus..... | 34 |
| Figure 2.13. Ratio of Saturated to Optimum Moisture Condition for the Modified Structural Number (SNC) for (a) Low Volume Sections (b) Interstate Sections Under Different Base Course Types | 35 |
| Figure 2.14. Ratio of Saturated to Optimum Moisture Condition for Modified Structural Number (MSN) For (a) Low Volume Sections (b) Interstate Sections Under Different Base Course Types | 36 |
| Figure 3.1. Illustration of Instrumentation Installation | 46 |
| Figure 3.2. Map Location of the LTPP Selected Sites..... | 49 |
| Figure 3.3. Schematic Demonstration of the Methods Used to Obtain an Equivalent Resilient Modulus | 55 |
| Figure 3.4. Moisture Content Profiles for (a) Minnesota Section; (b) Oklahoma Section | 58 |
| Figure 3.5. Measured and Predicted Deflection Basins for Minnesota Section..... | 61 |
| Figure 3.6. Measured and Predicted Deflection Basins for Oklahoma Section | 63 |
| Figure 3.7. Measured and Predicted D ₀ and D ₆ Deflections for All Seasons at (a) | |

| | |
|--|-----|
| Minnesota Section; (b) Oklahoma Section | 65 |
| Figure 3.8. Sensitivity Analysis Plots for Minnesota Section Based on a) Method A; b) Based on Method B&D; and c) Based on Method C | 67 |
| Figure 4.1. Pavement Cross Sections: (a) Thin; (b) Intermediate; (c) Thick | 77 |
| Figure 4.2. Schematics to Demonstrate (a) Locations of Water Level in a Pavement Cross Section (b) Example Analysis Approach of Water Level Number 7..... | 80 |
| Figure 4.3. Predicted SWRC for the Proposed Soils..... | 81 |
| Figure 4.4. Variation of the Maximum Surface Deflection with Depth of Subsurface Water Levels | 85 |
| Figure 4.5. Variation of the Horizontal Tensile Strain at the Bottom of the Asphalt Layer with Depth to Subsurface Water Levels..... | 86 |
| Figure 4.6. Variation of the Vertical Compressive Strain at the Top of the Subgrade Layer With Depth to Subsurface Water | 88 |
| Figure 4.7. Variation of the Modified Structural Number with Subsurface Water Levels | 90 |
| Figure 5.1. Predicted SWRC for the Proposed Soils..... | 108 |
| Figure 5.2. Schematic Demonstration of the Methods Used to Obtain Stress and Moisture-Dependent Resilient Modulus | 113 |
| Figure 5.3. Flow Diagram of the Procedure | 114 |
| Figure 5.4. TDR Measured And Suction - SWCC Predicted Moisture Content Profiles for (a) Maine Section; (b) Minnesota Section; (c) Texas Section; (d) Montana Section..... | 117 |
| Figure 5.5. Measured and Predicted Deflection Basins for Maine Section..... | 119 |
| Figure 5.6. Measured and Predicted Deflection Basins for Minnesota Section..... | 121 |
| Figure 5.7. Measured and Predicted Deflection Basins for Texas Section | 122 |

| | |
|---|-----|
| Figure 5.8. Measured and Predicted Deflection Basins for Montana Section | 123 |
| Figure 6.1. Predicted SWRC for the Proposed Soils | 133 |
| Figure 6.2. Schematic to Demonstrate the Pavement Cross Section and the Analysis Approach | 136 |
| Figure 6.3. Variation of Bearing Capacity with Groundwater Table Levels for the Proposed Soils | 138 |
| Figure 6.4. Ratio of Bearing Capacity with Groundwater Table Levels for the Proposed Soils | 139 |
| Figure 6.5. Tire Loads at Ultimate Bearing Capacity at Groundwater Table Levels for the Proposed Soils | 140 |

ABSTRACT

ASSESSING THE MECHANICAL RESPONSE OF PAVEMENTS DURING AND AFTER FLOODING

by

Mohamed Elshaer

University of New Hampshire, May, 2017

Flooding is recognized as a catastrophic event and a threat to the load carrying capacity of pavements around the world. In the aftermath of flooding, the pavement structure could be inundated and fully saturated. The significant increase of water within pavement layers may cause weakness and induce damage with traffic loading, subsequently increasing maintenance costs and shortening pavement service life.

The assessment of the structural performance and capacity of flooded pavements remains complicated due to lack of structural data immediately following flooding, and information about the pavement structure and materials is not always readily available. Currently, the decision to open roads for traffic is based on the assessment of the pavements, which relies on visual inspection and experience. An incorrect assessment of the flooded pavement structural capacity due to unforeseen conditions may lead to unexpected outcomes or failure. The objective of this dissertation is to advance the current knowledge of the behavior of flooded pavements, based on their performance properties and structural capacities.

Several methodologies have been developed and examined for a set of pavement

structures with different material types using layered elastic analysis to

- (1) investigate the pavement response to traffic loads under different moisture conditions,
- (2) identify the important parameters that affect the performance of inundated pavements,
- (3) investigate the influence depth of the subsurface water level at which the road can withstand traffic with zero to minimum deterioration,
- (4) estimate the in-situ pavement surface deflection, and
- (5) identify the catastrophic failure of pavements in post-flood events.

The findings showed a significant reduction in structural capacity when the pavement structure was in the fully saturated condition, but the road could regain its capacity after desaturation and recession of water level. The influence depth for the subsurface water level was found to be dependent on pavement structure and material type. The most accurate method to estimate the in-situ measured deflection is to divide the soil layer into several layers in the layered elastic analysis. Accurate layer thicknesses, traffic type, and interlayer bond condition are the important factors for evaluating changes in expected horizontal strain at the bottom of asphalt layer, used for predicting fatigue cracking pavement performance. The type of base and subgrade materials are the most important factors for evaluating the changes in expected vertical strain at the top of subgrade layer, used to predict pavement rutting performance. This dissertation provides information to agencies that will enhance their understanding of the performance and structural capacity of pavements in post-flood events.

CHAPTER 1

INTRODUCTION

1.1 STATEMENT OF PROBLEM

Roads are a vital part of the national infrastructure in moving people, freight, and services safely, and creating prosperity and welfare. Roads play a crucial role in the economic development at the national and local levels. Thus, investments in roads have many positive effects such as reducing travel times, increasing the resiliency of the transportation network and reducing user costs.

Extreme weather events, such as heavy rainfall, flooding, and heat waves can cause severe deterioration to the road infrastructure and increase intervention needs. One of the important challenges facing the pavement engineering community is assessing the behavior of pavements during and immediately following extreme weather events. For instance, flooding is recognized as a devastating event that can cause severe impact on the pavements through two different deteriorations: (1) substantial damage or washout and (2) distressed pavement that is still capable of the serving the community. In the latter, the floodwaters could completely saturate the unbound materials in the pavements. The pavement materials will become weakened and the road will not withstand the same traffic loading levels. Thus, the structural capacity of flooded pavements should be carefully investigated, and proactive actions considered to extend the pavement service life.

Another reason for advanced road deterioration post-flood events is a lack of guidelines

for agencies to determine the optimum time to reopen the road or restrict traffic loads to alleviate any potential damage in the weakened state. Generally, agencies are making the decision to reopen roads for traffic based on a visual inspection of the pavement and experience. An incorrect assessment can lead to further damage of flooded pavements, increasing rehabilitation needs. Thus, guidelines derived from performance-based assessments of flooded pavements are an appropriate tool to advance the current knowledge of flooded pavements for sustainability and resiliency planning.

This tool is important for monitoring the health of pavements to prevent further deteriorations and to make roads more sustainable and resilient. The American Society of Civil Engineers (ASCE) Infrastructure Report Card for 2017 stated that “roads in the United States are often crowded, frequently in poor condition, regularly underfunded, and are becoming more dangerous.” The report emphasized the increased backlog of rehabilitation needs due to the poor condition of highway pavement. A D grade is assigned to an overall condition of the nation roadways costing drivers an estimated \$112 billion in extra vehicle repairs and operating costs in 2014. Road construction costs rise faster than allocated funding, and at least 27 states and local governments reconsidered road materials, converting some low traffic, rural roads from asphalt to gravel for a sustainable solution. The lack of funding and future planning for the road infrastructure system is one of the main reason for the deteriorated condition. Tools to monitor the health of road infrastructure are needed for better planning.

In order to optimize the allocated funding, federal and state agencies have been investing in long-term programs to monitor the behavior of in-service pavements taking into account all potential factors related to pavement deterioration. Through such programs,

pavement behavior will be better understood and investment decisions will be more objective. Long-term pavement performance (LTPP) is one of the long-term programs that was introduced in 1987 as part of the Strategic Highway Research Program (SHRP) and has been managed by the Federal Highway Administration (FHWA) since 1992. LTPP is considered the most comprehensive pavement research program ever undertaken to address pavement performance. The primary goal of the LTPP program is to understand pavement performance. Since 1989, the LTPP database has grown exponentially and includes information collected from 2,509 pavement test sections throughout the United States and Canada. Understanding the behavior of pavements can improve by analyzing the LTPP data to increase the pavement service life and cost savings, and effectively implement interventions (preservation, rehabilitation, and maintenance).

1.2 OBJECTIVES

The primary objectives of this dissertation are to:

- 1- Provide robust performance-based assessment methodologies for pavements after flood events.
- 2- Improve understanding of how pavements perform under flooded conditions and how that changes as the floodwaters recede and moisture contents in the unbound materials return to normal.
- 3- Determine the most important information to gather for the assessment of pavements post flood events.
- 4- Develop a methodology for the state-of-practice to incorporate soil moisture profile into the evaluation of pavement structure.

- 5- Enhance understanding of the effect of subsurface water level on the structural capacity of pavements.
- 6- Assess the impact of the stress dependency coupled with moisture sensitivity of the unbound materials on pavement response.
- 7- Improve understanding of suction and its influence on the resilient behavior of unbound materials.
- 8- Provide a rational methodology to identifying the catastrophic failure of pavement structure due to the flooding events.

1.3 STRUCTURE OF DISSERTATION

This dissertation is intended to be a series of published or publishable technical papers devoted to advancing the current knowledge of the structural performance and capacity of pavements post flood events. Please note that the author of this dissertation is also the primary author of all technical chapters. **Chapter 1** provides an introduction to the problem, the objectives of the dissertation, and the scope.

Chapter 2 is a technical paper submitted for publication to the American Society of Civil Engineers Journal of Transportation Engineering, Part B. Pavements, entitled “Impacts of Pavement Layer Properties on Structural Performance of Inundated Pavements”. This paper identifies the most critical parameters affecting the performance of flooded pavements and investigates how much the variability in parameter properties impacts the pavement response. The structural capacity of thirteen different pavement sections with three different types of base course and three different subgrade soils from the Long-Term Pavement Performance (LTPP) database are evaluated using mechanistic and empirical approaches. The reduction of the structural capacity of pavements due to saturation

conditions is also discussed.

Chapter 3 presents a technical paper published by the Journal of Road Materials and Pavement Design, entitled “Methodology to Evaluate Performance of Pavement Structure Using Soil Moisture Profile”. Several methodologies are developed and tested to incorporate the soil moisture profile into flexible pavement evaluation, and to determine how the changes of groundwater table will affect the pavement deflection. In this paper, falling weight deflectometer (FWD) data from LTPP at two different flexible pavement sections in different climatic zones were used to estimate the in- situ measured pavement deflection with seasonal changes of water content. Comparisons of predicted deflection basins from layered elastic analysis using different methods with the measured FWD deflection basins for the selected LTPP sections at different times are presented.

Chapter 4 is a technical paper submitted for publication to the International Journal of Pavement Engineering, entitled “Impacts of Subsurface Water on the Structural Capacity of Inundated Flexible Pavements”. The primary focus of this portion of the dissertation is to investigate the impact of different subsurface water levels on the performance of pavements through a simplified approach. The paper uses different unbound material types with a variety of gradation and plasticity indexes from the LTPP database in different locations. This paper also provides insight into the effect of suction on the resilience behavior of different unbound material types and overall pavement structure. The critical subsurface water level at which the road can withstand traffic with minimum deterioration is also discussed.

Chapter 5 presents a manuscript to be submitted for publication, entitled “Assessing the Impact of Resilient Modulus Predictive Models of Unbound Materials on the Pavement Deflection Response”. This manuscript investigates the stress dependency coupled with

moisture sensitivity of the unbound materials on the estimated in-situ FWD deflection response through different methodologies. The paper uses four LTPP sections in different climatic zones to examine the sensitivity of each model on the pavement response. Soil moisture profile, AC temperature, material physical properties, groundwater table and depth to bedrock are the controlling parameters to be used in conjunction with the most accurate method of estimating the in-situ pavement deflection from chapter 3. The effect of the predicted moisture profile from suction distribution on the deflection response is also discussed.

Chapter 6 is a technical manuscript accepted for presentation and publication at the 10th International Conference on the Bearing Capacity of Roads, Railways and Airfields in Athens, Greece, entitled “Bearing Capacity Analysis of Pavement Structures for Short Term Flooding Events”. The paper presents a methodology to evaluate the bearing capacity of flooded pavements to provide an engineering basis for application of short-term load restrictions during and post flood events. Terzaghi’s bearing capacity formulation and the concept of effective stress in unsaturated soils are used. The paper also discussed the sudden failure of pavement structure caused by a relatively small number of passes over a severely weakened pavement structure. The maximum tire loads on the pavement surface that the road could withstand without any sudden shear failure are discussed. This approach can be extended to different pavement structures and material types and can be used to assist agencies in avoiding catastrophic failure in the pavement structures.

Chapter 7 is a closing discussion showing the author’s progression toward a performance-based evaluation of pavements and the range of application. Post-graduate plans for developing guidance based on the flooded pavements performance properties

and implementation as the state-of-practice useful to agencies are presented. **Chapter 8** is comprised of a master reference list.

CHAPTER 2

IMPACT OF PAVEMENT LAYER PROPERTIES ON STRUCTURAL PERFORMANCE OF INUNDATED PAVEMENTS

2.1 INTRODUCTION

Evaluating the structural function and integrity of pavements during flooding is complicated and challenges pavement engineers due to the existence of many unknowns during post-flood pavement assessments. In order to evaluate the performance or capacity of a pavement that has been inundated, full understanding of how asphalt pavement behaves under saturated conditions is required. Parameters such as traffic loads and environmental conditions such as temperature and moisture content will influence the amount of damage in pavements over time and, correspondingly, the reduced the structural capacity of the road. Pavement materials, bonding interface between layers, and thickness of pavement layers are examples of other parameters that determine the capacity of a pavement that has been flooded as well. The impact of these parameters on the performance of flooded pavements have not yet been widely investigated in most studies (Sultana et al. 2016).

Extreme changes in moisture content within a pavement structure during flooding can result in reduced load bearing capacity of the road. About 80% of pavement damage is related to the presence of excess water, which affects the performance of all pavement layers, especially the subgrade layer (Mndawe et al. 2015). The quality of unbound materials such as base, subbase, and subgrade layers determines the performance of the

pavement structure (Santero et al. 2011, Mallick and El-Korchi 2013, Elshaer et al. 2017). For short-term impacts; it is important to examine the behavior of unbound materials which are sensitive to moisture content under flooding and their influence on the pavement performance. For the assessment of long-term impacts due to floods, the sensitivity of the asphalt layer to water damage should also be considered.

Hurricanes Katrina and Rita caused devastating floods in 2005 that affected many roadways and called into question the appropriate way to evaluate the impact of flooding on the integrity of pavements. After these events, many agencies and researchers started to study the impact of flooding on pavement deterioration (Gaspard et al. 2007, Helali et al. 2008, Zhang et al. 2008, Vennapusa et al. 2013, Chen and Zhang 2014, Daniel et al. 2014, Khan et al. 2015, Mallick et al. 2015, Sultana et al. 2016). The lack of structural data for pavements before Hurricane Katrina made it difficult to perform a study to obtain the percent of reduction in the pavement strength after flooding. Thus, an alternative approach based on the comparison of the structural data for similar pavement structures, materials, environmental conditions, and traffic loads in different non-flooded areas was done. The research team studied the impact of road elevations, road pavement types, and AC pavement thickness. They observed that all damage caused by flooding happened during the first week of flooding. Based on the investigations, they suggested that the greatest impact from flooding is inundation which leads to change in the stiffness of pavements over time. The results showed that the thinner pavements were more vulnerable to the damage from flood waters than thicker pavements. The highest reduction in subgrade resilient modulus and the structural number was identified in thinner AC pavements. Flexible pavements were more vulnerable to flood water damage than rigid or composite pavements (Helali et al. 2008, Zhang et al. 2008).

Based on previous studies; there are many unknowns that impact the performance of flooded pavements that are not fully understood. In this study, six different parameters are investigated; these include asphalt layer thickness, base course layer thickness, base course material type, subgrade material type, interlayer bond condition, and traffic load. Analyses of these six different parameters for a low volume road and an interstate highway are conducted for two purposes: 1. to accurately determine which parameters affect the pavement's performance when the road is inundated and, 2. to determine the level of accuracy and/or resolution needed for the different parameters. In this study, the unbound layers are assumed to be at optimum moisture content during non-flood conditions; this represents the as-designed strength of the pavement structure. During the flooding event, the unbound layers are assumed to be fully saturated to evaluate the worst-case conditions where the pavement structure would be at its weakest. In other words, at the latter case the groundwater table level is assumed to be at the top of the subgrade layer. It is well known that the full saturation of the subgrade from excessive flood water is based on the exposure time to flood water and the soil type, but evaluating the time was not part of the scope of the study.

Two approaches were used to evaluate the structural capacity of pavement structure; 1. A Mechanistic approach, Layer Elastic Analysis (LEA) is used to predict the stresses and strains at the bottom of asphalt layer and at the top of subgrade layer to evaluate the impact of saturated conditions. 2. AASHTO Empirical approach, the structural number is calculated to evaluate the pavement structural capacity due to saturation condition. Then, the ratio of parameters calculated under saturated conditions to those calculated under optimum moisture conditions was determined. These ratios are used to identify the importance of various parameters. Statistical analysis using Analysis of Variance

(ANOVA) was conducted to provide a fair comparison amongst different parameters to investigate the impacts on the performance of inundated pavements.

This study will allow engineers to acquire a better understanding of how pavements perform under flooded conditions and to recognize the most critical parameters that affect the performance of flooded pavement structures. Based on this study, the most important information to collect during the post-flood assessments is the material characterizations of base course and subgrade layer for assessing the change in expected vertical strain, and therefore the rutting performance and the layer thickness, traffic loading types and interlayer bond conditions for assessing the change in expected horizontal strain, and therefore the fatigue performance.

2.2 METHODS AND DATA

In this study, the structural capacity of thirteen different pavement sections with three different types of base course and three different subgrade soils were evaluated. The cross sections chosen for a typical low-volume road and interstate highway are shown in Figure 2.1. A range of typical pavement layer thicknesses was used in this analysis to determine the sensitivity to thickness values. The intent is to provide guidance on the level of accuracy needed for these measurements to effectively determine the impact of the saturated conditions on the structural capacity of the pavement.

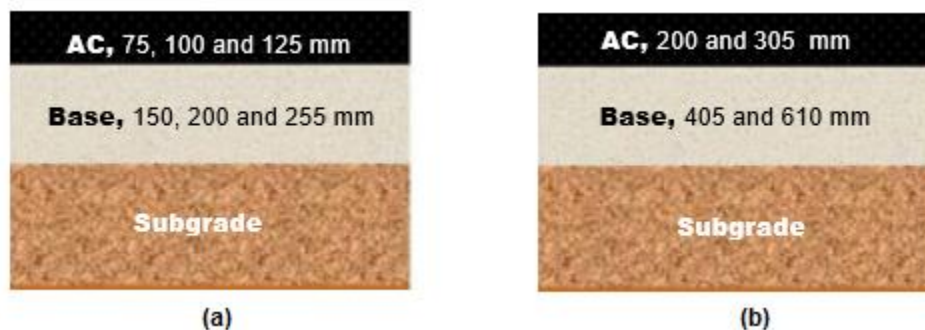


Figure 2.1. Typical cross section for a) Low-Volume Road b) Interstate Highway

The base course and subgrade soils represent a range of typical materials types across the U.S. For this study, the measured material physical properties for subgrade soils were obtained from the LTPP database for sites in Utah, Wyoming, and South Dakota and are presented in Table 2.1. These sites were chosen based on the variety of the gradation and plasticity index of the material types.

Table 2.1. Subgrade Soil Properties from Selected LTPP Sites

| LTPP Sites | 1 | 2 | 3 |
|--|-----------|--------------|-------------------|
| | 49-1017 | 56-6031 | 46-3012 |
| Location | Utah (UT) | Wyoming (WY) | South Dakota (SD) |
| AASHTO Classification | A-2-4 | A-4 | A-7-6 |
| Percent Passing # 200 | 8.9 | 35.7 | 83.1 |
| Liquid Limit (LL) | 20 | 25 | 58 |
| Plasticity Index (PI) | NP | 8 | 38 |
| Optimum Moisture % | 13.7 | 13.1 | 17.7 |
| Specific Gravity (Gs) | 2.650 | 2.706 | 2.762 |
| Void Ratio (e) | 0.48 | 0.44 | 0.54 |
| Max lab Dry Density (Kg/m ³) | 1794 | 1874 | 1794 |
| California Bearing Ratio test (CBR) | 32 | _____ | 10 |
| Resistance R-Value | _____ | 26 | _____ |

For the subgrade layer, the resilient modulus values at optimum moisture content and at full saturation are needed. Thus, Mechanistic-Empirical Pavement Design guide (MEPDG) Level 2 correlations between strength and stiffness of unbound materials were employed to estimate the resilient modulus (M_R) of the proposed soils at an optimum moisture content using Equation 2.1 or 2.2, based on available information.

$$M_R \text{ (MPa)} = 17.6(\text{CBR})^{0.64} \quad (2.1)$$

$$M_R \text{ (MPa)} = 8.0 + 3.8R \quad (2.2)$$

The MEPDG suggests that the ratio of resilient modulus values at different moisture contents to optimum moisture content (M_R/M_{Ropt}) ranges from 2.5 to 0.5 (NCHRP, 2004). The moisture content, and therefore resilient modulus of the subgrade under flooding conditions will depend on the infiltration rate, the permeability of the soil, and the flood duration. Vennapusa et al. (2013) proposed a study to evaluate the performance of pavement structures post-Missouri river flooding 2011. The findings from in-situ testing indicated that the reduction of resilient modulus of subgrade soils; A-2-4, A-4, A-6 and A-7 was 23 – 30% due to flooding at all times of testing. In this study, the resilient modulus of the saturated materials (worst case scenario) are assumed to be half the optimum moisture content value. The values of resilient modulus and Poisson's ratio for base course materials used in this analysis (Table 2.2) were obtained from the MEPDG level 3 inputs based on the AASHTO 180 soil classification for unbound materials (MEPDG, 2008) and Cornell typical values (Orr, 2014). For the asphalt layer, PG 64-28 with 5% void ratio and 5% effective binder with 2750 MPa average modulus value at 20°C was used; daily and seasonal variations are not considered in this analysis.

Table 2.2. Pavement Material Types and Material Properties

| Material Layer Type | AC | Base | | | Subgrade | | | |
|---------------------------|--------------------------------------|---------------|------------------|------|--------------------|-------|-------|-------|
| | Hot Mixed, Hot Laid AC, Dense Graded | Crushed Stone | Uncrushed Gravel | | Moisture Condition | A-2-4 | A-4 | A-7-6 |
| | | Well drained | Poorly drained | | | | | |
| Mr (MPa) | 2750 | 300 | 250 | 60 | Opt | 170 | 110 | 80 |
| | | | | | Sat | 85 | 55 | 40 |
| Poisson's ratio, v | 0.35 | 0.35 | 0.35 | 0.40 | Opt | 0.25 | 0.325 | 0.20 |
| | | | | | Sat | 0.25 | 0.35 | 0.45 |

2.2.1 Pavement Evaluation: Mechanistic Approach

Multi-layer elastic analysis Waterways Engineering Station Elastic Layer Analysis Pavement (WESLEA) software was used to calculate the stresses and strains in the pavement structures. The horizontal tensile strain at the bottom of AC layer and vertical compressive strain at the top of subgrade layer were calculated using layer modulus values corresponding to different moisture conditions. These parameters were selected as they are related to bottom-up fatigue cracking and rutting distress in the pavement. The interface condition was considered as both full bond and full slip to identify which is critical for pavement response. Traffic loads were broken down into light and heavy trucks to examine the impact on the flooded pavement response. Trucks were modeled in the WESLEA software and the maximum strains under each loading were used for further analysis. Table 2.3 shows the truck types, axle and tire types used in this analysis for low volume roads. The repair trucks such as dump truck 1, 2 and loader are considered in this analysis because they are typically used for removing debris after a flooding event. For the interstate analysis, only the single axle single tire load was evaluated.

Table 2.3. Truck, Axle and Tire Types

| Axle and Tire Type Truck Type | Front Axle (kN) | | | Rear Axle (kN) | | | Tire Pressure (MPa) |
|--------------------------------------|-------------------------|-----------------------|-----------------------|-------------------------|-----------------------|-----------------------|---------------------|
| | Single axle single tire | Single axle dual tire | Tandem axle dual tire | Single axle single tire | Single axle dual tire | Tandem axle dual tire | |
| Single axle single tire | 80 | _____ | _____ | 80 | _____ | _____ | 0.83 |
| FHWA Class 5 (Dump truck 1) | 65 | _____ | _____ | _____ | 100 | _____ | 0.83 |
| FHWA Class 6 (Dump truck 2) | 65 | _____ | _____ | _____ | _____ | 215 | 0.83 |
| FHWA Class 9 | 55 | _____ | 150 | _____ | _____ | 150 | 0.70 |
| Loader (15.5R25) | 115 | _____ | _____ | 115 | _____ | _____ | 0.50 |

JMP Software was used for statistical analysis. Analysis of Variance (ANOVA) was conducted to determine the influence of each pavement layer properties on the flooded pavements. A confidence level of 95 percent was used for all analysis. For this study, a substantial number of horizontal and vertical strains values were used for low volume cross sections (the total number of runs was 565) and the interstate cross sections (the total number of runs was 96). The ratio of horizontal and vertical strains at different moisture conditions was also investigated. Tukey-Kramer HSD test was conducted to determine the importance of each parameter on the performance of pavement structure. Table 2.4 shows the summary of the different combinations that were analyzed for the various cross sections and material types.

Table 2.4. Combinations of Material Types and Parameters Evaluated in This Study

| | Material Type/ Cross Section | Layer Thickness, mm | | Bond Interface | | Traffic Loading | | | | |
|--------------------------------------|--|---------------------|------|----------------|-----------|----------------------------|-----------------|-----------------|-----------------|--------|
| | | AC | Base | Full Bond | Full Slip | Single Axle Single Tire | FHWA Class 5 | FHWA Class 6 | FHWA Class 9 | Loader |
| | | | | | | | | | | |
| Low-Volume Road & Interstate Highway | | 75 | 150 | √ | √ | √ | √ | √ | √ | √ |
| | | 75 | 200 | √ | √ | √ | | | | |
| | | 75 | 255 | √ | √ | √ | √ | √ | √ | √ |
| | AC | 100 | 150 | √ | √ | √ | | | | |
| | | 100 | 200 | √ | √ | √ | | | | |
| | Crushed Stone | 100 | 255 | √ | √ | √ | | | | |
| | | 125 | 150 | √ | √ | √ | √ | √ | √ | √ |
| | | 125 | 200 | √ | √ | √ | | | | |
| | A-2-4, A-4 & A-7-6 Optimum Moisture Content Fully Saturated | 125 | 255 | √ | √ | √ | √ | √ | √ | √ |
| | | 200 | 405 | √ | √ | √ | | | | |
| | | 200 | 610 | √ | √ | √ | | | | |
| | | 305 | 405 | √ | √ | √ | | | | |
| | | 305 | 610 | √ | √ | √ | | | | |
| | AC | 75 | 150 | √ | √ | √ | √ | √ | √ | √ |
| | | 75 | 200 | √ | √ | √ | | | | |
| | Uncrushed Gravel Well Drained | 75 | 255 | √ | √ | √ | √ | √ | √ | √ |
| | | 100 | 150 | √ | √ | √ | | | | |
| | | 100 | 200 | √ | √ | √ | | | | |
| | A-2-4, A-4 & A-7-6 Optimum Moisture Content Fully Saturated | 100 | 255 | √ | √ | √ | | | | |
| | | 125 | 150 | √ | √ | √ | √ | √ | √ | √ |
| | | 125 | 200 | √ | √ | √ | | | | |
| | | 125 | 255 | √ | √ | √ | √ | √ | √ | √ |
| | | 75 | 150 | √ | √ | √ | √ | √ | √ | √ |
| | | 75 | 200 | √ | √ | √ | | | | |
| | AC | 75 | 255 | √ | √ | √ | √ | √ | √ | √ |
| | | 100 | 150 | √ | √ | √ | | | | |
| | Uncrushed Gravel Poorly Drained | 100 | 200 | √ | √ | √ | | | | |
| | | 100 | 255 | √ | √ | √ | | | | |
| | | 125 | 150 | √ | √ | √ | √ | √ | √ | √ |
| | A-2-4, A-4 & A-7-6 Optimum Moisture Content Fully Saturated | 125 | 200 | √ | √ | √ | | | | |
| | 125 | 255 | √ | √ | √ | √ | √ | √ | √ | |
| | 200 | 405 | √ | √ | √ | | | | | |
| | 200 | 610 | √ | √ | √ | | | | | |
| | 305 | 405 | √ | √ | √ | | | | | |
| | 305 | 610 | √ | √ | √ | | | | | |

2.2.2 Pavement Evaluation: AASHTO Empirical Approach

The AASHTO 1993 approach has been an important pavement design tool for several decades. It is still regularly used by pavement engineers around the world because it is simple to apply and is based on real data. Thus, this approach can be an effective way of looking at differences in the structural capacity for this particular problem of inundated pavements. The structural number (Equation 2.3) for a pavement cross section used in the AASHTO Empirical design approach is calculated only using the layers above the

subgrade and the contribution of the subgrade stiffness to the overall pavement performance is included as an independent parameter in Equation 2.4 (Rohde, 1994).

$$SN = a_1 D_1 + a_2 D_2 m_2 + a_3 D_3 m_3 \quad (2.3)$$

$$\log_{10}(W_{18}) = Z_R \times S_0 + 9.36 \times \log_{10}(SN + 1) - 0.20 + \frac{\log_{10}\left(\frac{\Delta PSI}{4.2-1.5}\right)}{0.40 + \frac{1094}{(SN+1)^{5.19}}} + 2.32 \times \log_{10}(M_R) - 8.07 \quad (2.4)$$

where SN = Structural Number; a_1, a_2, a_3 = layer coefficients of the surface, base, and subbase layers, respectively; D_1, D_2 and D_3 = layer thicknesses in inches of the surface, base, and subbase layers, respectively; m_2 and m_3 = layer drainage coefficients of the base, and subbase layers, respectively; W_{18} = Accumulated 18-kip Equivalent Single Axle Loads over the life of the project (18-kip) ESAL; Z_R = Standard Normal Deviate; S_0 = combined standard error of the traffic prediction and performance prediction; ΔPSI = Change in Serviceability; M_R = Resilient Modulus psi

In this study the traditional structural number (defined by Equation 2.3) was used as well as two modified SN approaches that include the subgrade material in the SN calculation. All three approaches were used to calculate the SN under different subgrade moisture conditions. The layer coefficient and drainage coefficient values used in this analysis are shown in Table 2.5 and Table 2.6 shows the reliability, standard deviation and terminal serviceability values used for low volume and interstate cross sections.

Table 2.5. Layer coefficient and drainage coefficient for the AASHTO method

| Material Layer Type | AC | Base | | | First layer of Subgrade (120-inch) | | | | | |
|--------------------------|------|---------------|------------------|----------------|------------------------------------|------|------|------|-------|------|
| | | Crushed Stone | Uncrushed Gravel | | A-2-4 | | A-4 | | A-7-6 | |
| | | | Well drained | Poorly drained | Opt | Sat | Opt | Sat | Opt | Sat |
| Layer coefficient (a) | 0.42 | 0.17 | 0.15 | 0.01 | 0.16 | 0.09 | 0.12 | 0.05 | 0.08 | 0.01 |
| Drainage coefficient (m) | -- | 1 | 1 | 0.60 | 1 | 1 | 1 | 1 | 1 | 1 |

Table 2.6. AASHTO input parameters

| Input Parameter | Reliability | Standard deviation | Terminal serviceability |
|----------------------------|-------------|--------------------|-------------------------|
| Low volume sections | 85 | 0.35 | 2.5 |
| Interstate sections | 95 | 0.45 | 3 |

Traditional SN Approach: The structural number (SN_{opt}) for each cross section was first calculated using Equation 2.3 with structural and drainage coefficient values for the AC and base layers in Table 2.6. The number of ESALs that each cross section could withstand (Equation 2.4) was then calculated using the resilient modulus of the subgrade layer at optimum moisture condition (M_{ROpt}). The structural number (SN_{sat}) required for the cross section to withstand the same level of traffic using the saturated resilient modulus of the subgrade layer (M_{RSat}) was then calculated. The ratio SN_{sat}/SN_{Opt} was calculated for the different cross sections and material types to evaluate the change in structural capacity due to saturated subgrade conditions. In this analysis, the SN_{sat} is greater than SN_{Opt} ($SN_{sat}/SN_{Opt} > 1.0$) because this SN represents the additional structural number needed under full saturation condition to withstand the same level of traffic the pavement was designed for under optimum moisture condition.

The relationship between change in subgrade modulus and number of ESALs was also determined in this approach and is applicable for all cross sections and material types.

Modified structural number (SNC): The modified structural number presented in Equation 2.5 is defined as the sum of the traditional structural number (Equation 2.3) and the contribution of subgrade (SN_{sg}) computed from Equation 2.6 using the CBR value of the subgrade (Watanatada et al. 1987). In this study, CBR values were obtained using the level 2 MEPDG correlation (Equation 2.1) assuming a 50% reduction in M_R under full saturation conditions.

$$SNC = SN + SN_{sg} \quad (2.5)$$

$$SN_{sg} = -0.85(\log CBR)^2 + 3.51(\log CBR) - 1.43 \quad (2.6)$$

where:

SN = Structural number; SN_{sg}= Subgrade structural number, determined by the Equation from Hodges et al. 1975.

Alternate Modified structural number (MSN): In this approach, the subgrade layer was divided into 2 layers, the upper layer is considered as subbase layer with a 120-inch thickness and the second layer is considered as infinite subgrade layer. The structural coefficients for the upper layer are determined using established empirical relationships between Mr and subbase structural coefficient values. The values used in this analysis are shown in Table 2.5. The MSN is calculated using Equation 2.3 with three layers: AC, base, and subbase. The 120-inch thickness for the subbase layer was determined through a sensitivity analysis. Subbase thicknesses greater than 120 inches did not result in a significant increase (less than 1 %) in the MSN value for any of the materials investigated. For the two modified structural numbers (SNC and MSN), values determined under fully saturated conditions are less than those determined at optimum moisture conditions because the contribution of the subgrade is taken into account ($SNC_{sat}/SNC_{opt} < 1.0$).

2.3 RESULTS AND DISCUSSION

2.3.1 Mechanistic Approach: Layer Elastic Analysis

2.3.1.1 Impact of Interlayer Bond Condition

The impact of the interlayer bond condition on the ratio of strain calculated using saturated condition to strain calculated using optimum moisture condition is shown in Figure 2.2. This figure represents the average strain ratios with the associated standard deviation from different asphalt and base layer thickness, base type, subgrade type and different traffic loads for low volume cross sections. Due to the difference in assumed Poisson's ratio of the A-7-6 soil for optimum and saturated conditions, the layered elastic analysis shows that the vertical strain at the top of subgrade soil at full saturation is less than that at optimum moisture condition at full slip condition at all traffic load types. This does not represent true behavior and thus, these data were excluded from the vertical strain comparison at full slip conditions.

Figure 2.2 shows that the full slip condition is critical (larger increase in ϵ_t under saturated conditions) for horizontal strain which is related to expected fatigue performance while the full bond condition is critical for vertical strains which are related to expected rutting performance. However, the actual interlayer bond condition in the field will fall somewhere between the full bond and full slip conditions. There is a statistically significant difference between the ratio of horizontal tensile strains at the full bond and full slip conditions while there is no significant difference for the ratio of vertical compressive strain between full bond and full slip for low volume and interstate cross sections as provided in Tables 2.7 and 2.8 respectively.

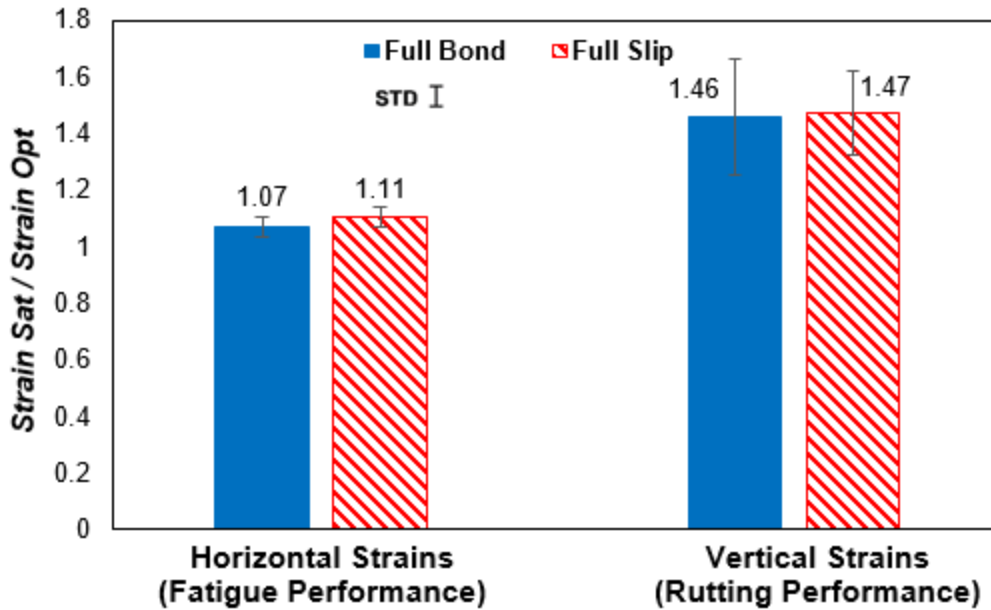


Figure 2.2. Ratio of saturated to optimum moisture condition for horizontal tensile strain and vertical compressive strain under full bond and full slip interlayer conditions for low volume roads.

Table 2.7. ANOVA Testing for the horizontal and vertical strain values and ratios for low volume cross sections (p-Value)

| Parameter | Strain values (n = 564) | | Strain Ratios (n=282) | |
|------------------------|-------------------------|----------|-----------------------|----------|
| | Horizontal | Vertical | Horizontal | Vertical |
| <i>Ac Thickness</i> | <0.0001 | <0.0001 | 0.17 | 0.45 |
| <i>Base Thickness</i> | <0.0001 | <0.0001 | <0.0001 | 0.48 |
| <i>Base Type</i> | <0.0001 | 0.50 | 0.13 | <0.0001 |
| <i>Subgrade Type</i> | 0.0157 | <0.0001 | 0.11 | <0.0001 |
| <i>Traffic Type</i> | 0.54 | <0.0001 | <0.0001 | 0.19 |
| <i>Bond interlayer</i> | <0.0001 | <0.0001 | <0.0001 | 0.55 |

Table 2.8. ANOVA Testing for the horizontal and vertical strain values and ratios for interstate cross sections at single axle single tire loading type (p-Value)

| Parameter | Strain values (n = 96) | | Strain Ratios (n=48) | |
|-----------------------|------------------------|----------|----------------------|----------|
| | Horizontal | Vertical | Horizontal | Vertical |
| <i>Ac Thickness</i> | <0.0001 | <0.0001 | 0.008 | 0.23 |
| <i>Base Thickness</i> | 0.81 | 0.0004 | <0.0001 | 0.69 |
| <i>Base Type</i> | 0.0002 | 0.88 | 0.87 | 0.004 |
| <i>Subgrade Type</i> | 0.99 | 0.011 | 0.66 | 0.008 |

| | | | | |
|------------------------|--------------|-------------------|---------------|------|
| <i>Bond interlayer</i> | 0.005 | <0.0001 | 0.0001 | 0.25 |
|------------------------|--------------|-------------------|---------------|------|

Note: Bold digits are less than 0.05 (95 % confidence); statistically significant.

2.3.1.2 Impact of Traffic Loading Type

Figures 2.3 and 2.4 show the impact of five different truck types (single axle single tire, FHWA Class 5, FHWA Class 6, FHWA Class 9 and Loader) on the saturated/optimum moisture condition ratios for horizontal and vertical strains. Figure 2.3 illustrates the average strain ratios associated with the standard deviation for all low volume cross sections at different asphalt and base layer thickness, base course type, subgrade type under five different truck types. The results for the thinnest and thickest low volume cross sections are shown in Figures 2.4a and 2.4b.

There is a significant difference from loading types on the ratio of horizontal strains while the ratio of vertical strains shows no significant difference in the performance of pavement structure as presented in Table 2.7 for low volume cross sections. Tukey-Kramer HSD test as presented in Table 2.9 shows that the loader is significantly different than other traffic loading types on the ratio of horizontal strains while the latter four traffic load types (single axle single tire, FHWA Class 5, 6 and 9) do not differ from one another. Therefore, the loader is the critical truck type for fatigue performance in the pavement structure under saturated conditions. For rutting performance, there is no statistically significant difference at all in ratios due to different truck types on the performance of pavement structure. The horizontal and vertical strains ratios are similar for the two different cross sections in Figure 2.4. The magnitude of the ratio changes with the different subgrade and base course types, but the trends with respect to loading type remain the same for a particular cross section. For the remaining analysis, the single axle single tire loading is used.

Table 2.9. Tukey-Kramer HSD Testing for the ratio of horizontal strain for low volume cross sections (p-Value)

| Level | level | p-Value |
|--------------|-------------------------|---------|
| Loader | Single Axle Single Tire | <0.0001 |
| Loader | FHWA Class 9 | 0.0007 |
| Loader | FHWA Class 6 | 0.0014 |
| Loader | FHWA Class 5 | 0.0068 |
| FHWA Class 5 | Single Axle Single Tire | 0.492 |
| FHWA Class 5 | FHWA Class 9 | 0.822 |
| FHWA Class 6 | Single Axle Single Tire | 0.872 |
| FHWA Class 6 | FHWA Class 9 | 0.971 |
| FHWA Class 5 | FHWA Class 6 | 0.986 |
| FHWA Class 9 | Single Axle Single Tire | 1.00 |

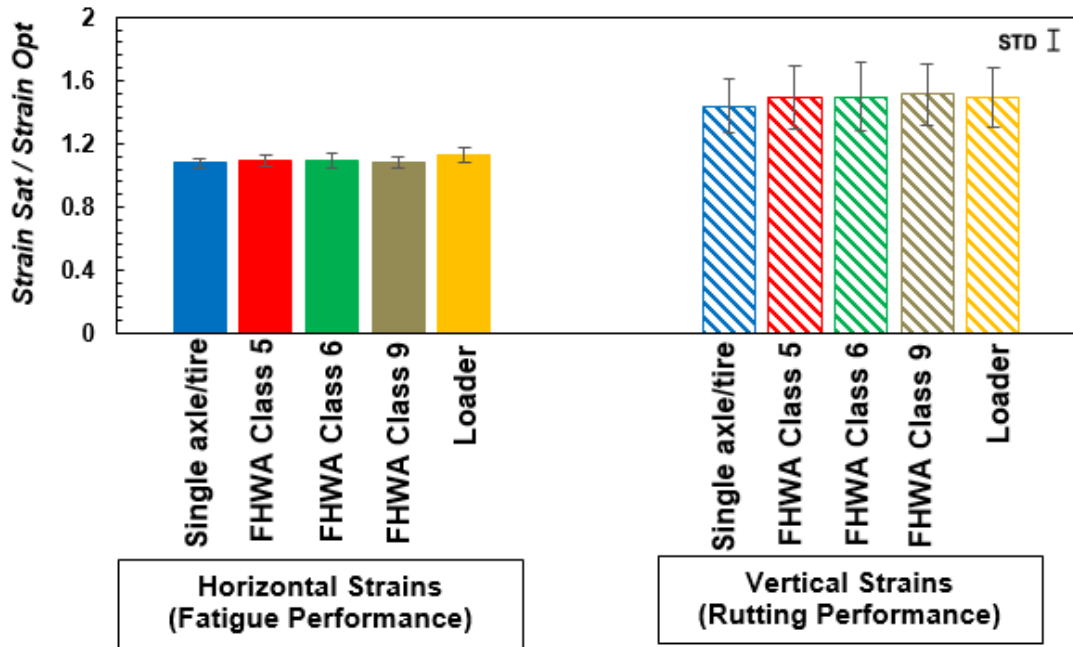


Figure 2.3. Ratio of saturated to optimum moisture condition for horizontal tensile strain and vertical compressive strain under different truck loading types for all low volume cross sections

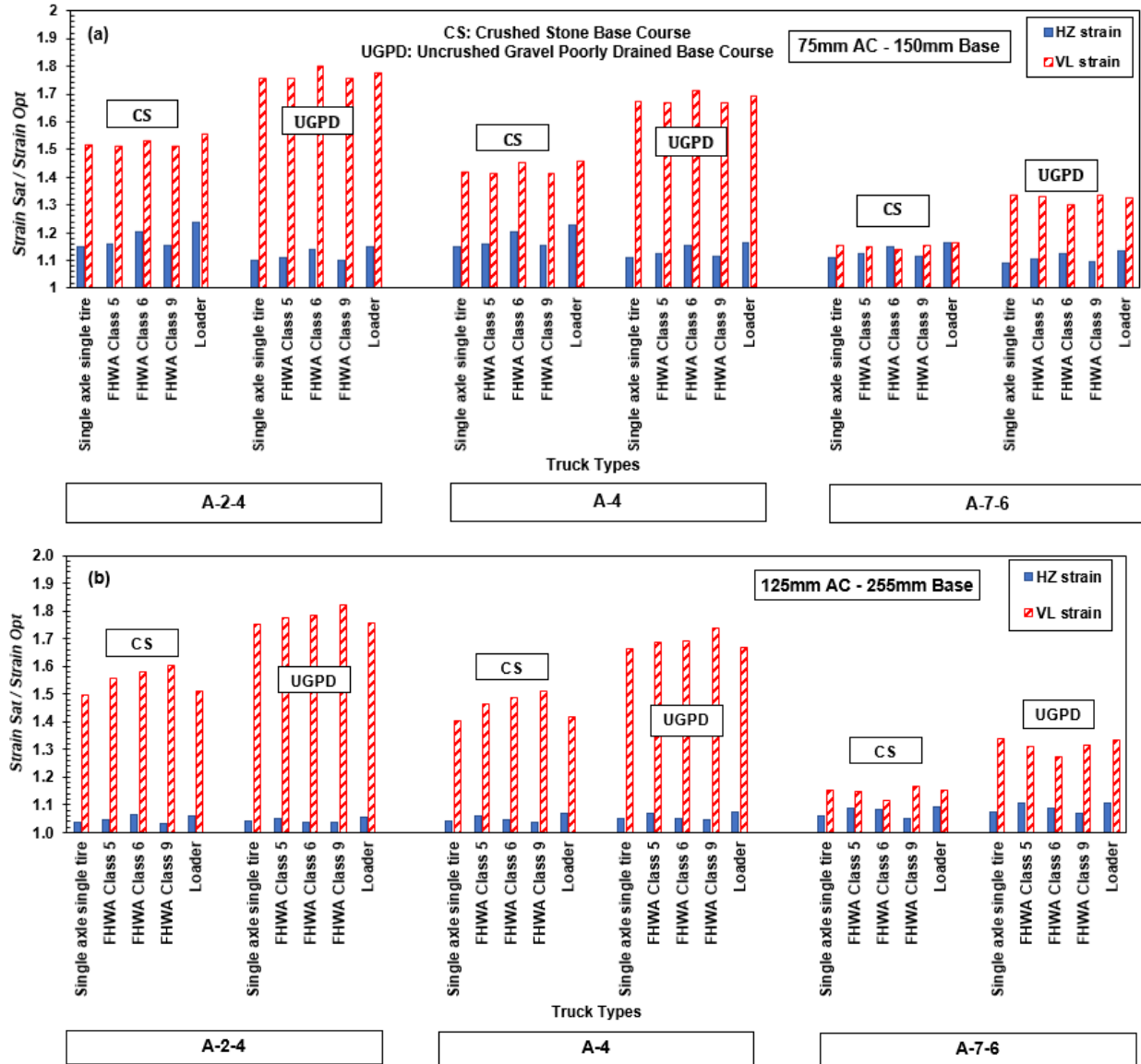


Figure 2.4. Ratio of saturated to optimum moisture condition for horizontal and vertical strain under different traffic loading types for (a) 75 mm AC, 150 mm base (b) 125 mm AC, 255 mm base cross section under different base course and subgrade material types

2.3.1.3 Impact of Layer Thickness and Material Type

Figures 2.5 and 2.6 show the calculated horizontal strains at the bottom of the asphalt layer and vertical strains at the top of subgrade layer under optimum moisture condition for the low volume road and interstate cross sections, respectively. The horizontal and

vertical strains follow expected trends under both optimum and saturated moisture conditions. The asphalt layer thickness, base course thickness, base course type, subgrade type and bond interlayer conditions all significantly impact the horizontal strain for low volume cross sections. In contrast, asphalt layer thickness, base course type, and interlayer bond condition are the only the significant parameters for interstate cross sections as shown in Tables 2.7 and 2.8. The crushed stone base course is slightly better than the well-drained uncrushed gravel base course, while the poorly drained uncrushed gravel shows the highest horizontal strain values.

The asphalt layer thickness, base course thickness, subgrade type, traffic loading types and interlayer bond conditions all significantly impact the vertical strain for low volume and interstate cross sections as shown in Tables 2.7 and 2.8. The base course type has the least impact. A-7-6 soil results in the highest strain values for all cross sections.

The ratio between the horizontal strain under saturated conditions to the horizontal strain under optimum moisture conditions is shown in Figures 2.7a and 2.7b for low-volume road and interstate cross-sections, respectively. The saturated conditions increase the strain by 6 to 15% for the low-volume road and 3 to 8% for the interstate section. The largest increases are for the thinner base course and the A-7-6 subgrade type. The asphalt thickness has a smaller impact on the increase in horizontal strain with thinner and poorly-drained base courses. The most important parameters that influence the increase in horizontal strain, and therefore the expected reduction in fatigue performance under saturated conditions, are base course type, traffic loading type, and interlayer bond conditions for low volume cross sections while the asphalt and base course layer thickness and bond interlayer conditions are the most significant parameters for interstate cross sections as shown in Tables 2.7 and 2.8.

Figures 2.8a and 2.8b show the ratio between the vertical strain at the top of subgrade layer under saturated and optimum moisture conditions for low-volume and interstate cross-sections, respectively. The vertical strain is more critical than horizontal strain under saturated conditions, with an increase in strain due to saturated conditions of 15 to 80% for the all the combinations evaluated. The base course and subgrade type have the most significant impact on the ratios for low volume and interstate cross sections as shown in Tables 2.7 and 2.8. The finer subgrades show a smaller change in vertical strain (although the actual magnitude of the vertical strain (ϵ_v) is lower than with coarse subgrade), and the poorly drained base course shows the largest difference. The asphalt and base course thicknesses do not have a significant impact on the increase in vertical strain due to saturated conditions.

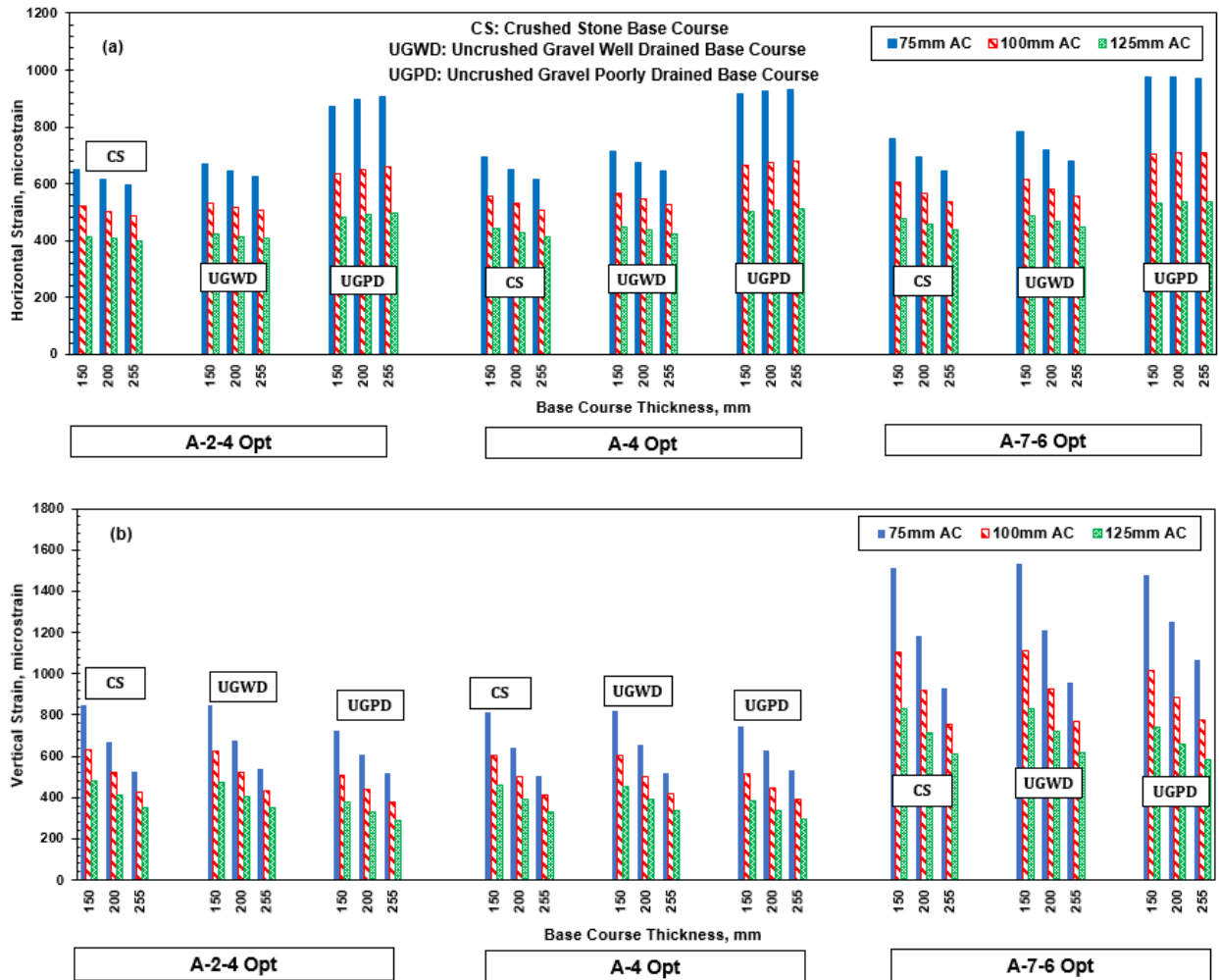


Figure 2.5. (a) Horizontal strain (b) Vertical strain at optimum moisture content under different base course and subgrade material types under single loading type on low volume cross sections

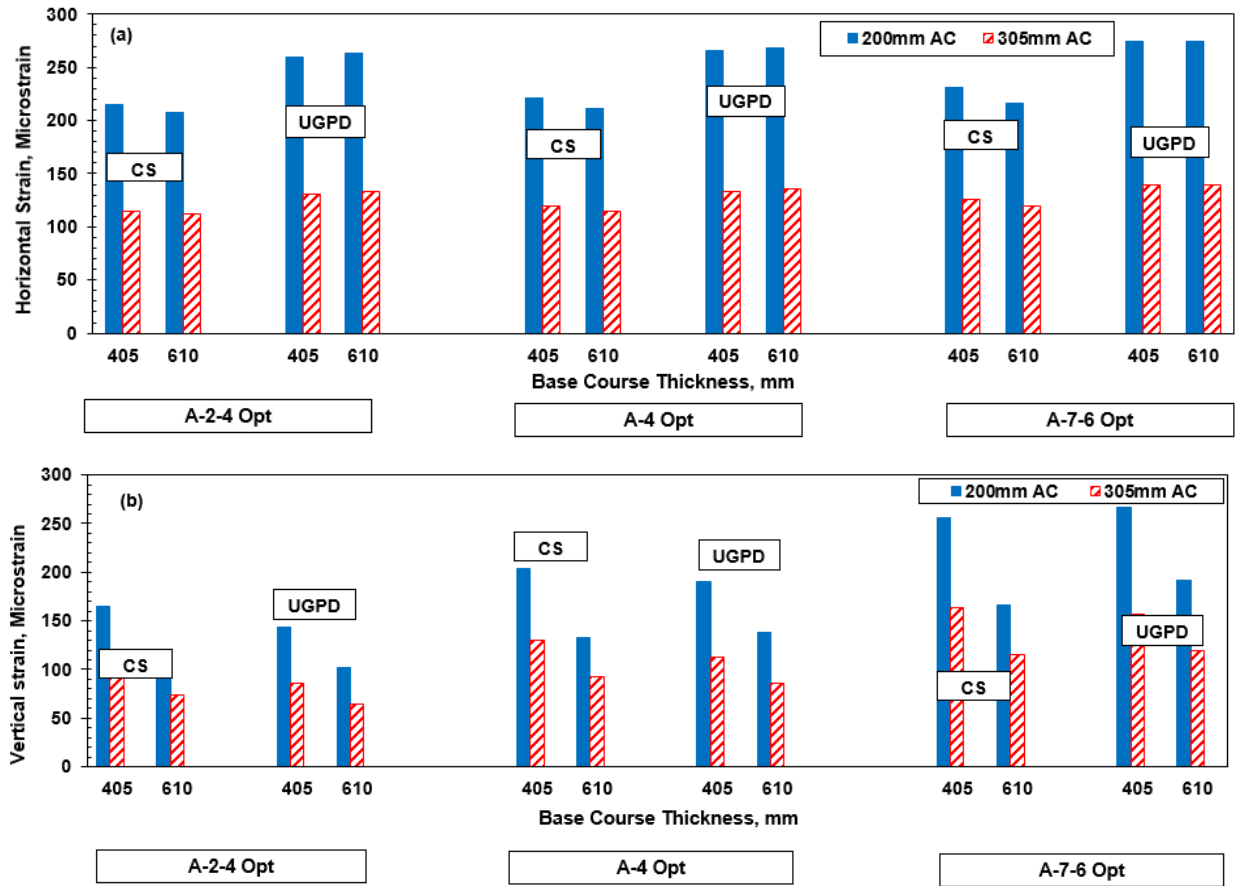


Figure 2.6. (a) Horizontal strain (b) Vertical strain at optimum moisture content under different base course and subgrade material types under single loading type on Interstate cross sections

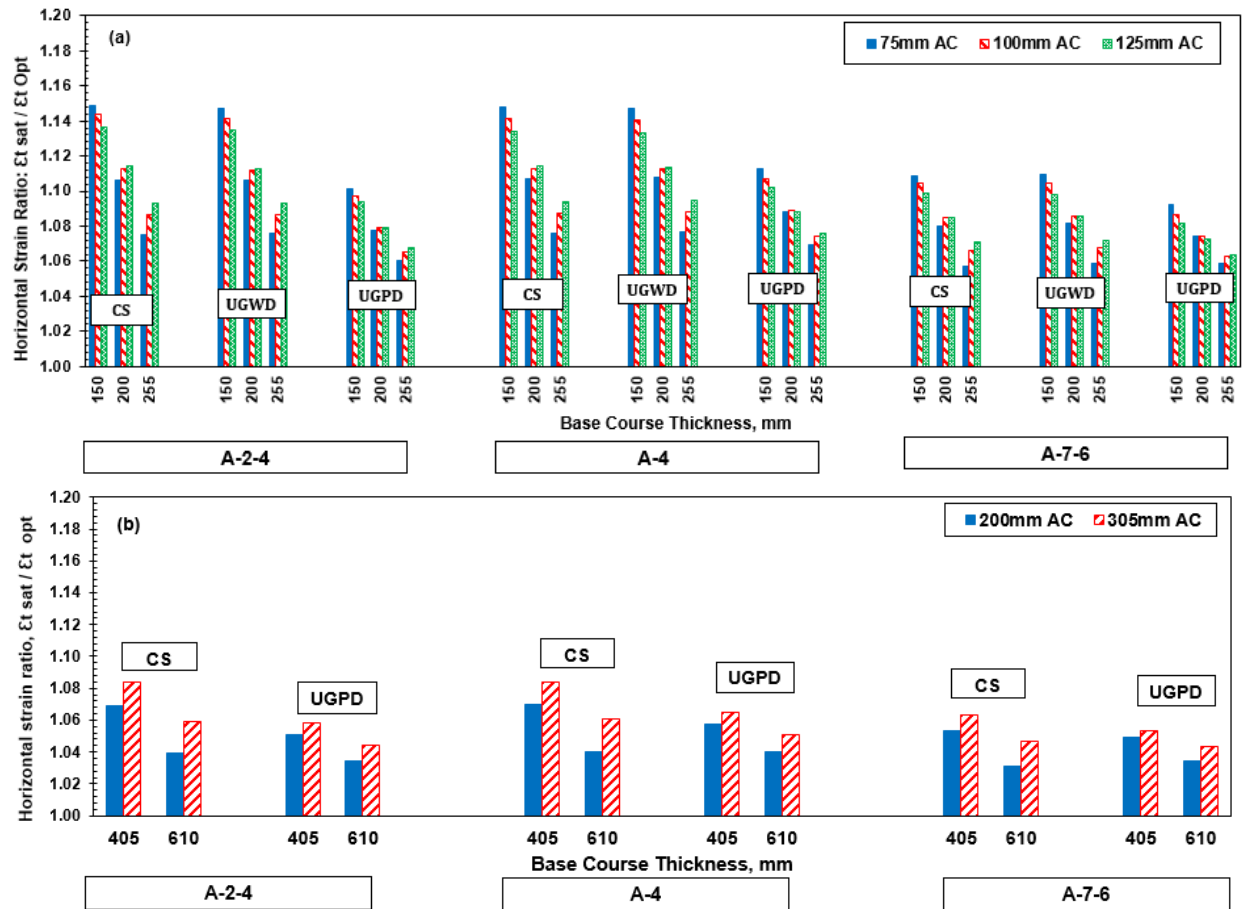


Figure 2.7. Ratio of saturated to optimum moisture condition for horizontal strains for (a) Low-volume sections (b) Interstate sections under different base course and subgrade material types under single loading type

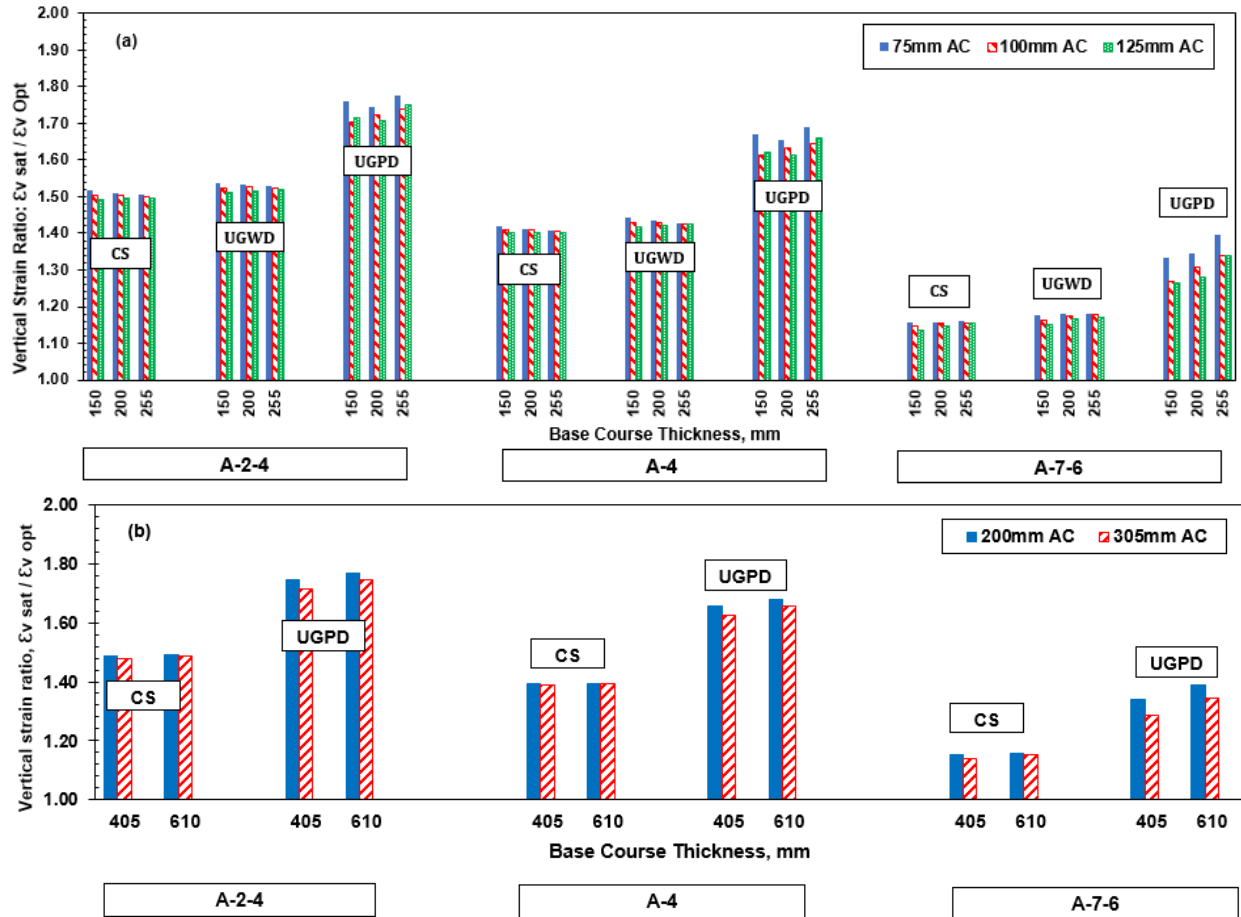


Figure 2.8. Ratio of saturated to optimum moisture condition for vertical strains for (a) Low-volume sections (b) Interstate sections under different base course and subgrade material types under single loading type

2.3.2 AASHTO Empirical Approach Results Discussion

Figures 2.9 and 2.10 show the calculated structural number (SN) and the corresponding number of ESALs for the low volume and interstate cross sections, respectively. The asphalt layer thickness, base course thickness, base course type and subgrade type all impact the number of ESALs, as expected with higher quality (stronger) materials having a larger number of ESALs.

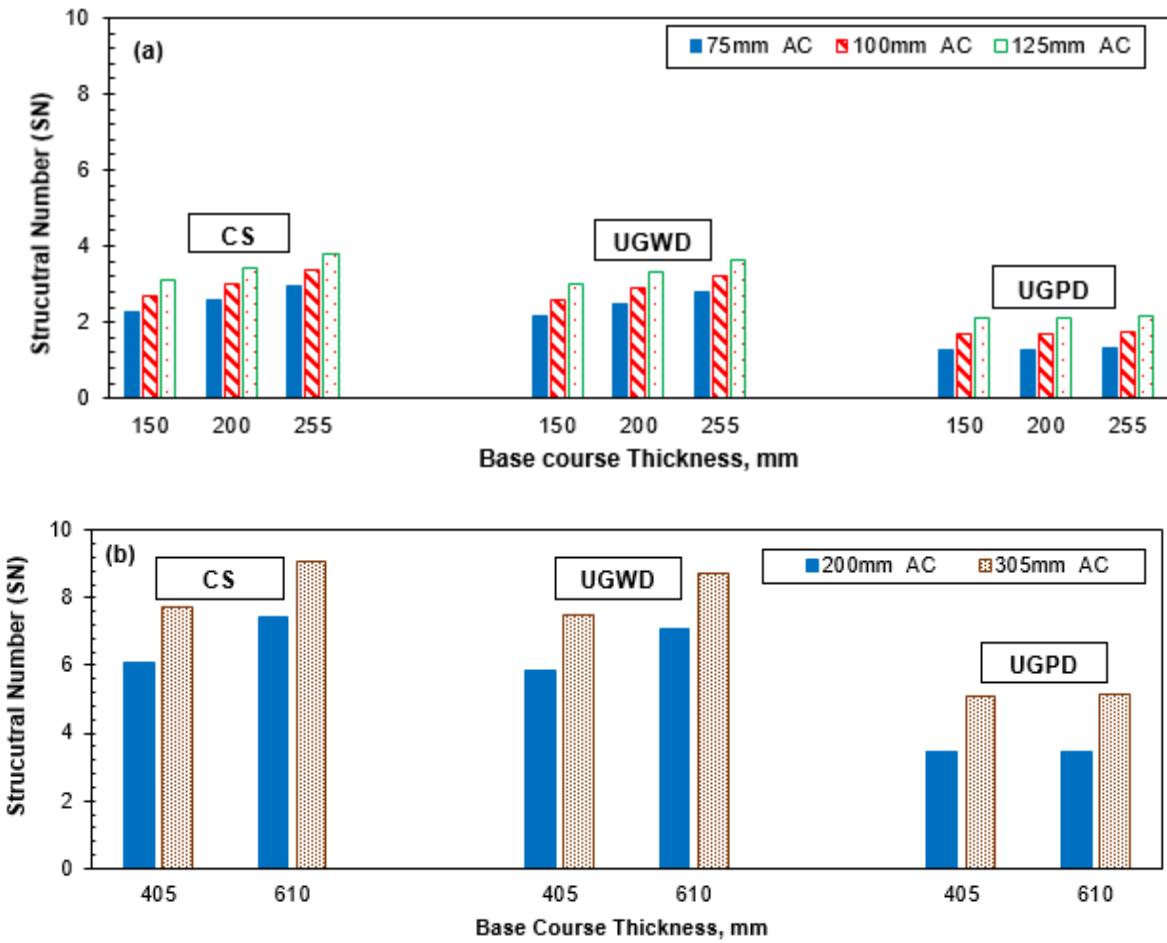


Figure 2.9. Structural number (SN) for (a) Low-volume sections (b) Interstate sections under different base course types

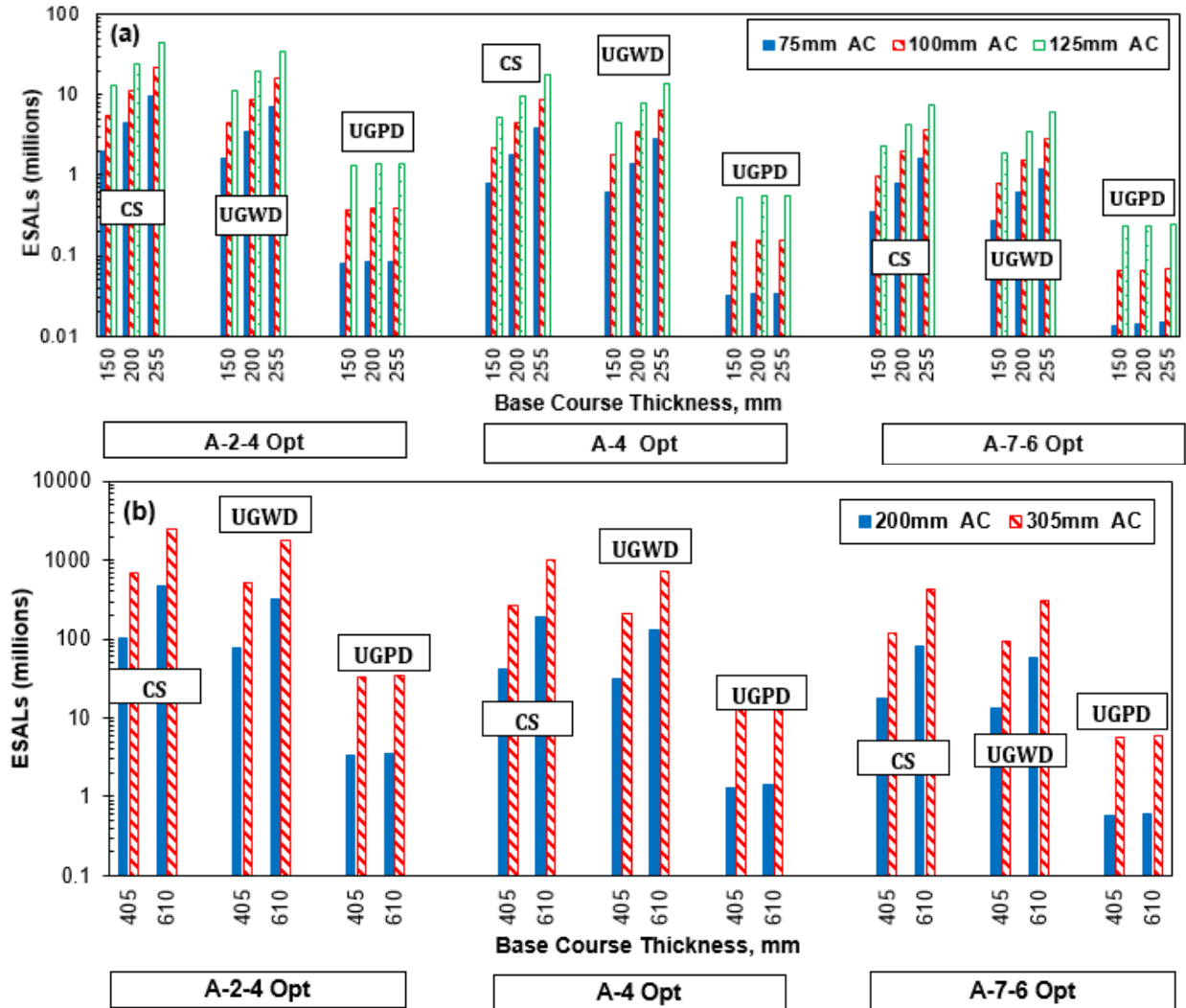


Figure 2.10. Number of ESALs for (a) Low-volume sections (b) Interstate sections under optimum moisture content condition

Figures 2.11a and 2.11b present the ratio between the structural number under the saturated condition (SN_{sat}) to structural number under optimum moisture condition (SN_{opt}) for low-volume and interstate cross-sections, respectively. The results show that the structural capacity needed under fully saturated conditions to withstand the same level of traffic that the pavement is designed for under optimum moisture conditions increased by 30-40 % for low volume sections and 20-30% for interstate sections. The

results also exhibit that the layer thicknesses and base course material types all impact the change in structural capacity of pavements.

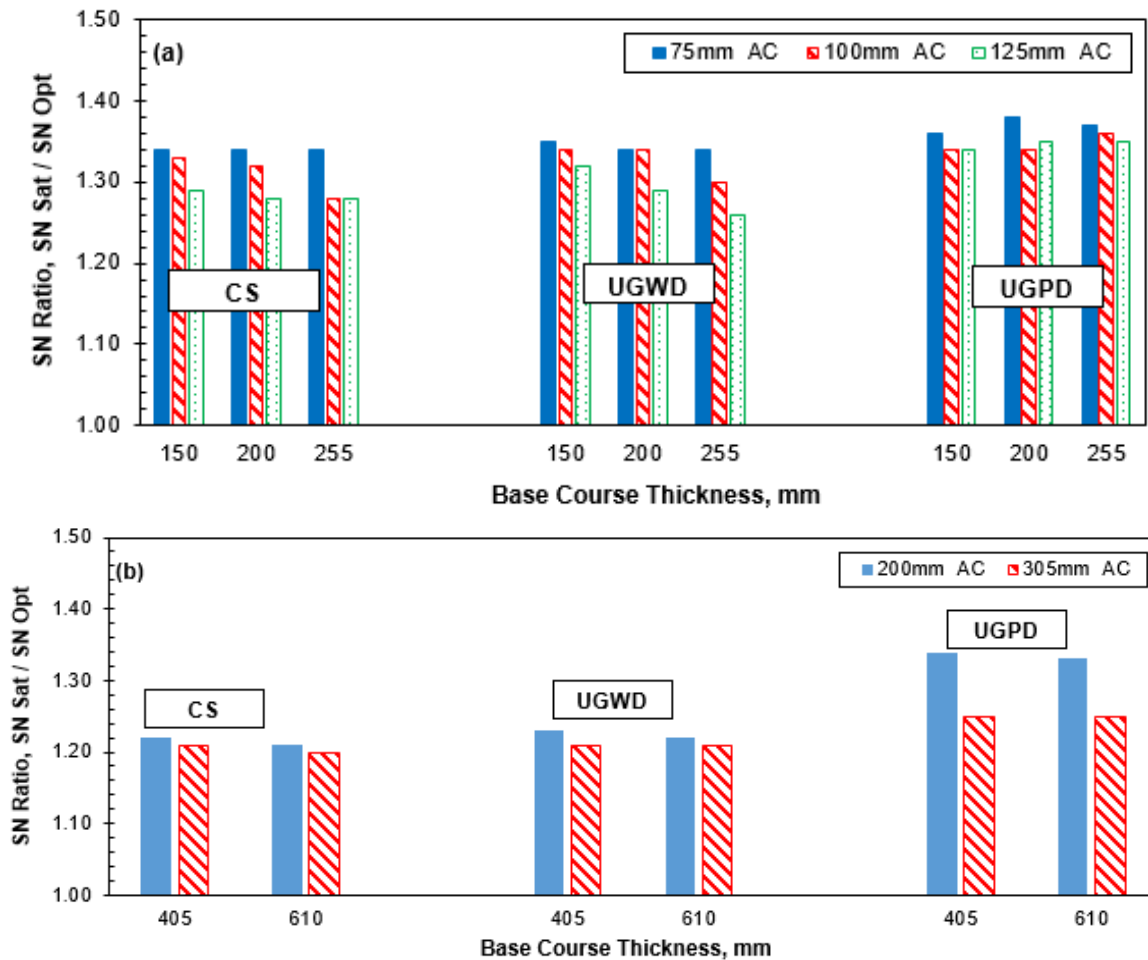


Figure 2.11. Ratio of saturated to optimum moisture condition for the structural Number (SN) for (a) Low volume sections (b) interstate sections under different base course types

The ratio of the subgrade resilient modulus at various moisture contents to the subgrade resilient modulus at optimum moisture content is related to the change in the number of ESALs as shown in Figure 2.12. This relationship holds for any cross section and shows the percent of load reductions if the resilient modulus of subgrade layer has changed due to changing moisture conditions in order to attain the same structural capacity that the pavement is designed for under optimum moisture conditions. In other

words, to minimize the deterioration that will occur due to changing in the moisture conditions.

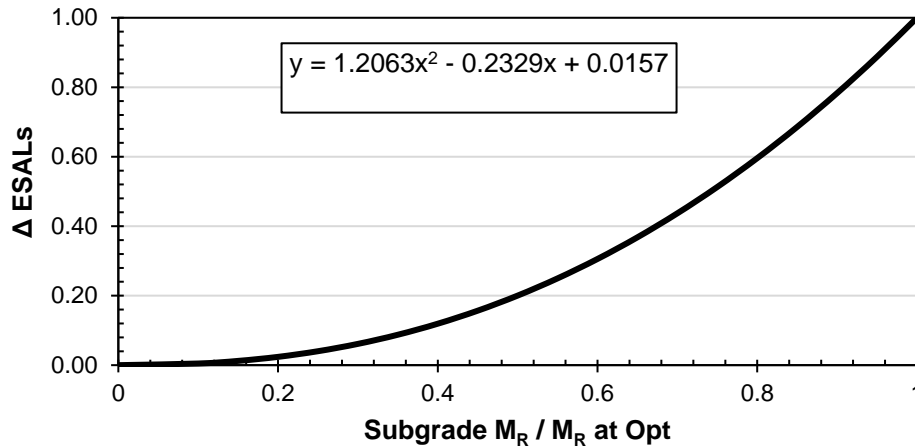


Figure 2.12. Change in ESALs versus change in subgrade resilient modulus

Figures 2.13a and 2.13b show the ratio of the modified structural number (SNC) for optimum and saturated moisture conditions for low volume and interstate cross sections respectively. The results show that there is a significant impact from all parameters on the modified structural number values for low volume and interstate cross sections. The SNC ratio shows that there is a significant impact from base and subgrade type while there is a slight impact from AC and base thickness. A 10-40% reduction of the structural capacity for low volume roads and 6-22% reduction for interstate cross sections are observed due to the saturated condition.

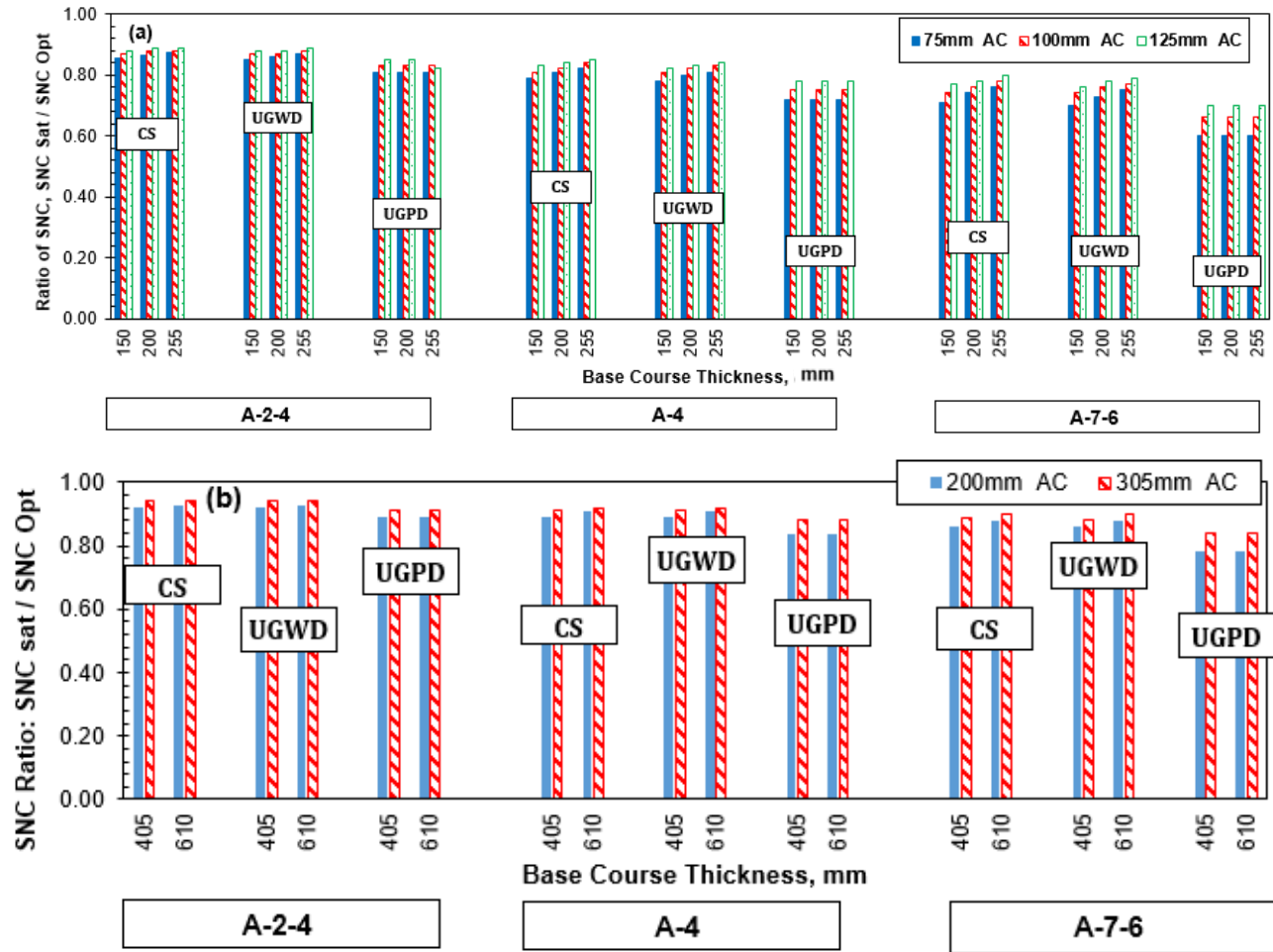


Figure 2.13. Ratio of saturated to optimum moisture condition for the modified structural Number (SNC) for (a) Low volume sections (b) interstate sections under different base course types

The ratio between the second modified structural number (MSN) under saturated conditions to modified structural number under optimum moisture conditions are shown in Figures 2.14a and 2.14b for low-volume road and interstate cross-sections, respectively. The saturated conditions reduce the structural capacity of the pavement by 35 to 73% for the low-volume road and 28 to 61% for the interstate section. The largest percentage of change are for A-7-6 subgrade type. The base course and subgrade type have the largest

impact on the ratios. The asphalt and base course thicknesses do not have a large impact on the ratio due to saturated conditions.

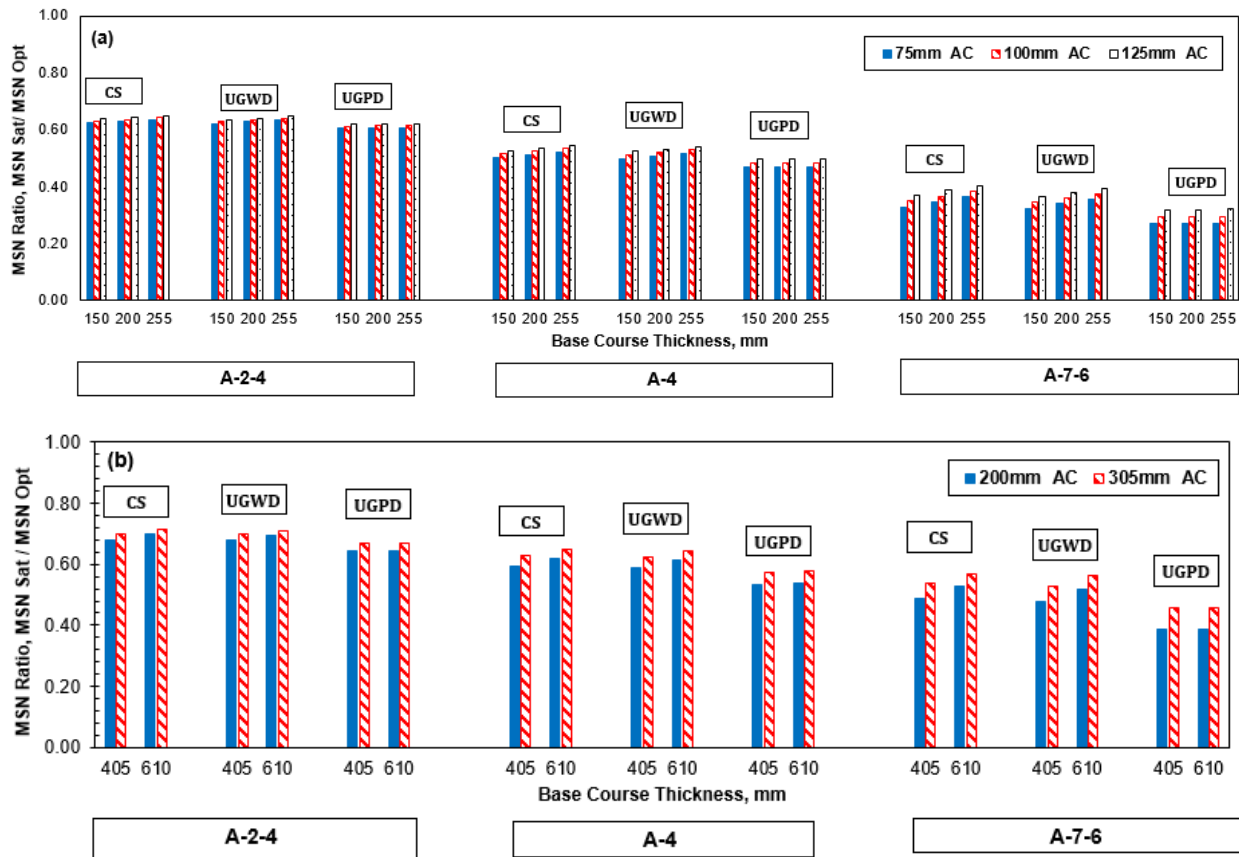


Figure 2.14. Ratio of saturated to optimum moisture condition for Modified Structural Number (MSN) for (a) Low volume sections (b) interstate sections under different base course types

2.4 SUMMARY AND CONCLUSIONS

Assessing the load carrying capacity of a pavement structure that has been inundated is difficult due to the combination of different parameters such as moisture content, material types, layer thickness, interlayer bond condition, and expected traffic loads on the pavement response. The values of these parameters are not always known, or easily measurable, during a flooding event. This study investigated the sensitivity of the

pavement response to variations in these parameters to determine which parameters have the largest impact on the change in expected pavement response under saturated conditions, and therefore, where time and resources should be dedicated to determining more accurate values of these parameters. Two approaches were used to evaluate the structural performance and capacity of inundated pavements; mechanistic approach using layer elastic analysis and AASHTO empirical approach. A series of pavement cross-sections that incorporate a typical range of material types and thicknesses that could be encountered in the field were evaluated.

The results from the mechanistic approach showed that saturated conditions have a larger impact on the vertical strain at the top of the subgrade layer (15 to 80% increases in vertical strains for low volume and interstate sections) of the pavements than the horizontal strain at the bottom of the asphalt layer (increase of 6 to 15% for low volume sections and 3 to 8% for interstate sections in horizontal strain). The type of base course and subgrade had the most influence on the change in vertical strain and therefore would be the important parameters to identify for assessment of a flooded pavement with respect to rutting. For fatigue performance (related to horizontal strain), the ratios were most sensitive to interlayer bond conditions and base course thickness for low volume roads and asphalt and base layer thicknesses and interlayer bond conditions for interstate sections. The type of loading has only a significant impact on the horizontal strain ratios.

The results from the AASHTO empirical approach exhibited that the percent of change in the structural capacity of pavements due to saturated conditions was based on the type of pavement cross section. The SN required under fully saturated conditions to withstand the same level of traffic that the pavements is designed for under optimum moisture conditions increased by 30-40% for low volume sections and 20-30% for interstate

sections. The modified structural capacity (expressed as SNC) reduced by 10-40% for low volume sections and 6-22% for interstate sections due to saturation conditions. Finally, the reduction of the structural capacity (expressed as MSN) were found to be 35-73% for low volume sections and 28-61% for interstate sections due to saturation conditions. For the latter modified SN approaches, the SNC and MSN show the percent of reduction under fully saturated conditions due to the contribution of the subgrade soil.

This study was limited by estimating the structural capacity of inundated pavements for three soils types; non-plastic and plastic (A-2-4, A-4, and A-7-6). Further studies are needed to investigate other pavement structures with different soil types from different locations. Despite this limitation, the use of this information can be adapted to develop a more comprehensive engineering-based approach for agencies to assist engineers throughout the assessment of flooded pavements.

2.5 ACKNOWLEDGEMENT

The author would like to thank the Federal Highway Administration for acting as a project sponsor. Thanks, are also extended to the coauthor of this work: Dr. Jo Sias Daniel of University of New Hampshire. The author also thanks Dr. Rajib Malick of Worcester Polytechnic Institute, Dr. Leslie McCarthy of Villanova University, Dr. Eshan Dave and Dr. Majid Ghayoomi, both of University of New Hampshire for their feedback.

CHAPTER 3

METHODOLOGY TO EVALUATE PERFORMANCE OF PAVEMENT STRUCTURE USING SOIL MOISTURE PROFILE

3.1 INTRODUCTION

Parameters such as traffic loading, pavement materials, and environmental conditions impact the structural capacity and deformation behavior of pavements and, therefore, influence their long-term performance. The typical pavement structure is comprised of unbound and bound materials placed on a subgrade layer to support and distribute the traffic loads. The subgrade layer is required to provide adequate support in order to retard permanent deformation, increase the bearing capacity, and enhance the serviceability. Environmental factors that can vary seasonally play a critical role in pavement performance where temperature affects the behavior of asphalt material and moisture content affects the soil behavior in unbound and subgrade layers. Moisture content has been shown to influence the stress state in the soil and consequently the moduli of the unbound pavement material. For example, increasing the moisture content results in a reduction in soil material moduli (Seed et al. 1962, Hicks and Monismith 1971, Rada and Witczak 1981, Lary and Mahoney 1984, Carmichael and Stewart 1985, Nouredin 1994, Richter 2006). It is believed that the deformation that a traffic load would induce is a function of soil type, porosity of the material, and the rate of loading. Therefore, the deformation is at its maximum when the subgrade layer is fully saturated as the soil layer loses its stiffness gradually when the water table rises (Ovik et al. 2000). On the other hand, the rate of loading plays a significant role in controlling the strength of fully

saturated fine grain soil where the pore pressure increases with rapid loading. Thus, fluctuation of moisture in the soil can impact the performance of pavement systems leading to excessive deformations and failures. To this end, developing a simple and precise, yet conservative method to estimate the moisture-dependent pavement deformation would be valuable in pavement engineering.

In situ testing is used to evaluate the capacity of a pavement structure. For instance, Falling Weight Deflectometer (FWD) is a field test to measure the deflection in pavement surface under dynamic loading. The measured deflection basin is then employed to evaluate the bearing capacity and structural condition of pavements. The Long Term Pavement Performance (LTPP) program conducted the Seasonal Monitoring Program (SMP) to study the environmental impacts on pavement performance. The SMP study is designed to measure the impact of changes of daily and annual temperature, moisture content, and frost/thaw on pavement structure and monitor the pavement response at sixty-four sites (Elkins et al. 2003). The continuous pavement behavioral response obtained from LTPP data can be used to interpret moisture-pavement interaction mechanisms.

Layered elastic models are widely accepted and implemented for predicting stress, strain, and deflection in the pavements by knowing the characteristics of pavement layers such as stiffness, thickness, Poisson's ratio, and magnitude of loading. This type of analysis can be employed to examine the sensitivity of the pavement performance to each of the contributing factors or to calibrate the material properties or constitutive models using the field data such as that from FWD. In order to evaluate the pavement performance and then compare it with FWD data, input parameters such as subgrade resilient modulus must be estimated and input to the predictive tools like layer elastic

analysis. Since the modulus varies as the soil moisture content changes in depth, selection of the representative modulus is a challenging task. Different approaches can be implemented to incorporate spatial variability of moisture content and its effects on the resilient modulus of saturated and unsaturated subgrade soil and propose an “effective” or “equivalent” resilient modulus for the subgrade layer.

This paper combines the seasonal, in-depth data from Long Term Pavement Performance - Seasonal Monitoring Program (LTPP-SMP) sections and the layer elastic analysis to investigate different approaches to incorporate resilient modulus of subgrade soil layers with variable moisture content in pavement performance evaluation. Specifically, pavement characteristics, moisture content profiles with depth, and bedrock and water table elevations were synthesized and inserted into the layer elastic analysis to predict the pavement deflection under loads similar to the FWD test. Different strategies were evaluated for the choice of the depth up to which the moisture content influences the response. This process was repeated for seasonally variable moisture content profiles and two sites with different subgrade soils, and the predictions were compared and verified with measured FWD deflections obtained from LTPP data.

3.2 BACKGROUND

3.2.1 Resilience Modulus Models for Unsaturated Subgrade Soils

Resilient modulus is an important soil characteristic that plays a critical role in pavement performance and has been shown to be affected by changes in moisture content (Richter, 2006). The stress state of the soil can significantly change due to the variation of moisture content of the soil. The change in stress state in unsaturated soil where the soil layer is above the groundwater table is generally expressed as matric suction, which is defined as the pressure difference between pore air and pore water pressures in the soil

matrix. Therefore, matric suction is adopted as an independent stress state variable and considered in dealing with the mechanical behavior of unsaturated soil. The Soil Water Characteristic Curve (SWCC) defines the relationship between the soil suction and water content or the degree of saturation. The more common SWCC model implemented in the pavement community was proposed by Fredlund and Xing 1994 (NCHRP, 2004). It is well known that the effects of soil type and plasticity on matric suction are substantial where fine grained soils can retain water to higher matric suctions than coarse grained soils. Previous studies investigated the effect of changes of moisture content and suction on the resilience modulus of subgrade soils using both laboratory and field testing (Sauer and Monismith 1968, Edris and Lytton 1976, Fredlund and Morgenstern 1977, Noureldin 1994, Drumm et al. 1997, Ceratti et al. 2004, Yang et al. 2008, Khoury and Khoury 2009, Sawangsuriya et al. 2009, Khoury et al. 2010, Cary and Zapata 2010, Han and Vanapalli 2015). As a result, several empirical models have been developed to predict the resilient modulus of subgrade soils in various moisture conditions and stress states (Witczak et al. 2000, Khoury and Zaman 2004, Yang et al. 2005, Liang et al. 2008, Cary and Zapata 2010 and 2011, Sivakumar et al. 2013). Findings from these studies have shown a significant influence of moisture content and matric suction on the resilient modulus of unsaturated soils especially in fine grain soils, where the modulus increases by desaturating the soil.

Traditionally, empirical resilient modulus Equations could only capture the effect of stress state (Seed et al. 1967, Moossazadeh and Witczak 1981, Witczak and Uzan 1988). For example, in the Mechanistic-Empirical Pavement Design Guide (MEPDG), resilient modulus of subgrade soil is predicted using a model similar to the universal model developed by Uzan (1992) as shown in the following Equation:

$$M_R = K_1 P_a \left(\frac{\theta}{P_a} \right)^{K_2} \left(\frac{\tau_{oct}}{P_a} + 1 \right)^{K_3} \quad (3.1)$$

where θ = bulk stress, τ_{oct} = octahedral shear stress, P_a = atmospheric pressure and K_1 , K_2 , and K_3 are regression constants.

Witczak et al. (2000) proposed a generalized model to include the variation of the degree of saturation in the modulus of unbound materials that illustrated a general agreement with the behavior of unsaturated soils (NCHRP, 2000). This model, which is also the state of the practice in the M-E Design Guide, presented in Equation 3.2, is widely accepted by the pavement community for the purpose of moisture-dependent pavement analysis.

$$\log \frac{M_R}{M_{Ropt}} = a + \frac{b-a}{1 + \exp \left[\ln \frac{-b}{a} + k_m (S - S_{opt}) \right]} \quad (3.2)$$

where M_R/M_{Ropt} = resilient modulus ratio; M_R = resilient modulus at any degree of saturation; M_{Ropt} = resilient modulus at a reference condition; a = minimum of $\log M_R/M_{Ropt}$, b = maximum of $\log M_R/M_{Ropt}$; k_m = regression parameter; and $S - S_{opt}$ = variation in degree of saturation expressed in decimals. The model is designed to provide reliable M_R predictions at high moisture contents up to the fully saturated condition.

Over the past decade, more complex and inclusive relations have been proposed to incorporate the environmental variation and matric suction as a stress state variable (e.g. Khoury et al. 2010, Cary and Zapata 2010 and 2011, Han and Vanapalli 2015, Khosravifar et al. 2015, Khoury 2016). Cary and Zapata 2011 proposed an enhanced resilient modulus model that accounts for seasonal environmental variations by incorporating matric suction as a stress state variable (presented in Equation 3.3) instead of using a resilient modulus adjustment factor determined from the degree of saturation as in Equation 3.2.

$$M_R = K_1 P_a \left[\frac{\theta_{net} - 3\Delta u_w sat}{P_a} \right]^{K_2} \left[\frac{\tau_{oct}}{P_a} + 1 \right]^{K_3} \left[\frac{\psi_{m0} - \Delta \psi_m}{P_a} + 1 \right]^{K_4} \quad (3.3)$$

where K_{1-4} = regression constants, p_a = atmospheric pressure, θ_{net} = net bulk stress ($\theta - 3u_a$), $\theta = \sigma_1 + \sigma_2 + \sigma_3$, τ_{oct} = octahedral shear stress, u_a = pore air pressure, $\Delta u_{w \text{ sat}}$ = pore water pressure buildup under a saturated condition ($\psi_m = 0$), ψ_{m0} = initial matric soil suction, and $\Delta\psi_m$ = relative change in soil matric suction with respect to ψ_{m0} caused by pore water pressure buildup under an unsaturated condition ($\Delta u_{w \text{ sat}} = 0$). Combining the stress state and environmental variation in one model as in Equation 3.3 requires more input parameters that may not be easily available from field measurements such as LTPP data. Thus, application of simple and yet approximately accurate relations such as Equation 3.2 remains attractive to the pavement engineering community.

3.2.2 In Situ Pavement Response Evaluation

Non-Destructive Testing (NDT) methods have been shown to be effective in assessing the performance of pavement structures (Goel et al. 2008). The results of NDT are normally used to determine proper maintenance and rehabilitation strategies for a road (Li, 2004). Falling Weight Deflectometer (FWD) is a common NDT system to monitor the structural integrity of pavements by measuring the deflection of the pavement surface. These deflections are registered by seven to nine transducer sensors (geophones) installed at -305, 0, 203, 305, 457, 610, 914, and 1524 mm away from the center of the loading plate. Then 16 drops are applied at each FWD testing point with different loads (Von Quintus and Simpson, 2002).

The pavement surface deflection data is the primary tool in assessing the bearing capacity of the pavement. The magnitude and shape of the pavement deflection is a function of traffic load, pavement structure, temperature, and moisture (pavement interactive, 2010). The magnitude of the load, pulse shape and duration, and the type of NDT device are very influential, so when the deflection is measured, it is important to

simulate the right design load (Li, 2004). The shape of the deflection basin provides a detailed description of the response of the pavement structure. Fundamentally, the basin shape close to the loading plate represents the stiffness of the near surface layers while the furthest deflections reflect the stiffness of the subgrade layer (Tonkin et al. 1998). Maximum deflection (Do) gives an indication of all structural layers with about 70% contribution from the subgrade (Horak et al. 1989).

3.2.3 Long Term Pavement Performance (LTPP) Program

The Federal Highway Administration (FHWA) LTPP team launched the Seasonal Monitoring Program (SMP) as a part of the LTPP database to study the temporal variation in material properties and pavement response due to the environmental effects such as temperature and moisture content. Environmental factors such as temperature and moisture content can have a significant impact on the pavement surface deflection under the loading. Time Domain Reflectometry (TDR) probes are commonly used to measure soil moisture content at multiple depths without disturbing the soil profile (Topp et al. 1980). TDR probes determine the soil moisture content by measuring its apparent dielectric constant (Hanek et al. 2001).

The LTPP-Seasonal Monitoring Program (SMP) installed sensors in 64 sections to evaluate the environmental status of pavement. Ten TDR probe sensors were placed in one hole located in the outer wheel path to measure the water content of granular layer material and subgrade layer at depths up to 1.90 m from pavement surface throughout the study periods (Zollinger et al. 2008). Figure 3.1 provides a schematic of the instrumentation in the sites. Common LTPP data and the corresponding instrumentation that were also used in this study are presented in Table 3.1.

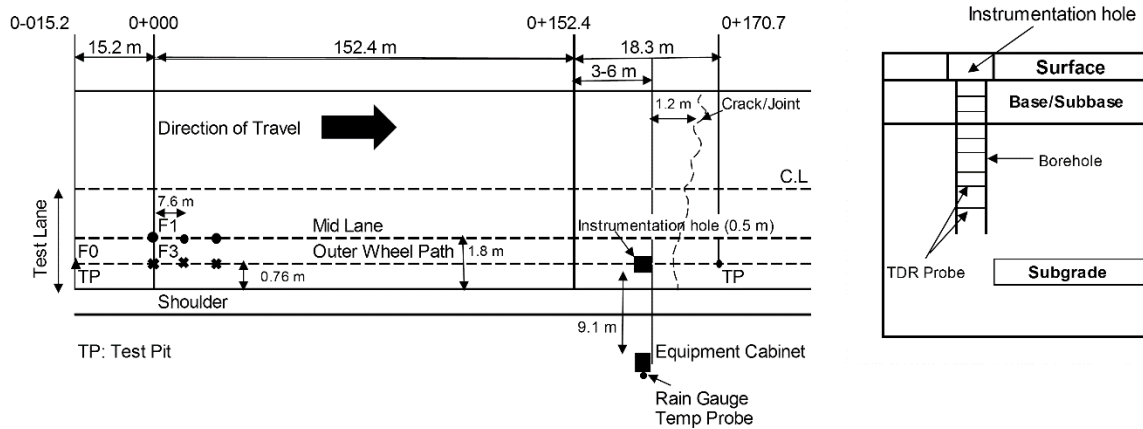


Figure 3.1. Illustration of instrumentation installation. (after Zollinger et al. 2008)

Table 3.1. Employed LTPP data

| Instruments | Measurement |
|------------------------------------|--|
| FWD (Falling Weight Deflectometer) | Deflection basin |
| Thermistor Sensor | Pavement temperature and air temperature |
| TDR (Time Domain Reflectometer) | Moisture content of subsurface |
| Piezometer | Depth the ground water table |

3.2.4 Layered Elastic Analysis (LEA) of Pavements

Layer elastic analysis is a mechanistic model that mathematically simulates pavement response. The origin of layered elastic theory is credited to V.J. Boussinesq in 1885. In a typical layered elastic analysis, the system is divided into an arbitrary number of horizontal layers (Vokas et al. 1985). The thickness of the individual layers and material properties may vary from one layer to another. Each layer is assumed to be homogeneous and linearly elastic with a finite thickness. Circular uniform pressure is applied on the pavement surface and the interface between two adjacent layers are set to have the same response such as deflection, vertical stress, shear stress, and radial displacement. The application of the layered elastic method can be extended to multiple-layer systems (Wang, 2001). Given the material properties of each layer such as modulus of elasticity

and Poisson's ratio, the thickness of different pavement layers, and the loading condition the stresses, strains, and deflections in the pavement depth can be predicted. The critical locations include: the pavement surface for the deflection calculation, the bottom of the asphalt layer to calculate the horizontal tensile strain to predict the fatigue failure in the asphalt layer, the top of the base/subbase layer to calculate vertical compressive strain in order to predict rutting failure in the base/subbase, and the top of the subgrade soil layer to calculate vertical compressive strain in order to predict rutting failure in the subgrade soil. Thus, application of such models will be valuable in predicting the pavement performance given an accurate estimation of material properties.

Truss (2004) showed that flexible pavements can be modeled using BISAR layer elastic analysis program. Predicted FWD behavior at different times during the year for 16 frozen and 6 non-frozen LTPP-SMP sites was used to predict times where overload could be permitted during winter and loads should be restricted during the spring thaw. The subgrade layer was divided into 6 sublayers up to the depth of freeze/thaw for the analysis. Accordingly, the top half of the subgrade was divided into 4 equal layers and the bottom half was divided into 2 equal layers. The modulus of the AC layer was obtained from the relationship developed from the LTPP data between asphalt modulus and pavement surface temperature. Base and subgrade modulus were calculated from back calculated deflection from the measured FWD during the late summer and early fall. Then the modulus was adjusted by multiplying by 2 for the frozen months and 0.5 for the thaw months.

Salour et al. (2015) measured the in-situ moisture contents at different depths including 50, 90, 120 and 150 cm in a Swedish pavement structure. These depths were associated with the subbase layer (the top one) and the subgrade layer (the rest). The FWD test was

performed with multilevel loads at different moisture content and depths by manipulating the drainage system of the road section. The silty sand subgrade layer was divided into a different number of sublayers and the non-linear resilient modulus of unbound material was calculated using the universal model in Equation 3.1 using ERAPave software. Then, the estimated modulus was compared with the moisture-dependent predictive Equation by Cary and Zapata (2010) incorporating matric suction in unsaturated soils. An acceptable correlation was observed between the predicted and FWD-back calculated resilient modulus at different moisture contents, including the fully saturated condition.

In general, previous studies used resilient modulus predictive models for soils (e.g. Cary and Zapata (2010)) as a tool to validate the back calculated resilient modulus from FWD testing at different stress states and moisture contents. In this paper, however, the resilient modulus in the subgrade layer was estimated directly from the measured soil moisture profile to evaluate the performance of the pavement structure independent of FWD test results. The proposed approach will lead to a good understanding of the pavement performance in various moisture conditions and potentially provide a cost-effective predictive tool once the method is calibrated and verified.

3.3 PROCEDURES

3.3.1 LTPP Sites Selection

Two flexible pavement sections from two different climate zones; one from Minnesota and the other from Oklahoma, shown in Figure 3.2, were selected for this study. The pavement structure and material physical properties for the two sections are presented in Table 3.2.



Figure 3.2. Map location of the LTPP selected sites.

Table 3.2. Selected LTPP Sites and Subgrade Soil Characterizations

| LTPP Sites | 1 | 2 |
|--|---------------------------|----------------|
| | 27-1018 | 40-4165 |
| Location | Minnesota (MN) | Oklahoma (OK) |
| Surface type | AC (112 mm) | AC (69 mm) |
| Base Layer properties | | |
| Base material type | Uncrushed Gravel (132 mm) | *HMAC (140 mm) |
| AASHTO Classification | A-1-b | - |
| Optimum Moisture % | 7 | - |
| In situ Dry Density (kg/m ³) | 2030 | - |
| Specific Gravity (Gs) | 2.713 | - |
| Void Ratio (e) | 0.34 | - |
| Max lab Dry Density (kg/m ³) | 2195 | - |
| Subgrade Layer properties | | |

| LTPP Soil type | Coarse-Grained Soils: Poorly Graded Sand with Silt | Coarse-Grained Soil: Silty Sand |
|---|---|---|
| AASHTO Classification | A-3 | A-2-4 |
| Percent Passing # 200 | 6.2 | 28.2 |
| Plasticity index PI | NP | NP |
| Percent of Coarse Sand | 42 | 8 |
| Percent of Fine Sand | 34 | 64 |
| Percent of Silt | 4.5 | 19.2 |
| Percent of Clay | 1.5 | 9 |
| Optimum Moisture % | 8 | 14 |
| In situ Dry Density (kg/m³) | 1828 | 1345 |
| Specific Gravity (Gs) | 2.65 | 2.65 |
| Void Ratio (e) | 0.45 | 0.97 |
| Max lab Dry Density (kg/m³) | 1970.3 | 1778 |
| Porosity | 0.31 | 0.49 |
| Depth to bedrock | 2.5 m from top of subgrade layer | Infinite |
| Moisture and deflection data year | (1994) 25 April, 13 June, 8 August and 10 October | (1994) 25 July and October 13 (1995) 18 April and 16 May |

***HMAC:** Hot mix asphalt concrete

The LTPP data evaluated at these sites included the FWD deflection measured in the outer wheel path (at last drop of 40 kN load), thickness of pavement layers, gravimetric moisture content of subgrade soil with depth, temperature profile with depth for pavement layers, and the depth to the groundwater table. The depth to bedrock was extracted from the NCHRP 2003 report.

3.3.2 Methodologies to Estimate a Moisture-Dependent Resilient Modulus from Field Data

In order to gain more insight into the behavior of saturated and unsaturated subgrade soil and its role in pavement evaluation, an approach should be developed that considers soil moisture profile with depth. This can be accomplished by relating the depth-dependent stiffness of the subgrade soil with moisture content; four different methods are proposed in the analysis. Level 3 typical values of resilient modulus at optimum moisture content were obtained based on the AASHTO 180 soil classification for unbound materials, which is used in the Enhanced Integrated Climatic Model (EICM) implemented in the MEPDG (MEPDG, 2008). Then, these values were modified for the given moisture content using Equation 3.2 due to the lack of the measured matric suction in the LTPP database. Using the available data from the literature and assuming a maximum modulus ratio of 2.5 for fine-grained materials and 2 for coarse-grained materials, the values of a , b , and k_m for coarse-grained and fine-grained materials are summarized in Table 3.3 (Witczak et al. 2000). For purposes of this study, the degree of saturation at any given moisture content was computed using Equations 3.4 and 3.5.

$$\gamma_d = \frac{G_s}{1+e} \gamma_w \quad (3.4)$$

$$S_r = G_s \frac{w}{e} \quad (3.5)$$

where: S_r = degree of saturation, G_s = specific gravity, w = moisture content, γ_w = unit weight of water, γ_d = dry unit weight, e = void ratio

The type of soil, density, and porosity control the permeability and infiltration rate of the soil. As shown in Table 3.2, the percent of fines for the Oklahoma soil is larger than

that for the Minnesota soil, which resulted in a higher porosity in the Oklahoma soil and, in turn, lowered the resilient modulus.

Table 3.3. Regression parameters of Equation 3.2

| Parameter | Coarse- grain materials | Fine- grain materials |
|-----------|-------------------------|-----------------------|
| a | -0.3123 | -0.5934 |
| b | 0.3 | 0.4 |
| k_m | 6.8157 | 6.1324 |

The four methods for including depth- and moisture-dependent modulus are explained in the following sections and schematically shown in Figure 3.3. Then, according to the layering strategy in each method, the estimated moisture-dependent resilient moduli were input to the layer elastic analysis.

Method A:

In this method, the subgrade layer was divided into several sublayers from the top of the subgrade to the groundwater table based on the TDR location depths. The sublayers were selected so that the TDRs fall in the middle of sublayers. The rest of subgrade layer, i.e. below the water table, was also sub-layered depending on the depth of bedrock. If the depth to the bedrock was shallow; in this case was less than 3 m, then the rest of subgrade was divided into 2 layers; 1 layer from the groundwater table to the bedrock and the bedrock layer itself. If the depth to the bedrock was deep, then the rest of the subgrade layer considered as an infinite layer from the groundwater table below. The layer below the groundwater table was considered fully saturated, ($S_r = 1$). The resilient modulus of each layer was calculated based on Equation 3.2.

Method B:

In this method, the subgrade layer above the water table was considered as one layer. The effective resilient modulus associated with this layer was estimated based on a

weighted average moisture content above the water table measured at TDR locations.

The moisture weight for each TDR measurement was assumed to be equal to the height of the zone of influence between the mid-points of the consecutive TDR locations. The rest of the soil below the groundwater level was treated similarly to method A.

Method C:

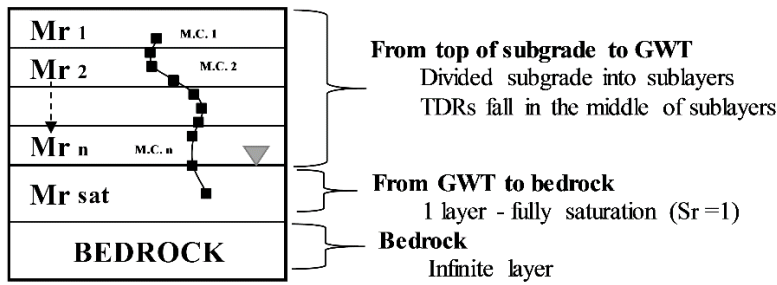
In this method, the subgrade layer, both above and below the water table, was considered as one layer. However, the effective resilient modulus of the subgrade layer soil was calculated based on a weighted average of moisture content measurements above the ground water table. The moisture content weights were determined using the same procedure as in method B.

Method D:

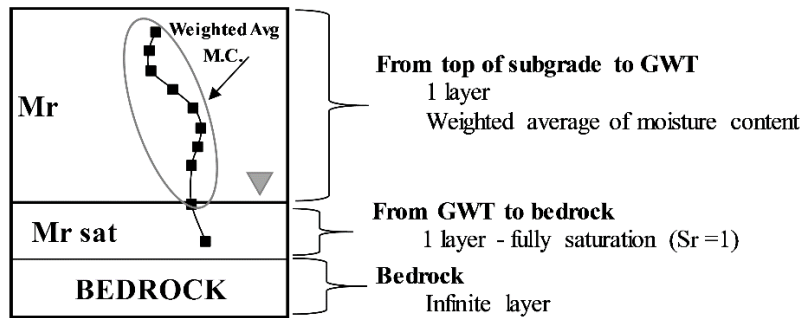
Originated from the theory of elastic stress distribution in an infinite half space (Boussinesq's theory, 1885), an influence zone was defined to project the stresses caused by surface loading of a pavement structure. Thus, approximate vertical stress profiles inside the subgrade soil were estimated for the pavement structure using linear layer elastic analysis KENLAYER software for the most critical condition. The modulus of unbound materials at optimum moisture content was determined from level 3 default values and the minimum value of asphalt modulus was used. The influence zone was defined above the location where the induced stress reduces to at least 10% of the applied surface pressure. This zone was then considered as the representative subgrade layer, for which the resilient modulus was calculated based on a weighted average moisture content. A second layer was considered from that depth to the groundwater table if appropriate. The resilient modulus of this layer was calculated using the lowest moisture content data measured at the above layer. The rest of subgrade layer from the ground

water table to the bedrock was evaluated using the same procedure as in method A and B. If the depth to bedrock is deep, the layer from groundwater table is considered to be an infinite layer in all four methods.

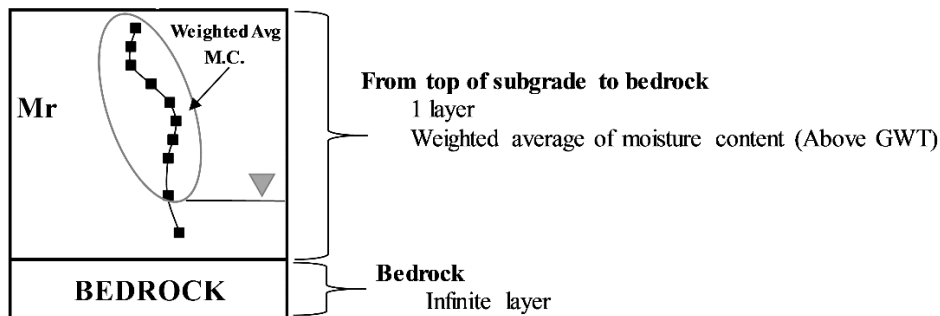
Method A:



Method B:



Method C:



Method D:

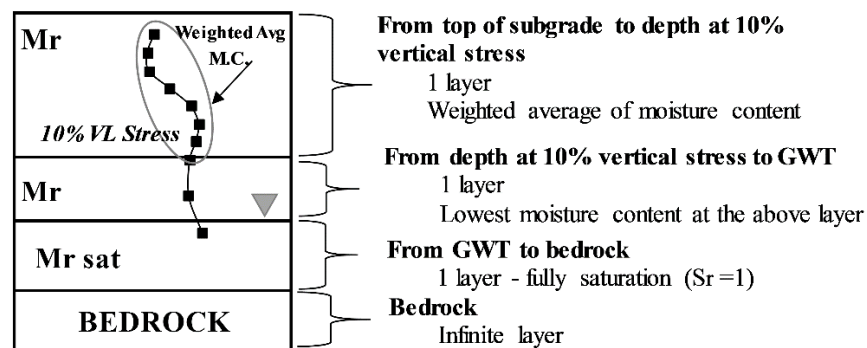


Figure 3.3. Schematic demonstration of the methods used to obtain an equivalent resilient modulus

3.3.3 Asphalt Modulus Correction

The moduli of the asphalt layers varied seasonally with temperature. Thus, the stiffness of the asphalt concrete (E_T) at a specific temperature (T) was corrected according to the following relationship (Erlingsson 2010):

$$E_T = e^{-b \times (T - T_{ref})} \times E_{ref} \quad (3.6)$$

where T_{ref} = reference temperature, T = AC temperature at the time of testing, E_T = back-calculated AC modulus at tested temperature, E_{ref} = reference AC modulus at the reference temperature and b = material constant estimated in Indirect Tensile Test (IDT) stiffness tests carried out at different temperatures equal to 0.065.

In this study, air, surface, and mid-depth asphalt temperature gradient data were measured during FWD testing. The mid-depth asphalt temperature has been chosen simultaneously with the time of measured moisture content and groundwater table to correct the modulus of asphalt layer using Equation 3.6 to be used in the proposed analysis.

3.3.4 Linear Elastic Analysis (LEA) Method

The KENLAYER multi-layer elastic analysis computer program was used to calculate the deflection basin and vertical stress profile. The response analysis by KENLAYER program was conducted using the given FWD load, FWD plate radius, the thickness of all layers, Poisson's ratio of materials and the modulus of all materials. Table 3.4 presents a summary of sources of information for all the input parameters used to predict pavement deflection basins.

Table 3.4. Input parameters and source of information

| Input Parameter | Source of Information |
|--|---|
| FWD data file | |
| Deflection data file at 40 kN load at last drop, air temperatures, surface temperatures and asphalt temperatures | LTPP Sources (standard data release 29) |
| TRAFFIC | |
| FWD Load | 40-kN |
| FWD contact radius of circular loaded | 150.114 mm |
| Type of loading | single axle with single tire |
| points to be analyzed | 0, 203, 305, 457, 610, 914, 1524 mm |
| STRUCTURE | |
| Asphalt Concrete: layer thickness | Cores and historical data (TST_L05B) |
| Asphalt Concrete: AC modulus correction to a reference temperature at the time of testing. | Equation 3.5 AC modulus = 2000 MPa at 20 C (typical modulus values) |
| Base/subbase Layers: layer thickness | Cores and historical data (TST_L05B) |
| Base/subbase Layers: Poisson's ratio, Modulus | Default values and State specifications Witczak model (Equation 3.2) |
| Subgrade Layer: Modulus based on the proposed methods | Witczak model (Equation 3.2) |
| Poisson's ratio | Default values and State specifications |

3.4 RESULTS AND DISCUSSIONS

3.4.1 Interpretation of the Results from the Selected LTPP Sections

Figures 3.4 (a) and (b) show the moisture content profiles with depth and the groundwater table locations on different dates for the Minnesota and Oklahoma sections, respectively. The moisture content variations in these figures indicated that the

groundwater table changes seasonally where it elevated in the spring and dropped in the fall.

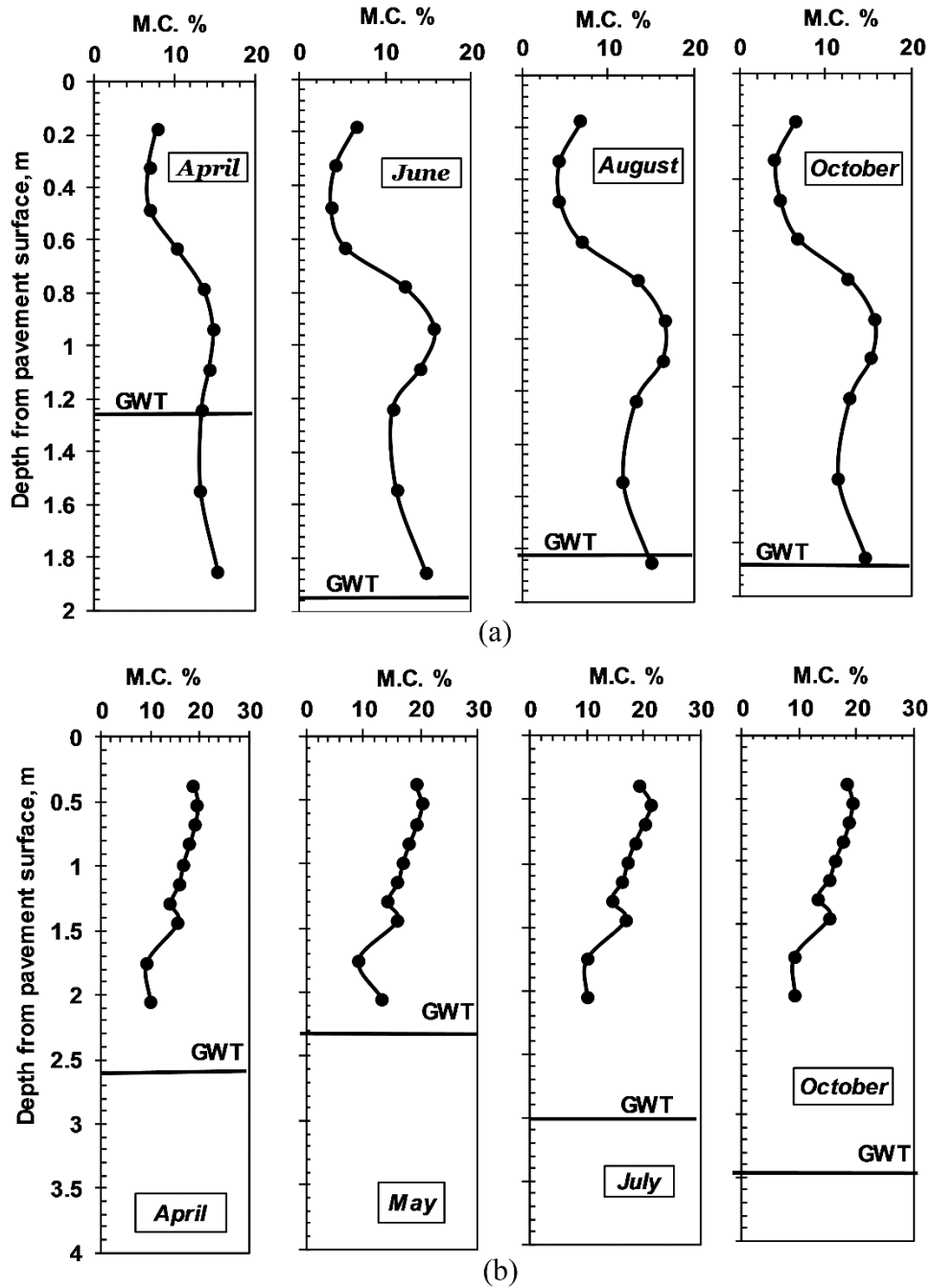


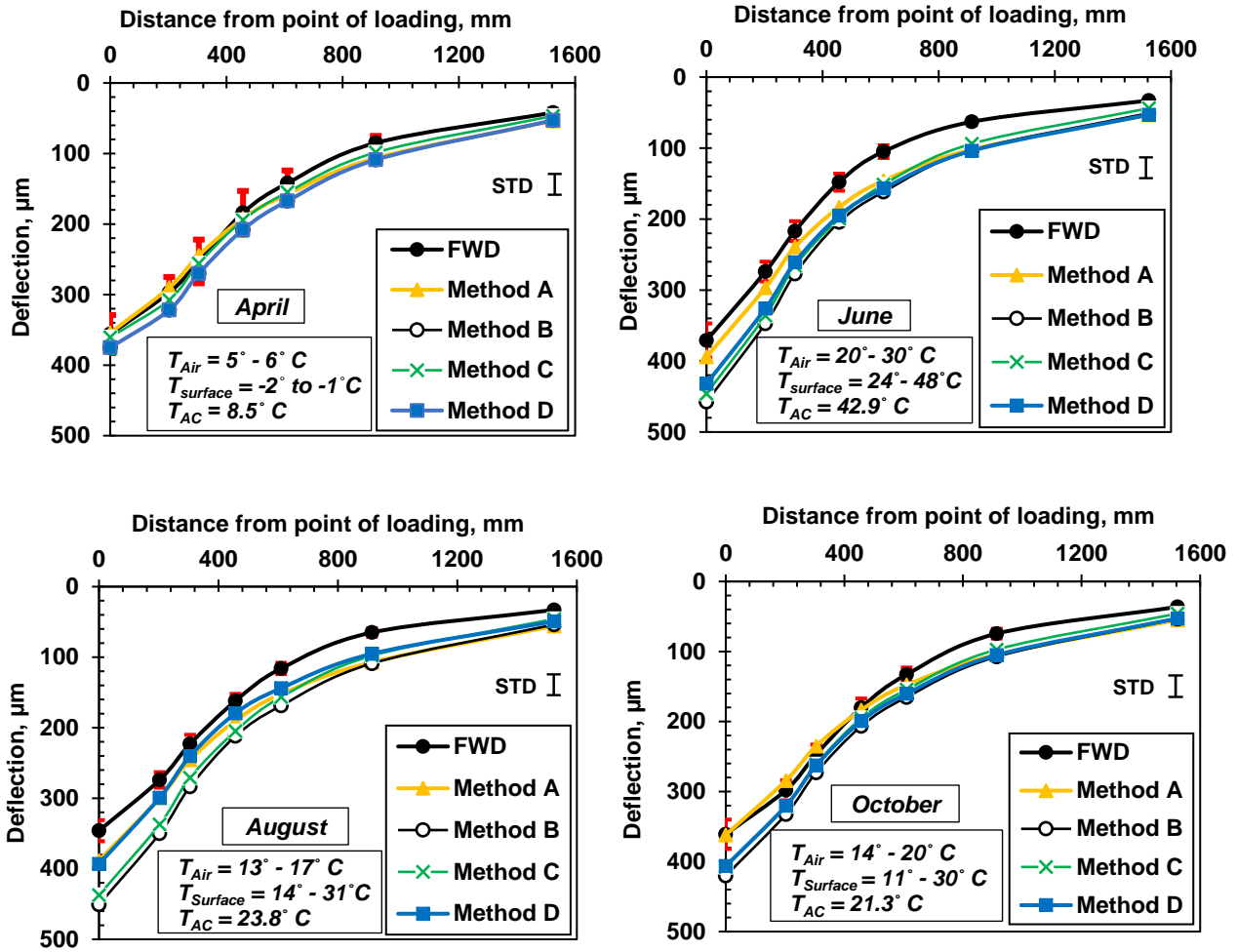
Figure 3.4. Moisture content profiles for (a) Minnesota section; (b) Oklahoma section

Figures 3.5 illustrates the comparison between average measured FWD-based deflections adjusted to 40 kN load with the associated standard deviation and the predicted deflection from LEA using the four methods for the Minnesota sections. Overall, it can be seen that the magnitude and the shape of deflection basins fit reasonably well with the predicted values. However, there are slight differences in magnitude, which could be because of the assumptions that were made in the selection of material properties in the proposed methods.

In this section, the predicted deflection basins for all the proposed methods are very well in agreement with the measured values in April. The similarity between the different methods could be because of the elevated groundwater table due to spring thaw that resulted in the same moisture distribution form in all the proposed methods. Therefore, based on the results in April, all the proposed methods would be good indicators of the FWD deflection during high water table seasons. In the other seasons (i.e. June, August, and October) the predictive methodologies overestimated the actual average deformations consistently among all four methods. This can be considered conservative and practically acceptable with regards to deflection evaluation and mechanical response. However, overly conservative estimates may result in uneconomical actions. The predicted deflection basin using the methods B and C are identical in all the times because ultimately the same moisture content distribution strategy was considered, but with different layer thicknesses. This means that the FWD-based deflection is mostly affected by the top most portion of the subgrade soil, not the lower portion.

Based on the data in Figures 3.4 (a), from April to June, the measured moisture content decreased in the base and subgrade layers as the water receded. Moreover, the measured and predicted FWD deflection basins decreased in all points except the

maximum deflection (D_0). The maximum deflection is expected to decrease as the GWT drops to 1.95m (Figure 3.4a) and the water recedes from the soil surface, but the deflection increased in June. One potential reason could be the significant difference in the temperature from April to June (Figure 3.5) causing the asphalt layer to behave viscoelastically, causing a higher deflection. That signifies the importance of incorporating a multivariable environmental effect. On the other hand, from June to August, the measured moisture content is identical in the base layer while it slightly increased in the subgrade layer. Thus, the measured and predicted FWD deflection basin increased in all points except the furthest point where they are identical, knowing that the furthest point defines the stiffness of the subgrade layer. Further, the measured moisture content is identical in unbound layers from August to October. Therefore, the measured and predicted FWD deflection basins are the same considering the associated standard deviation in all points.



*STD: standard deviation, T_{AC} : temperature at mid-depth asphalt layer

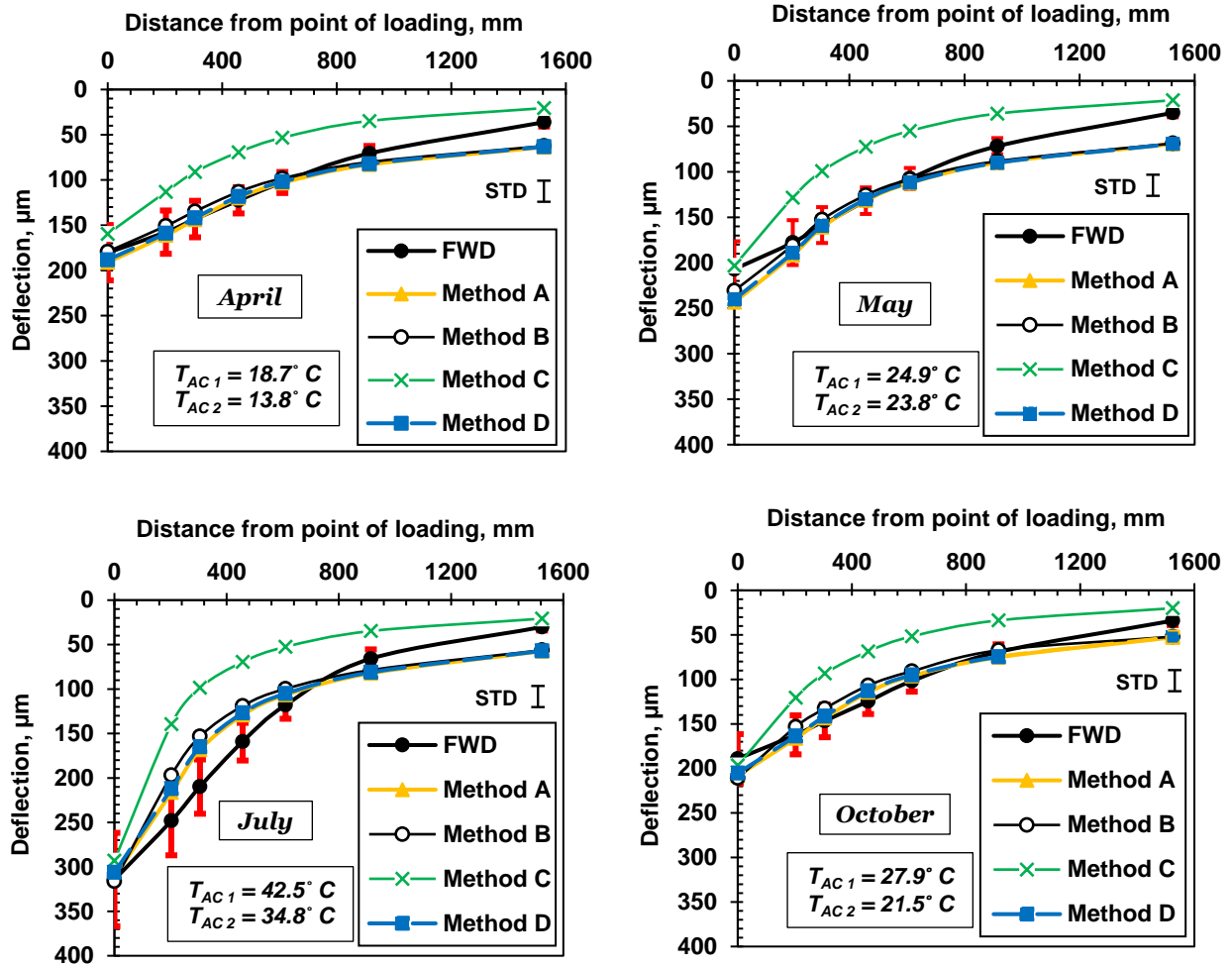
Figure 3.5. Measured and Predicted Deflection Basins for Minnesota Section

Figures 3.6 illustrates the comparison between the average measured FWD-based deflections adjusted to 40 kN load with the associated standard deviation and the predicted deflection from LEA using the four methods for the Oklahoma section. In this section, the magnitude of the measured and predicted deflection basins agreed well for three methods A, B, and D, in all points except the furthest point (D6). The predicted deflection magnitude using method C showed lower values than the FWD measured deflection basin in all points except in maximum deflection (D0) and furthest deflection

(D6) over the three seasons. Overall, the shape of the deflection profile did not always agree with the measured values.

The predicted response using methods A, B, and D all resulted in conservative solutions except in the dry month of July near the loading location. The clear differences between the quality of predictions in this section compared with the Minnesota section could be attributed to the following factors: 1) in this section the depth to the bedrock was very deep, thus, method C might not work the best; however this assumption might be suitable for predicting the maximum deflection (D_0) and furthest deflection (D_6); 2) the base material type was hot mix asphalt; a bound layer that is stiff and prevented the excess water from penetrating underneath; and 3) the soil-water retention selection is very sensitive to this type of subgrade material that may have resulted in a poorer prediction.

In this section, due to the lack of the simultaneous data measurement from the LTPP database in the same year for various seasons, the comparison between FWD measured and predicted deflection basins were examined based on the measurement in four seasons in two different years. The comparison between April and May (1995) indicates that the moisture content increased and the measured and predicted FWD deflection basin increased. On the other hand, the comparison between July and October (1994), showed that the moisture content decreased due to water receding and the measured and predicted FWD deflection basin decreased as well. It can be observed that the moisture content in October 1994 and April 1995 are identical, resulting in the same measured and predicted FWD deflection basins considering the standard deviation. Moreover, when the moisture content increased in the soil, the soil becomes softer until the water recedes, thus the deflection increased, predicting the poor performance of the pavement structure.



*STD: standard deviation, T_{AC1} : temperature at mid-depth asphalt layer 1, T_{AC2} : temperature at mid-depth asphalt layer 2

Figure 3.6. Measured and Predicted Deflection Basins for Oklahoma Section

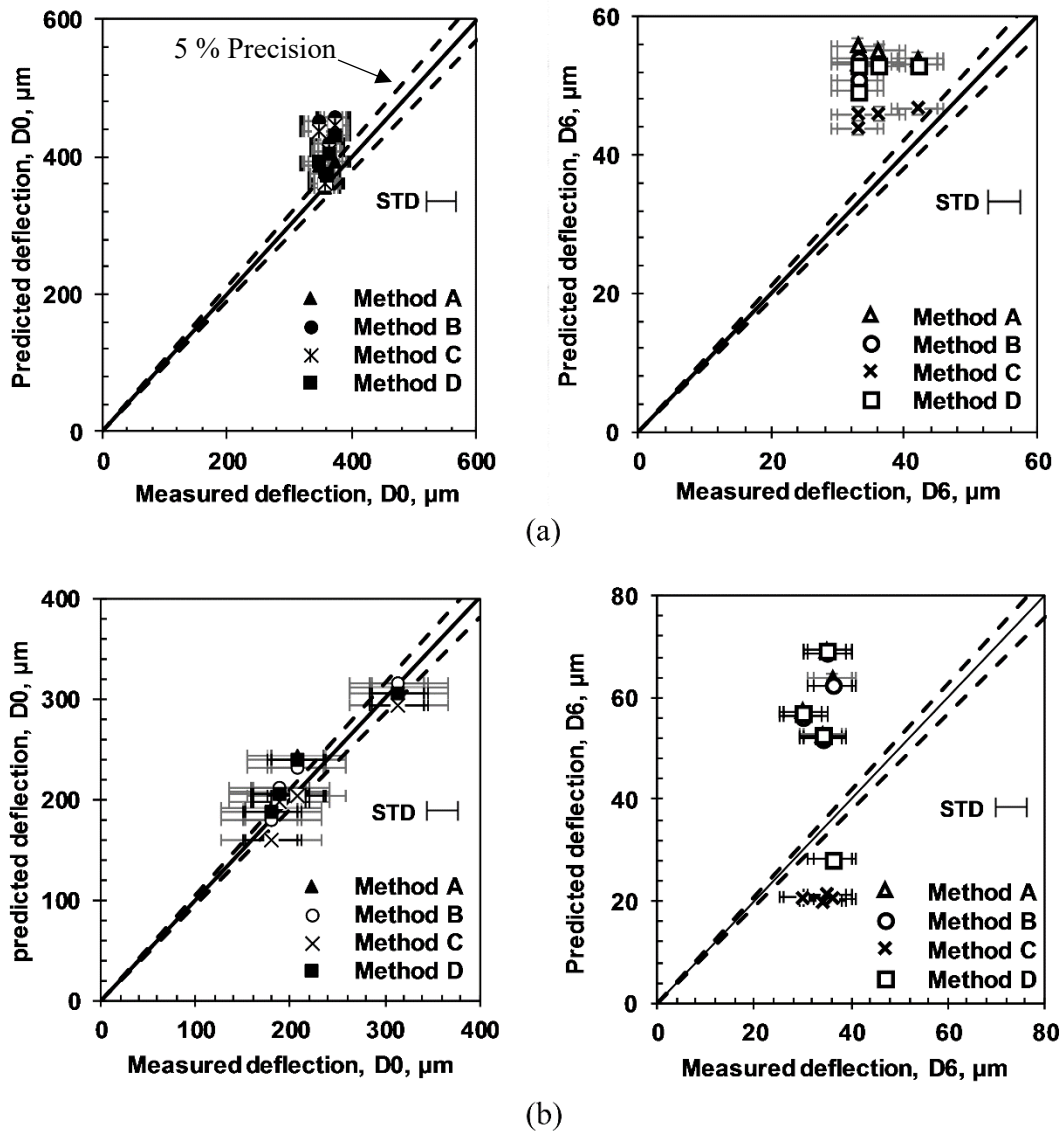
Based on the above analyses, it is concluded that the method of dividing subgrade into sublayers to the groundwater table (Method A) is the most appropriate method of predicting the FWD deflection basin for all seasons. Incorporating the stiffness of each sublayer individually into analysis with respect to the moisture content is closer to reality in a linear elastic analysis framework. Using the moisture profile up to a depth of 10 % vertical stress from subgrade surface (Method D) is the next most appropriate method based on this analysis. This is because the stress below that depth minimally influenced

the overall stiffness of pavement structure. Application of Method D instead of Method A in practice may reduce the instrumentation and consequently the cost of LTPP database program. However, if the base layer is a bound layer and the bedrock is infinite, all the proposed methods work the same way except the method of considering subgrade as one infinite layer (Method C).

Witczak et al. (2000) performed a study to adjust the resilient modulus of unbound materials in Equation 3.2 for frozen and thaw periods. The authors recommended that the least of the resilient modulus at optimum moisture content or the resilient modulus at any degree of saturation would be used to estimate the resilient modulus after thawing by conducting the resilient modulus reduction factor (RF) as a function of soil index (Janoo et al. 1997). Then, the authors suggested using the adjusted resilient modulus to compute a recovery ratio (RR) from soil moisture suction to compute the resilient modulus during the recovery period. Considering the reduction factor for the thaw period, the resilient modulus would become up to 50% less than the predicted resilient modulus. Due to this degradation in the resilient modulus for thawing period and knowing that the resilient modulus implemented into layer elastic analysis set in this paper resulted in a conservative prediction of the deflection basins, reduction factors can be ignored for these two sections.

Maximum and furthest predicted deflection based on the four methods are compared with the field average measured including the associated standard deviation in Figures 3.7 (a) and (b), for all seasons in the Minnesota and Oklahoma sections, respectively. The dashed line is at 5% precision between the predicted and measured deflection according to FHWA. It can be seen that the proposed methods give a relatively good prediction of the deflections due to changes of moisture content. The predicted deflections using the

proposed methods are conservative, which could be due to the application of the minimum value of modulus for asphalt concrete layer. Although the measured moisture contents were 6 m away from the end on the test sections, they appropriately predicted the behavior of pavement structure by using the proposed methods.



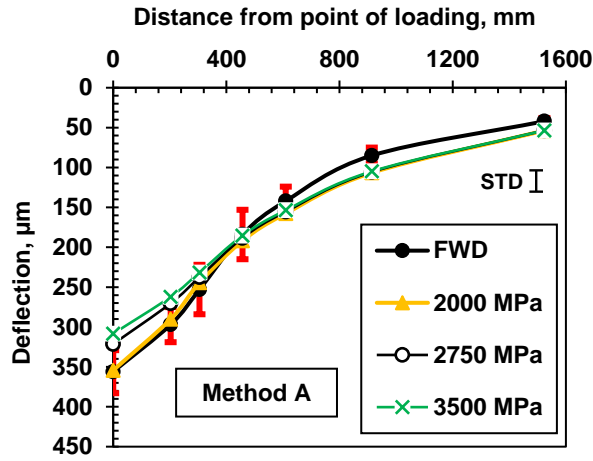
*STD: standard deviation

Figure 3.7. Measured and Predicted D0 and D6 Deflections for All Seasons at (a) Minnesota Section; (b) Oklahoma Section

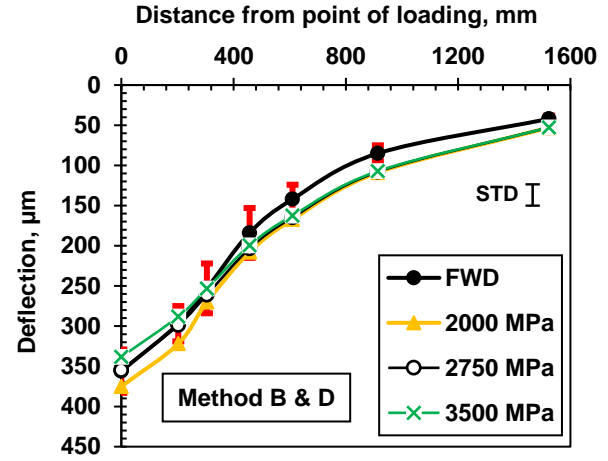
3.4.2 Effect of Asphalt Concrete Modulus on the Deflection Prediction

A sensitivity analysis was performed on the data recorded at the Minnesota section (27-1018) on April 25th, 1994 to study the impact of asphalt concrete initial material properties on the deflection prediction using the four different methods. This sensitivity analysis included different modulus values of the asphalt concrete layer (2000-3500 MPa) at 20°C, corrected to the reference temperature at the time of testing using Equation 3.5. The values of modulus of pavement materials were chosen according to the MEPDG.

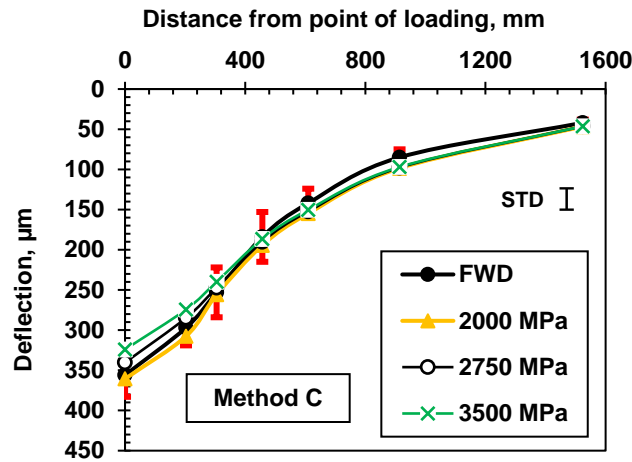
The vertical stress results showed that the depth to 10% vertical stress from subgrade surface at this date and section was the same depth from the top of subgrade layer to the groundwater table. Thus, these methods D and B would be identical. Figures 3.8 (a)-(c) show the comparison between the average FWD-measured deflection basin adjusted to 40 kN with the standard deviation and the predicted deflection basin from LEA using different AC modulus and different methods. The results indicated that the overall shape of the deflection basin is in agreement with the predicted deflection basin. Using Methods B and D resulted in relatively close, yet conservative prediction of deflection regardless of the choice of the asphalt modulus. Application of Method A and C may result in lower deflection, especially at the maximum deflection point (D_0). However, they mostly fit in the experimental standard deviation range. Overall, selecting 2000 MPa for AC modulus would be the most appropriate as it resulted in the best match with the FWD-measured deflection data while it stayed on the conservative side.



(a)



(b)



(c)

*STD: Standard deviation

Figure 3.8. Sensitivity analysis plots for Minnesota section based on a) Method A; b) based on Method B&D; and c) based on Method C

3.5 CONCLUSION

A set of predictive procedures were developed to estimate the pavement deflection with seasonally and spatially variable moisture content profiles. This included incorporating moisture-dependent resilient modulus values into Layer Elastic Analysis where the subgrade was divided into various forms of sublayers with different moisture

contents. Then, the predicted deformation was compared with the FWD-based estimated deformation basin in four different seasons for two pavement sections in Minnesota and Oklahoma.

In general, there was good agreement between the predicted deflection shape from layer elastic analysis and FWD measured deflection for the proposed sections. In addition, the way the subgrade was divided into sublayers influenced the results. Dividing the layers according to the location of moisture measurements for as many TDR measurements as possible led to the most accurate deflection prediction. However, considering only the layers located above the depth of 10% stress increment in the analysis may result in a sufficient estimate and reduce the cost of the monitoring program. If the pavement evaluation was to be performed based on the maximum deflection and furthest deflection, the method of treating moisture content in the subgrade layers would not impact the outcome of furthest deflection but it would impact the outcome of maximum deflection in the case of unbound base course. However, if the base course layer is the bound material the method of treating subgrade moisture content is significant for furthest deflection but does not make any difference for the maximum deflection.

The Witczak Model for resilient modulus prediction was found to work well under both saturated and unsaturated soil conditions (for A-1-b, A-2-4, and A-3 soils in this study; A-1-b for base course and A-2-4 and A-3 for subgrade). Based on these analyses, the pavement structure can be evaluated using these methodologies as a first-hand estimate of pavement deflection, if an appropriate moisture content profile is used and the limitation is considered correctly. Based on the deflection comparison results, the measured FWD deflection basin at the last drop of 40 kN load shown to be an effective tool to test the proposed methodologies to predict the structural capacity of roads. Finally,

the base course and subgrade material type, the thickness of pavement layers, temperature and moisture content have a significant impact on the overall performance of pavement structure.

This study was limited by estimating the pavement deflection with seasonally and spatially variable moisture content profiles for three non-plastic soils types (A-1-b, A-3 and A-2-4) from Minnesota and Oklahoma in April, May, June, July, August and October. Further studies are needed to investigate other pavement structures with different soil types from different locations and at different testing times. Despite this limitation, this study will be practically valuable for the pavements with the similar climatic zone conditions, pavement structure, and soil types. Further studies are recommended to conduct probabilistic method solution to obtain different predicted deflection basins at different testing location rather than the average for comparison with the measured FWD deflection.

3.6 ACKNOWLEDGEMENT

The author would like to thank the Federal Highway Administration for acting as a project sponsor. Thanks, are also extended to the coauthors of this work: Dr. Majid Ghayoomi and Dr. Jo Sias Daniel, both of University of New Hampshire. The author also thanks Dr. Eshan Dave of University of New Hampshire for his feedback and cooperation.

CHAPTER 4

IMPACT OF SUBSURFACE WATER ON THE STRUCTURAL CAPACITY OF INUNDATED FLEXIBLE PAVEMENTS

4.1 INTRODUCTION

Flooding is a natural disaster that can have a severe impact on road infrastructure; even when it does not completely wash away the roadway, the structural capacity of the pavement can be significantly reduced due to the inundation of unbound materials. In such circumstances, road agents have to determine if the pavement structure is capable of withstanding the traffic load without excessive damage or sudden failure and when the roadway can be reopened to traffic upon flood water recession. Therefore, the structural capacity of saturated and unsaturated pavements should be carefully investigated, which requires knowledge of material properties, pavement section and geometry, and expected traffic load.

When a flooding event occurs, the water level rises above the normal groundwater table and the pavement structure becomes submerged. Then, after a period of time, the flood water recedes from the pavement surface down to the unbound material layers. Unbound layers such as base, subbase, and subgrade play vital roles in structural performance of pavements. An increase in moisture content can significantly reduce the stiffness of these materials (Hicks and Monismith, 1971, Rada and Witczak 1981, Lary and Mahoney 1984, Khoury and Zaman 2004, Cary and Zapata 2010). The duration of exposure to excessive moisture content can result in a severe loss of bearing capacity of pavement structure, excessive permanent deformation, degradation of material integrity, and loss of bonding between pavement layers especially when it coincides with heavy traffic (Salour and

Erlingsson 2014). The subsurface water level typically divides the unbound layer into two layers: above the water level where the material is unsaturated (vadose zone) and below the water level where it is fully saturated. Numerous studies have investigated the behavior of unsaturated soil by incorporating the matric suction in a form of stress state in unsaturated soils (Drumm et al. 1997, Khalili et al. 2004, Sawangsuriya et al. 2009, Liang et al. 2008, Khoury et al. 2010, Cary and Zapata 2011, Han and Vanapalli, 2015) or the degree of saturation through modified effective stress relationships (Witczak et al. 2000).

Previous studies (Gaspard et al. 2007, Zhang et al. 2008, Helali et al. 2008, Vennapusa et al. 2013, Chen and Zhang 2014) showed that, although difficult, it is crucial to estimate the percent changes of pavement strength capacity and stiffness during and after flooding with time. The results obtained from such analyses will be valuable for the pavement community and agencies to assess the flooded pavement condition and to determine a timeline for opening the road to traffic balancing the need for access and the damage that may occur to the pavement. Thus, the objective of this study is to develop an approach to evaluate the structural capacity of inundated pavement at different subsurface water levels. The influence depth of the water level up to which the excessive moisture significantly impacts the structural performance of pavements was investigated. In other words, the changes in the pavement structural capacity are minimal when the water level is below the influence depth. In this study, the flooded conditions were simulated using a hydrostatic pressure distribution by lowering the subsurface water level to multiple elevations in the unbound material layers. Matric suction was incorporated indirectly to determine the resilient modulus of unsaturated unbound material layers. The layered elastic approach was used to predict the maximum surface deflection, horizontal tensile

strain at the bottom of asphalt layer, and vertical compressive strain at the top of subgrade layer at different water levels to evaluate the impact of unsaturated and saturated conditions on overall pavement performance. The proposed study will be instrumental to pavement performance evaluation by road agencies to determine the structural capacity of inundated pavements with different water levels and shed light in future studies potentially incorporating time and traffic restrictions to avoid pavement failure.

4.2 BACKGROUND

The degree of water saturation impacts the behavior of unbound materials in the pavement system due to significantly different stress states and stiffness in soils (Sauer and Monismith 1968, Edris and Lytton, 1976, Fredlund and Morgenstern, 1977, Noureldin 1994, Witczak, et al. 2000, Ceratti et al. 2004). Several models have been developed to account the impact of stress state and moisture variation on the resilient modulus of unbound layers (Khoury and Zaman 2004, Yang et al. 2008, Cary and Zapata 2010, 2011, Khoury et al. 2011, Sivakumar et al. 2013). Most of the models showed an increase in modulus as the soil moisture decreases (Sauer and Monismith 1968, Hicks and Monismith 1971, Carmichael and Stuart 1985, Drumm et al. 1997, Witczak et al. 2000, Cary and Zapata 2010, Sivakumar et al. 2013, Khoury 2016). Among these models is the model introduced in the Mechanistic–Empirical Pavement Design Guide (MEPDG) proposed by Witczak et al. 2000 to adjust the resilient modulus of unbound materials at given degree of saturation; expressed in Equation 4.1.

$$\log \frac{M_R}{M_{Ropt}} = a + \frac{b-a}{1+\exp\left[\ln\frac{-b}{a}+k_m(S-S_{opt})\right]} \quad (4.1)$$

where M_R/M_{Ropt} = resilient modulus ratio; M_R = resilient modulus at any degree of saturation; M_{Ropt} = resilient modulus at a reference condition; a = minimum of log

M_R/M_{Ropt} , b = maximum of $\log M_R/M_{R opt}$; k_m = regression parameter; and $S-S_{opt}$ = variation in degree of saturation expressed in decimals.

An unsaturated soil layer in the vadose zone and a fully saturated layer are separated by the water table level. In the unsaturated soil layer, the variation in moisture content results in changes of the stress state in the soil. This includes suction stresses due to the presence of inter-particle matric suction defined as the difference between pore air and water pressures in the soil matrix. The matric suction could be measured in-situ using sensors such as tensiometers or be predicted through the hydrostatic capillary pressure given the height above the water level as shown in Equation 4.2.

$$u_a - u_w = -\gamma_w h \quad (4.2)$$

where: u_a is pore air pressure, u_w is pore water pressure, γ_w is unit weight of water, h is the average distance from the point of interest to the water table for a period of time for which the water level has been fairly stable.

The Soil-Water Characteristic Curve (SWCC) defines the relationship between the soil matric suction and volumetric water content or the degree of saturation of soil. Fredlund and Xing (1994) proposed a SWCC relationship to predict the degree of saturation from matric suction or vice versa as presented in Equations 4.3 and 4.4. Perera et al. (2005) presented a methodology to predict the Fredlund and Xing's fitting parameters for different types of soil based on soil index properties as shown in Equations 4.5-4.11. Fredlund and Xing's model and Perera et al.'s correlations are used in the Enhanced Integrated Climatic Model (EICM) and implemented in the MEPDG to predict the degree of saturation to be used in Equation 4.1, in order to adjust the resilient modulus of unbound layers.

$$S = C(h) \times \left[\frac{1}{\left[\ln \left[\exp(1) + \left(\frac{h}{a} \right)^b \right] \right]^c} \right] \quad (4.3)$$

$$C(h) = \left[1 - \frac{\ln \left(1 + \frac{h}{h_r} \right)}{\ln \left(1 + \frac{10^6}{h_r} \right)} \right] \quad (4.4)$$

where

S: Degree of saturation, h: matric suction (ua-uw), a, b, c, hr: fitting parameters to the equation.

- **For soils with plasticity index = 0**

$$a = 0.8627(D_{60})^{-0.751} \quad (4.5)$$

$$\bar{b} = 7.5$$

$$c = 0.1772 \ln(D_{60}) + 0.7734 \quad (4.6)$$

$$\frac{h_r}{a} = \frac{1}{D_{60} + 9.7e^{-4}} \quad (4.7)$$

- **For soils with plasticity index > 0**

$$a = 0.00364(wPI)^{3.35} + 4(wPI) + 11 \quad (4.8)$$

$$\frac{b}{c} = -2.313(wPI)^{0.14} + 5 \quad (4.9)$$

$$c = 0.514(wPI)^{0.465} + 0.5 \quad (4.10)$$

$$\frac{h_r}{a} = 32.44e^{0.0186(wPI)} \quad (4.11)$$

where \bar{b} = Average value of fitting parameter b.

Excessive water from flooding can cause a faster rate of deterioration in pavements. Many agencies and researchers have studied the impact of flooding on pavement deterioration (Clarke and Cosby, 2007, Gaspard et al. 2007, Zhang et al. 2008, Helali et al. 2008, Vennapusa et al. 2013, Chen and Zhang, 2014, Mallick et al. 2015, Khan et al. 2015, Sultana et al. 2016). Zhang et al. (2008) investigated the performance of pavements that were flooded during the 2005 Hurricane Katrina in New Orleans, Louisiana. Due to the lack of structural data before flooding, the flooded pavement structure was compared with similar non-flooded pavements in nearby areas. The research team observed that all damage caused by flooding occurred during the first week of flooding. The comparison

between flooded and non-flooded pavements indicated that there is 18% reduction in the structural number (SN) and 25% reduction in the subgrade modulus due to the effects of saturation. The authors suggested that the flooded pavements substantially affected by inundation. Thinner pavements were shown to be more vulnerable than thicker pavements, where thinner pavements showed more reductions in SN_{eff} and subgrade modulus and higher surface deflection. Clarke and Cosby (2007) conducted a study on the flooded HMA pavements on State Highway 24 in McClain County, Oklahoma after the road was closed to traffic for 14 hrs. They observed a reduction in the Falling Weight Deflectometer (FWD) surface deflection of 12 % for the areas were flooded for about 14 hours. Vennapusa et al. (2013) evaluated flooded pavements during Missouri River flooding in 2011. The research team visited the flooded sites to test the pavement shortly after the flood water receded and again 6 to 8 months after the flooding on different types of roads at different locations. They observed a reduction of 25-28% in subgrade modulus and the overall pavement stiffness due to the flooding for 20 days after the flood water recedes. The percent reductions obtained about 6 to 8 months after the flooding was, on average, similar to the results obtained shortly after the flooding. Sultana et al. (2016) studied the structural performance of pavements after January 2011 flooding in Queensland, Australia. In-situ tests were conducted within 6 weeks and 2 to 4 years post-flood. FWD surface deflection and Modified Structural Number (SNC) were used for comparison before and after flooding. The results showed that a 25 - 40% reduction in FWD surface deflection and 1.5 to 50% reduction in structural number were observed within 6 weeks of flooding while the pavements regained their structural strength 4 years post flooding due to rehabilitation works. A statistical analysis was performed based on the observed data collected within 6 weeks after the flood that showed a significant

reduction of strength. A deterministic model was developed that expressed the structural strength of pavements as a function of time. This model was limited to light traffic on thin asphalt pavement surface for short-term floods.

In general, previous studies showed the percent reduction in the structural capacity of pavements based on the limited measurements made after flood events. However, these measurements were also time consuming and expensive. Hence, in this paper, a parametric analytical analysis is presented based on unsaturated and saturated mechanical behavior of pavement materials to simulate the effect of floodwater recession on the performance of pavement systems. This work will advance the understanding of the structural performance and capacity of flooded pavements at different subsurface water levels incorporating various effective stresses and moisture conditions. This study will provide a platform for a future cost-effective tool to evaluate the time to open the road for traffic, once the method is correlated with the water recession time through unbound materials.

4.3 PAVEMENT SECTIONS AND PROCEDURES

4.3.1 Pavement Section Characterizations

Three pavement cross sections with different subgrade soils were evaluated in this study and are shown in Figure 4.1. The pavement materials were selected from LTPP sites to represent a variety of gradation and plasticity index of pavement materials across the U.S. The physical soil index properties were obtained from Arizona State University application maps (NCHRP 9-23b, 2012); presented in Table 4.1.

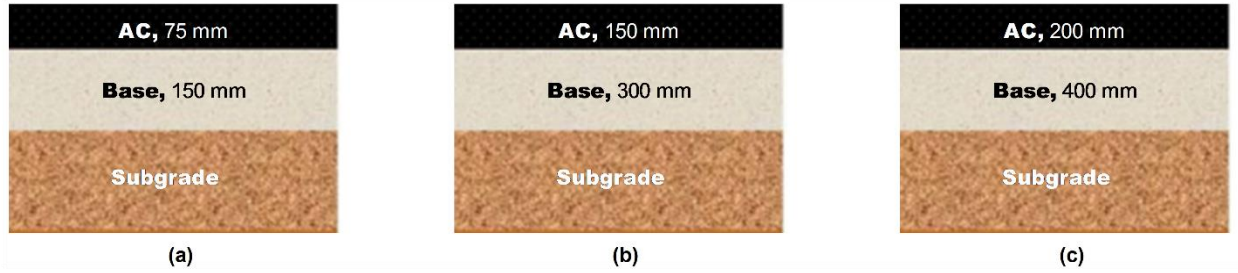


Figure 4.1. Pavement cross sections: (a) Thin; (b) Intermediate; (c) Thick

Available correlations from pavement Mechanistic-Empirical Design Guide (MEPDG) Level 2 were used to predict the water content, degree of saturation, specific unit weight, void ratio, and dry densities from physical soil indices as presented in Equations 4.12-4.17.

$$S_{opt} (\%) = 6.752(WPI)^{0.147} + 78 \quad (4.12)$$

$$G_s = 0.041(WPI)^{0.29} + 2.65 \quad (4.13)$$

$$S \times e = W \times G_s \quad (4.14)$$

$$\rho_{dry} = \frac{G_s \times \gamma_w}{1+e} \quad (4.15)$$

$$W_{opt}(\%) = 8.6425D_{60}^{-0.1038} \quad \text{If PI} = \text{zero} \quad (4.16)$$

$$W_{opt}(\%) = 1.3(WPI)^{0.73} + 11 \quad \text{If PI} > \text{zero} \quad (4.17)$$

where:

WPI = Percent of passing#200 × plasticity index, D₆₀: Grain diameter corresponding to 60% passing by weight or mass (mm), S_{opt}: degree of saturation at the optimum moisture content, W_{opt}: optimum moisture content, e: void ratio, ρ_{dry}: max dry density of the soil, G_s: specific gravity

MEPDG Level 2 correlations between strength and stiffness of unbound materials and physical soil indices were also employed. The California Bearing Ratio (CBR) and resilient modulus (M_R) of the proposed soils at optimum moisture content were estimated from Equations 4.18 and 4.19, respectively. Table 4.1 shows the estimated soil properties and

the strength and stiffness of the materials determined from the MEPDG Level 2 relationships.

$$CBR = \frac{75}{1+0.728(wpl)} \quad (18)$$

$$M_{R_{opt}} = 17.6(CBR)^{0.64} \quad (19)$$

where

CBR: California bearing ratio test, %, $M_{R_{opt}}$: Resilient modulus at optimum moisture content, MPa

Table 4.1. Unbound Materials Properties

| Pavement layer type | Base course | Subgrade | | |
|--|--------------------|-----------------|-------|-------|
| AASHTO Classification | A-1-a | A-2-4 | A-4 | A-7-5 |
| Passing # 200, % | 7.6 | 22.5 | 80 | 92.5 |
| Liquid Limit, L.L | 0 | 17.5 | 26 | 60 |
| Plasticity Index, PI | NP | NP | 9 | 30 |
| WPI = P₂₀₀ × PI | 0 | 0 | 7.2 | 27.75 |
| D60 (mm) | 7.7 | 0.25 | - | - |
| Specific Gravity, G_s | 2.650 | 2.650 | 2.723 | 2.757 |
| Void Ratio, e | 0.216 | 0.339 | 0.516 | 0.796 |
| Max Dry Density, gm/cm³ | 2.18 | 1.980 | 1.798 | 1.535 |
| Optimum moisture content, W_{opt} % | 7 | 10 | 16.50 | 25.71 |
| Degree of saturation, S_{r opt} % | 78 | 78 | 87 | 89 |
| California Bearing Ratio, CBR % | 70 | 20 | 12 | 3.5 |
| Resilience modulus, M_{R opt} (MPa) | 270 | 120 | 86 | 40 |
| Water Table Depth Annual Min (m) | N.A. | N.A. | 1.53 | 0.61 |

4.3.2 Subsurface Water Level and water pressure distribution

The subsurface water level was located at different elevations in the pavement structure for this analysis:

1. At the top of base course layer: In this case, all the unbound materials, i.e. base course and subgrade soil, were considered fully saturated.
2. At the top of subgrade layer: In this case, the subgrade was considered fully saturated and the base course was considered unsaturated.
3. The water level was lowered in 150 mm intervals down to the point where no significant impact on the performance of pavement structure was observed, or up to 3 meters below the pavement surface. The subgrade below the subsurface water level location was considered fully saturated and the subgrade material above the water level was considered unsaturated

The unsaturated subgrade layer above the subsurface water level was then divided into sublayers (150 mm each) and the layer below the water level was considered as one infinite fully saturated layer. A hydrostatic pressure distribution was considered at any given water level neglecting transient flow and evaporation-precipitation events. The pressure was set to zero at the water level (fully saturated) followed by positive pressure below the subsurface water level. A hydrostatic suction was calculated from Equation 4.2 for soils above the subsurface water level. The matric suction in each unsaturated sublayer of unbound layers was calculated at the mid-depth of the sublayer given the water pressure distribution. Figure 4.2 shows a schematic of the approach.

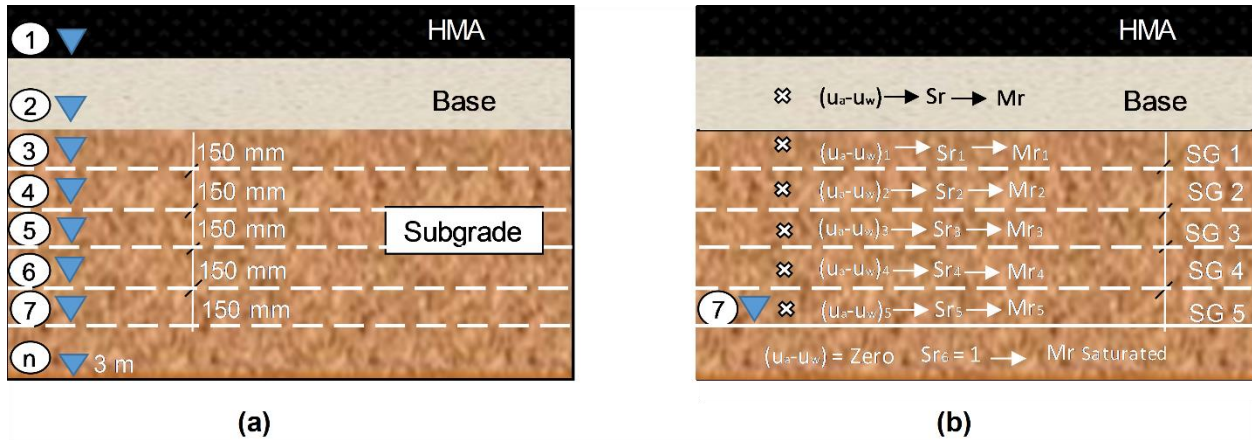


Figure 4.2. Schematics to demonstrate (a) locations of water level in a pavement cross section (b) example analysis approach of water level number 7

4.3.3 SWCC and degree of saturation

The Soil-Water Characteristic Curve (SWCC) proposed by Fredlund and Xing (1994) presented in Equations 4.3 and 4.4 and fitting parameters in Equations 4.5-4.11 were used to predict the degree of saturation given the suction in each sublayer of the subgrade. Figure 4.3 depicts the estimated SWRC for the three subgrade soil types; A-2-4, A-4, and A-7-5 using the Fredlund and Xing and Perera's correlation models. The figure illustrates that the soils with more fine materials and more plasticity have higher Air Entry Values (AEV); ranging from 2 kPa for A-2-4 to 14 kPa for A-4, and 90 kPa for A-7-5 soils. The air entry value indicates when the saturated soil transitions to the unsaturated condition as the matric suction exceeds these values.

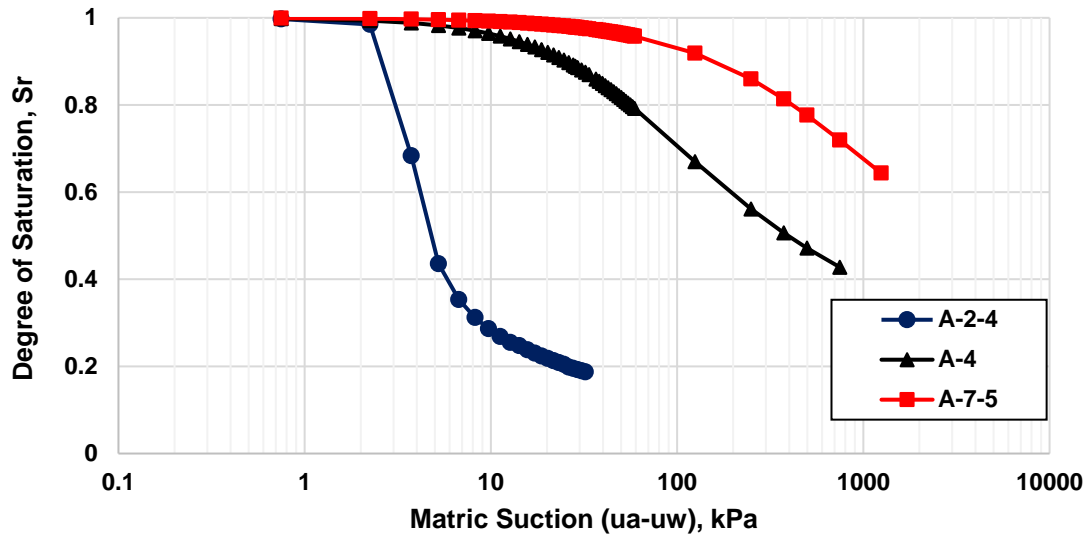


Figure 4.3. Predicted SWRC for the proposed soils

4.3.4 Resilient Modulus, Mr

After estimating the degree of saturation at each sublayer from the SWRC, the resilient modulus of the soil corresponding to each sublayer in subgrade was estimated using Equation 4.1. The coefficient parameters in this Equation; i.e. a , b , and k_m , were determined using available data from the literature and assuming a maximum modulus ratio of 2 for coarse-grained materials and 2.5 for fine-grained materials with respect to degree of saturation. The values of a , b , and k_m for coarse-grained and fine-grained materials are summarized in Table 4.2 (Witczak et al. 2000).

Table 4.2. Regression parameters of Equation 4.1

| Parameter | Coarse- grain materials | Fine- grain materials |
|-----------|-------------------------|-----------------------|
| A | -0.3123 | -0.5934 |
| B | 0.3 | 0.4 |
| k_m | 6.8157 | 6.1324 |

4.3.5 Linear Elastic Analysis (LEA)

Elshaer et al. (2017) showed that flexible pavements can be modeled using KENLAYER layer elastic analysis program given the soil moisture profile to estimate the FWD deflection at different times. In this study, the moisture-dependent resilient moduli for each sublayer were used in the layer elastic analysis. As a result, the subgrade layer in this study was divided into sublayers above the subsurface water level, while the layer below the subsurface water level was considered as one infinite fully saturated layer to simulate the pavement response from FWD testing.

The KENLAYER multi-layer elastic analysis computer program was used to calculate the deflection, stresses, and strains in the pavement. The maximum surface deflection, the horizontal tensile strain at the bottom of asphalt layer, and the vertical compressive strain at the top of subgrade layer were computed given the load, the thickness of all layers, Poisson's ratio and the modulus of materials. For the asphalt layer, PG 64-28 with 5% void ratio and 5% effective binder with 300,000 psi average modulus value at 20°C was used in the analysis; daily and seasonal variations were not considered in this analysis. For unbound layers, the resilient modulus of the base course layer and subgrade sublayers were calculated from Equation 4.1 based on the estimated degree of saturation from the SWRC. The Poisson's ratio of all the materials used in this analysis was obtained from the MEPDG Level 3 inputs. FWD testing configuration and single axle dual tires loading were simulated in KENLAYER and the maximum surface deflection, vertical and horizontal strains were calculated. Table 4.3 summarizes the axle and tire types used in this analysis.

Table 4.3. Axle and Tire Types

| Axle types | Contact radius, mm | Tire pressure, Mpa | Load, kN |
|-----------------------|---------------------------|---------------------------|-----------------|
| FWD, Steer | 150 | 0.57 | 40 |
| Single axle dual tire | 124 | 0.83 | 40 |

The structural capacity was then computed using the modified structural number (SNC) from the FWD maximum deflection value (D_0) for asphalt pavement; as presented in Equation 4.20 (World bank, 1987). Then, the percent of reduction in pavement strength due to saturated conditions was calculated.

$$SNC = 3.2D_0^{-0.63} \quad (4.20)$$

where SNC is the modified structural number, D_0 is the maximum deflection, mm

4.4 RESULTS AND DISCUSSION

The results of the multi-layer linear elastic analysis are presented herein by looking at the changes in maximum deflection, horizontal tensile strain at the bottom of asphalt layer, vertical compressive strain at the top of subgrade layer, and modified structural number at various subsurface water levels for the three soil types and three pavement structures. The impact of pavement structure and soil types on the structural performance of pavements with different subsurface water levels is discussed.

4.4.1 Maximum Surface Deflection

The changes in maximum surface deflection as the subsurface water level was dropped are shown in Figure 4.4 for the selected subgrade soils and the three pavement cross sections. The figure clearly exhibits the impact of pavement structure and soil type with varying water level on the maximum deflection. When the water level was at the interface between the asphalt layer and the base course layer the maximum surface deflection was

the highest due to the full saturation of the unbound material layers. Once the water level moved to the interface between the base course layer and subgrade layer, the maximum deflection quickly decreased due to the relative contribution of the base course layer to the overall structural capacity of pavement structure. The pavement structure cross section had a significant impact on the maximum surface deflection where the thinnest pavement structure showed more than twice the maximum deflection of the thickest pavement structure for all types of soils.

Soil gradation, plasticity, and infiltration rate affected the soil suction, the saturation condition, and consequently resilient modulus of subgrade soil, and therefore the deflection magnitudes. In general, the resilient modulus of subgrade with fine-grained soils (A-4 and A-7-5) is lower than the ones with coarse-grained soil (A-2-4), which resulted in the greater deflection values for pavements. The rate of the change in the maximum surface deflection for A-2-4 and A-4 subgrade soil types was more than the one for A-7-5 subgrade soil due to the minimal changes in resilient modulus of the fine clayey soil in sublayers where the soil stayed close to saturated condition (above 98 % degree of saturation) as the water level dropped. The rate of the change in the maximum surface deflection also appeared to decrease for some materials once the water level dropped below a certain depth (approx. 1.5 meters from the pavement surface).

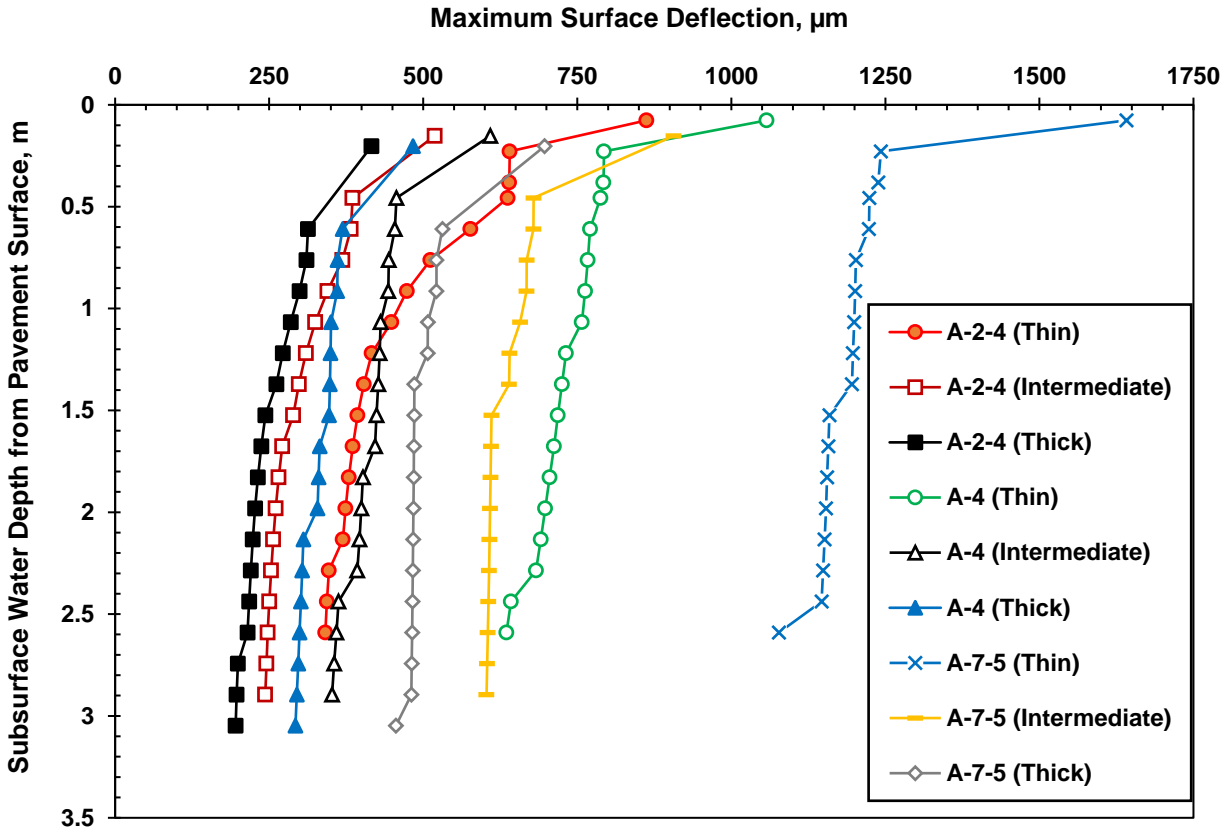


Figure 4.4. Variation of the maximum surface deflection with depth of subsurface water levels

4.4.2 Horizontal Tensile Strain at the Bottom of Asphalt Layer

Figure 4.5 shows the changes in the horizontal tensile strain at the bottom of the asphalt layer as the water level dropped in 150 mm intervals down to 3 meters for the selected soil types and different pavement cross sections. In this figure, the impact of the type of subgrade layer and the pavement cross section on the induced strain were investigated to determine the parameter that is most influential in the horizontal strain and, therefore the fatigue performance of pavement structure. The horizontal strain was at the highest magnitude when the water level was at the interface between the asphalt layer and the base course layer due to the full saturation of the unbound materials in the pavement

cross section. Then, when the water level moved down to the interface between the base course layer and the subgrade layer, the horizontal strain magnitudes rapidly decreased to less than half their value under full saturated conditions. Figure 4.5 shows that the pavement structure had also a significant impact on the horizontal tensile strain at the bottom of asphalt layer; the thinner the pavement structure the highest horizontal strain. In most cases, the changes in the horizontal strain were minimal after the water level dropped below the subgrade surface. However, for the pavements with A-2-4 subgrade soil, some changes were observed when the water level was still in the top portion of the subgrade layer (until 0.50 meter from subgrade surface). In general, there is a very limited impact from subgrade type on the horizontal strain, especially for the intermediate and thick pavement cross sections.

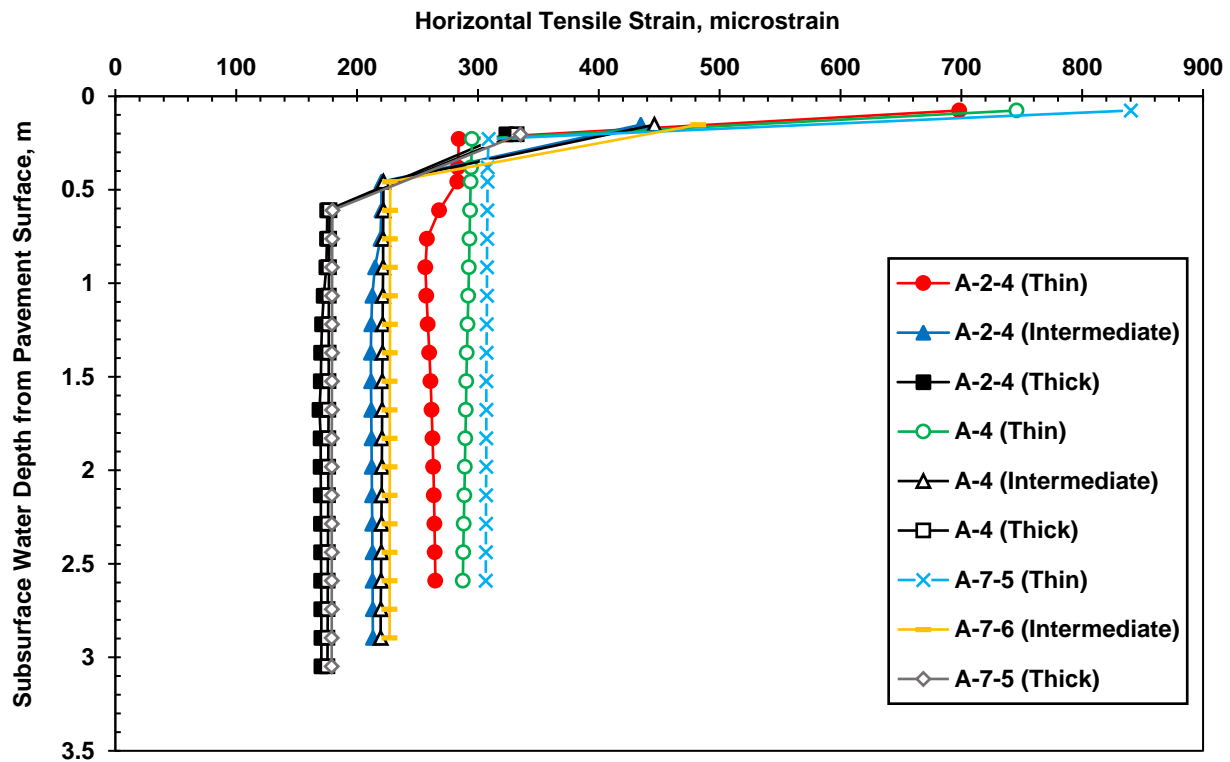


Figure 4.5. Variation of the horizontal tensile strain at the bottom of the asphalt layer with depth to subsurface water levels

4.4.3 Vertical Compressive Strain at the Top of Subgrade Layer

Figure 4.6 presents the changes in vertical compressive strain at the top of subgrade soil with different subsurface water levels for three different soil types and three different pavement cross sections. The figure indicates a maximum vertical compressive strain when the water level was at the interface between the asphalt layer and the base course layer. Then, the vertical strain decreased rapidly as the water level lowered to the interface between the base course layer and the subgrade layer because of the relative contribution of the base course layer to the overall pavement strength. This figure shows that the pavement structure significantly impacted the vertical strain at the top of the subgrade for all soils.

The soils with finer subgrade material exhibited the highest vertical strain; i.e. the pavement with A-7-5 subgrade soil had the largest vertical strain magnitudes in depth. For the pavement with A-2-4 subgrade soil type, the vertical strain started to decrease gradually with a lower water level. But, then, it significantly decreased to half the value under fully saturated subgrade layer (subsurface water level at the top of subgrade layer) up to a certain depth; the extent of which greatly depended on the pavement structure. Further, the changes in the vertical strain became insignificant (less than 1%) when the water table passed a certain depth; “an influence depth”. This influence depth was 0.53 meter from the top of the subgrade for the thinnest pavement structure and 0.60 meter for the thickest pavement structure. Based on this variation, 0.60 meters from the subgrade surface was chosen to be a threshold influence depth in all pavement cross sections with A-2-4 subgrade soil type. In other words, when water levels dropped below that depth, there was no longer an impact on the vertical strain and therefore the expected rutting performance.

For the pavements with A-4 subgrade soil, the slope of the vertical strain profile in depth remained relatively constant for water levels below the subgrade surface regardless of the cross-section type. However, this slope was steeper for the thinnest pavement structure due to the higher effects of suction on the resilient modulus of subgrade soil. This slope became almost vertical for the thicker sections showing the minimal impact of the location of the water level in the subgrade layer on the vertical strain. Similarly, for the pavements with A-7-5 subgrade soil, there is no change in the vertical strain once the water level lowered to the interface between the base course layer and the subgrade layer. This might be because of the slight changes in the degree of saturation for fine material for the range of induced suctions; which led to a very minimal change in the resilient modulus.

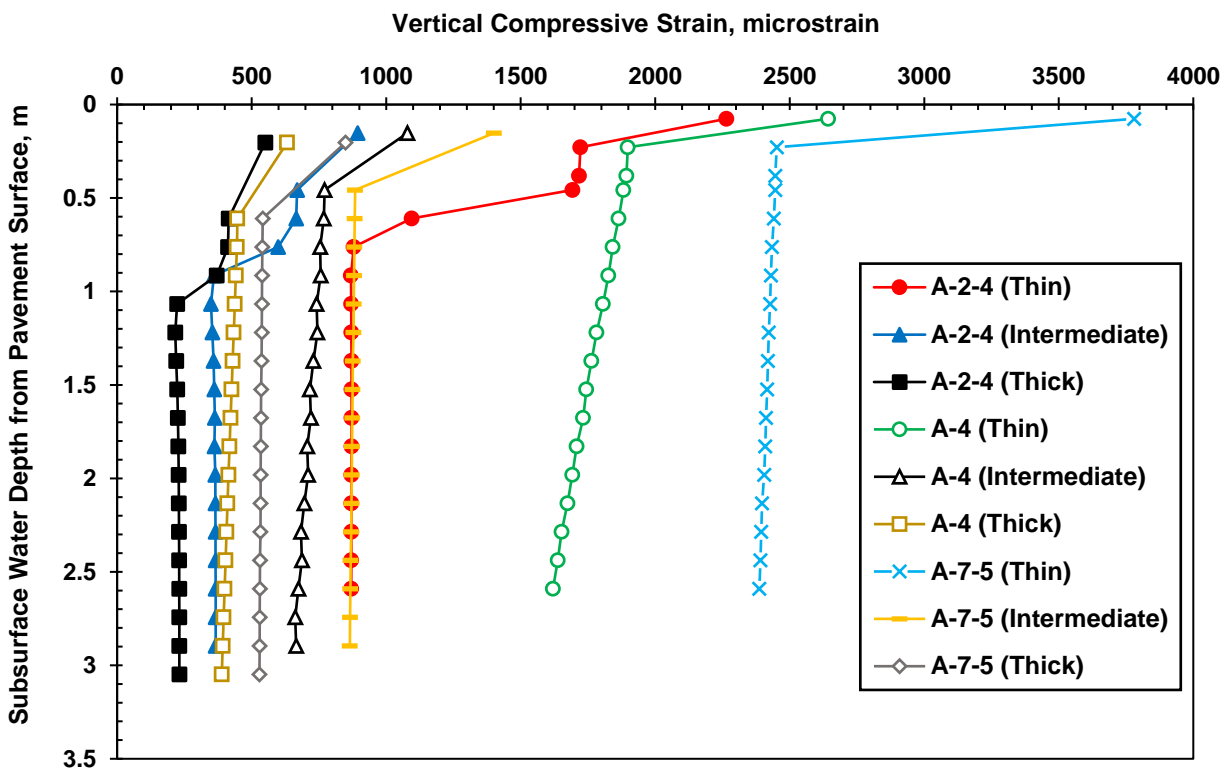


Figure 4.6. Variation of the vertical compressive strain at the top of the subgrade layer with depth to subsurface water

4.4.4 Structural Capacity of Pavements

Figure 4.7 shows the calculated modified structural number (SNC) of pavements with different subsurface water levels for the three different soil types and three different pavement cross sections. This figure exhibits that the structural capacity of the pavement cross section was the weakest when the water level was at the interface between asphalt layer and base course layer. Then, the pavement gradually started to gain its strength once the water level dropped down to the interface between the base course layer and subgrade layer.

There was a significant change in the structural capacity with varying water levels for pavements with different soils and different pavement cross sections where the thicker pavement showed the higher SNC values. The rate of SNC change was higher for A-2-4 subgrades than A-4 and A-7-5 materials because of the higher influence of desaturation on the resilient modulus of the sublayers, which impacted the overall pavement performance.

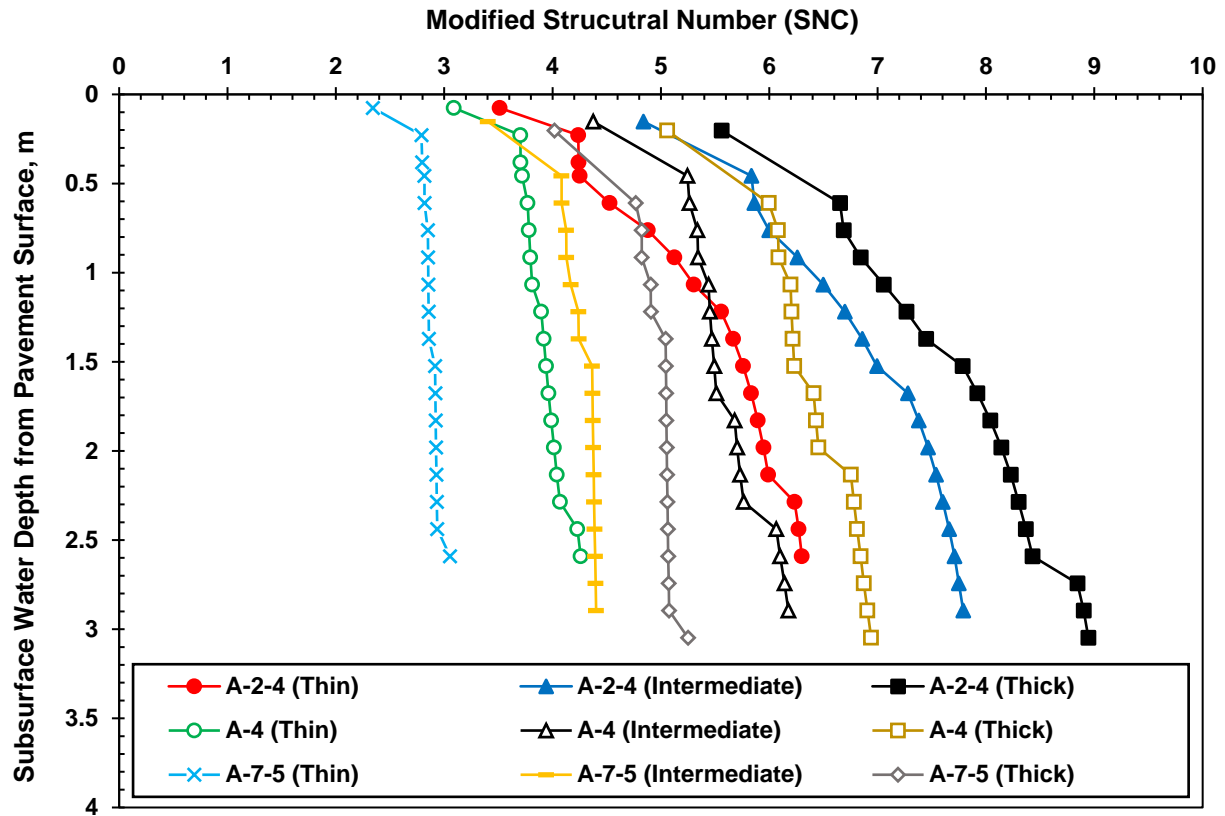


Figure 4.7. Variation of the modified structural number with subsurface water levels

Based on the above analyses, the base course layer had the most influence on the structural capacity of pavements under fully saturated conditions. In addition, pavement structure and subgrade type significantly impacted the surface deflection, modified structural number and vertical strain, and therefore the rutting performance. Subgrade type showed a smaller impact on the horizontal strain, and therefore the fatigue performance while the pavement structure had the largest impact on horizontal strain.

4.4.5 Influence Depths

For each pavement model with different cross section thicknesses and subgrade soil types, an “influence depth” of the subsurface water level was defined, measured from the subgrade surface, beyond which the pavement performance would be acceptable for the

specific traffic load. Although determining the criteria for such definition requires further investigation, Table 4.4 summarizes these depths from subgrade surface for each of the pavement models with three pavement structure and three soil types evaluated in this study. The influence depth was defined based on the changes in the slope of the pavement response in depth (e.g. in subgrade layer) with different water levels; listed for different models in Table 4.4. The influence depth was selected where the change in the evaluated parameter became less than 2% in three consecutive intervals. It is also important to mention that in some cases, such as in fine-grained soils, no change in the slope was observed, which marked as N.A. in the table. In addition, based on the past experience the threshold for maximum deflection before inducing significant damage was reported to be between 500 – 750 micrometers (Horak and Emery 2006). Therefore, if the maximum deflection exceeded this range it was recommended to perform a further investigation to determine the cause of the pavement deterioration. In this study, the influence depth was intended to represent the critical zone for the subsurface water level at which the road can withstand traffic with minimum deterioration based on the pavement structure and soil type. As demonstrated in Table 4.4, this range was appropriate and conservative for all pavement structures and soil types except the thin pavement with A-7-5 subgrade soil type.

Table 4.4. Influence depth from top of subgrade surface in **meter**

| Pavement section | Thin | | | Intermediate | | | Thick | | |
|--------------------------|--------------|------------|-------------|---------------|----------------|---------------|---------------|---------------|---------------|
| | A-2-4 | A-4 | A-7-5 | A-2-4 | A-4 | A-7-5 | A-2-4 | A-4 | A-7-5 |
| Subgrade type | A-2-4 | A-4 | A-7-5 | A-2-4 | A-4 | A-7-5 | A-2-4 | A-4 | A-7-5 |
| Deflection | 1 (431)** | 1 (732) | 1 (1194) | 1.07 (280) | N.A.* (457) | 1.07 (610) | 0.91 (244) | N.A. (368) | 0.76 (485) |
| Horizontal strain | 0.53 | N.A. | N.A. | N.A. | N.A. | N.A. | N.A. | N.A. | N.A. |
| Vertical strain | 0.53 | 2.80 | N.A. | 0.50 | 2.1 | N.A. | 0.60 | 0.41 | N.A. |

N.A.*: a vertical line from subgrade surface; there is no change in pavement response at different subsurface water level,

**Number between brackets are the surface deflection magnitudes (μm)

4.5 CONCLUSIONS

The load bearing capacity of inundated pavements was evaluated using multi-layer elastic analysis. Matric suction was utilized to determine the resilient modulus of unsaturated unbound material layers divided into sublayers at different subsurface water levels. The pavement responses; maximum surface deflection, horizontal strain at the bottom of asphalt layer and vertical strain at the top of subgrade layer were calculated under different moisture conditions ranging from unsaturated to flooded, fully saturated condition. The flooded condition was attained by placing the water level at the surface of the pavement layer and a hydrostatic pressure distribution (positive and negative) was assigned while the subsurface water level was levered through the unbound material layers.

The analysis results showed that the pavement structure loses significant structural capacity when the unbound material layers are submerged. The pavement structure rapidly regains strength once the subsurface water level dropped below the base course layer.

The base course, subgrade type, and pavement structure were shown to have the most influence on the changes in surface deflection, modified structural number and vertical strain and therefore would be the most significant parameters to identify for the assessment of inundated pavements with respect to rutting. For fatigue performance (related to horizontal strain), the change is the most affected by the pavement structure. In addition, the gradation and plasticity of unbound materials were one of the most

important parameters to determine the structural capacity of the pavements. Moreover, the materials from non-to-low plasticity index show significant impact on the structural capacity at different water levels while the high plastic material depicted no impact on the pavement response at different water levels due to very minimal change in the degree of saturation of the material. Finally, the influence depth for the subsurface water level at which the road can withstand traffic with minimum damage was shown to depend on the pavement structure and soil type.

This study would allow agencies to get a better understanding of how inundated pavements behave when the floodwater recedes in order to apply a traffic load restriction to avoid pavement failure. The knowledge gained from this study can be adapted to develop an engineering-based approach for agencies for the assessment of inundated pavements. Future work will be investigated different cross sections with different unbound material types and correlate the time of water recedes in pavement materials post-flooding with pavement performance. This correlation will assist agencies to determine the optimum time to reopen a flooded pavement to traffic.

4.6 ACKNOWLEDGEMENT

The author would like to thank the Federal Highway Administration for acting as a project sponsor. Thanks, are also extended to the coauthors of this work: Dr. Majid Ghayoomi and Dr. Jo Sias Daniel, both of University of New Hampshire. The author also thanks Dr. Eshan Dave of University of New Hampshire and Dr. Rajib Malick of Worcester Polytechnic Institute for the suggestions and feedbacks.

CHAPTER 5

ASSESSING THE IMPACT OF RESILIENT MODULUS PREDICTIVE MODELS OF UNBOUND MATERIALS ON THE PAVEMENT DEFLECTION RESPONSE

5.1 INTRODUCTION

Falling Weight Deflectometer (FWD) is an in-situ test used to determine the structural capacity of pavements by measuring the pavement surface deflection under different loads simulating moving traffic. Parameters such as temperature, moisture content, groundwater table, and depth to bedrock have a significant impact on the measured FWD deflection. The shape and the magnitude of the FWD deflection basins can be used to back calculate the stiffness of pavement materials. The high cost of FWD device including any associated labor testing time and data analysis, the limited availability among the transportation agencies, and the uncertainty of results in extreme weather events fortified researchers to think about cost-effective alternatives. In order to assess the structural capacity of pavements without conducting a FWD test, an alternative method will be very attractive and valuable to the pavement engineering community. This alternative method could serve as a first-hand evaluation of the structural performance of pavements.

Layered elastic analysis could predict the FWD deflection basins when correct parameters are implemented (Elshaer et al. 2017). Input parameters such as layer thicknesses, stiffnesses of pavement materials, and traffic loads are required to perform such analysis. The stiffness of the unbound materials in pavement systems, expressed as resilient modulus (M_R), is the most important input parameter for base, subbase and subgrade

soils in a layered elastic analysis. The resilient modulus can vary significantly within the soil layers due to changes in the moisture, plasticity index, density and stress levels. Soil material behave nonlinearly; therefore, in order to characterize their nonlinear modulus, tests incorporating changes in stresses and moisture content are needed. Several researchers developed nonlinear constitutive models based on the bulk stress and octahedral shear stress (Seed et al. 1967, Moossazadeh and Witczak 1981, Witczak and Uzan 1988). Effective stress in the unsaturated soil can be calculated using Bishop's formula as a function of matric suction defining the difference between pore air and pore water pressures ($u_a - u_w$). Matric suction can be related to soil moisture content through Soil-Water Characteristic Curve (SWCC) (Fredlund and Xing 1994), which is function of different parameters such as grain size geometry and distribution. Thus, assessing moisture-dependent resilient modulus is vital to provide a reliable assessment of pavement structural capacity.

This paper utilizes the data such as temperature, moisture content, groundwater table, bedrock location, and FWD deflection obtained from the Long-Term Pavement Performance program (LTPP). These data were deployed in the layered elastic analysis to assess the impact of implementing different resilient modulus models for unbound materials. The proposed methods were all based on dividing unbound material layers into several layers to predict the FWD deflection basins, where different resilient modulus predictive models were incorporated in the analysis. Moisture content profiles from Time Domain Reflectometer (TDR) and hydrostatic matric suction profiles from the water level were introduced in to the analysis based on four LTPP sites with different subgrade soils. Then, layered elastic analyses were performed to predict the pavement deflection using FWD load configuration and resilient modulus of materials at different moisture contents

to examine the sensitivity of the pavement structural capacity to different modulus predictive models.

5.2 BACKGROUND

5.2.1 Resilient Modulus Models for Unbound Materials

5.2.1.1 Nonlinear Models

The behavior of flexible pavement under wheel loads can be simulated using a homogeneous half-space. Boussinesq (1885) derived the solution to a concentrated load applied on an elastic half-space based on a linear material assumption. It is well known that subgrade soils are not elastic and experience permanent deformation under constant loads. However, under the repeated traffic loads, most of the deformations in pavement system are recoverable and can be considered elastic (Huang 2004). The stiffness and strength characteristics of soils are pressure dependent, therefore, the impact of this change on Boussinesq's solution is of practical interest. One approximate method to examine the pressure-dependency in a nonlinear half-space is to divide it into sublayers and determine the stresses at the mid-height of each layer by Boussinesq's equations as presented in Equations 5.1 and 5.2 based on linear theory. Then, based on the calculated stresses the nonlinear resilient modulus for each sublayer can be determined from the universal or constitutive equations. The Boussinesq's method of stress distribution was used by Vesic and Domaschuk (1964) to predict the shape of deflection basins on highway pavements, and reasonable agreements were stated (Huang 2004)

$$\sigma_z = q \left[1 - \frac{z^3}{(a^2+z^2)^{1.5}} \right] \quad (5.1)$$

$$\sigma_r = \sigma_t = \frac{q}{2} \left[1 + 2\nu - \frac{2(1+\nu)z}{(a^2+z^2)^{0.5}} + \frac{z^3}{(a^2+z^2)^{1.5}} \right] \quad (5.2)$$

where σ_z , σ_r , and σ_t are the vertical, radial, and tangential stresses due to loading; a is the plate radius, q is the uniform pressure; ν is the Poisson's ratio; z is the distance below ground surface at which the stress is computed.

One of the constitutive models that implemented in the Mechanistic-Empirical Pavement Design Guide (MEPDG) to determine the nonlinear resilient modulus of unbound materials is presented in Equation 5.3. This constitutive model captures the effect of stress state and is applicable to all types of unbound materials ranging from very plastic clays to clean granular bases (NCHRP, 2004).

$$M_R = K_1 P_a \left(\frac{\theta}{P_a} \right)^{K_2} \left(\frac{\tau_{oct}}{P_a} + 1 \right)^{K_3} \quad (5.3)$$

Where M_R is the resilient modulus, P_a is the atmospheric pressure to normalize stresses and modulus; K_1 , K_2 , K_3 are the regression constants; θ = bulk stress; can be expressed as $\theta = \sigma_z + \sigma_r + \sigma_t + \gamma z(1 + 2k_0)$; and τ_{oct} = octahedral shear stress; can be expressed as $\frac{1}{3} \sqrt{(\sigma_1 - \sigma_2)^2 + (\sigma_2 - \sigma_3)^2 + (\sigma_1 - \sigma_3)^2}$

where γ is the unit weight of soil; z is the distance below ground surface at which the stress invariant is computed; and K_0 is the coefficient of earth pressure at rest.

The nonlinear regression coefficients K_1 , K_2 , and K_3 are constants, dependent on the material type and physical properties. The coefficient K_1 is proportional to Young's modulus, thus, it should be positive as the modulus can never be negative. The coefficient K_2 should be positive, because increasing the volumetric stress produces stiffening or hardening of the material, yielding to higher modulus. The coefficient K_3 should be negative because an increase in the shear stress softens the material, thus yielding lower modulus. If nonlinear property coefficients K_2 and K_3 are set to zero, then the model can be simplified as linear elastic. If K_3 is zero, the behavior might be non-linear hardening

and if K_2 is zero, the behavior is non-linear softening (Yau and Von Quintus 2002).

Several empirical models have been developed to predict the nonlinear regression parameters (K_{1-3}) of the constitutive equation based on soil properties and stress state at various moisture conditions (Santha 1994, Mohammad et al. 1999, Yau and Von Quintus 2002, and Dai et al. 2002). Yau and Von Quintus (2002) developed correlations based on the unbound materials from the LTPP test sections to predict the resilient modulus from physical properties of the base materials and soils at a specific stress state using nonlinear regression optimization techniques. George (2004) compared the measured resilient modulus in laboratory and predicted resilient modulus based on the proposed equations by several researchers (e.g. Long Term Pavement Performance (LTPP), Minnesota Road Research Project, Georgia DOT, Carmichael and Stuart 1985, Drumm et al. 1990, Wyoming DOT, and Mississippi DOT) of eight subgrade soil types. The author exhibited that the LTPP correlation showed the best results in predicting the resilient modulus of those soils.

The regression constants K_1 , K_2 and K_3 from the LTPP correlation equations are listed below (Equations 5.4-5.21) based on the material type. These correlation equations were used in this study.

- **For crushed stone base material, the $K_1 - K_3$ constants are the following:**

$$K_1 = 0.7632 + 0.0084 P_{\frac{3}{8}} + 0.0088 LL - 0.0371W_{opt} - 0.0001\gamma_{opt} \quad (5.4)$$

$$K_2 = 2.2159 - 0.0016 P_{\frac{3}{8}} + 0.0008 LL - 0.038W_{opt} - 0.0006\gamma_{opt} + 2.4 \times 10^{-7} \left(\frac{\gamma_{opt}^2}{P_{40}} \right) \quad (5.5)$$

$$K_3 = -1.1720 - 0.0082 LL - 0.0014W_{opt} + 0.0005\gamma_{opt} \quad (5.6)$$

- **For crushed gravel base material, the K1 – K3 constants are the following:**

$$K_1 = -0.8282 - 0.0065 P_{\frac{3}{8}} + 0.0114 LL + 0.0004 PI - 0.0187W_{opt} + 0.0036W_s + 0.0013\gamma_s - 2.6 \times 10^{-6} \left(\frac{\gamma_{opt}^2}{P_{40}} \right) \quad (5.7)$$

$$K_2 = 4.9555 - 0.0057 LL - 0.0075 PI - 0.0470W_s - 0.0022\gamma_{opt} + 2.8 \times 10^{-6} \left(\frac{\gamma_{opt}^2}{P_{40}} \right) \quad (5.8)$$

$$K_3 = -3.514 + 0.0016\gamma_s \quad (5.9)$$

- **For uncrushed gravel base material, the K1 – K3 constants are the following:**

$$K_1 = -1.8961 + 0.0014\gamma_s - 0.1184 \left(\frac{W_s}{W_{opt}} \right) \quad (5.10)$$

$$K_2 = 0.4960 - 0.0074 P_{200} - 0.0007\gamma_s + 1.6972 \left(\frac{\gamma_s}{\gamma_{opt}} \right) + 0.1199 \left(\frac{W_s}{W_{opt}} \right) \quad (5.11)$$

$$K_3 = -0.5979 + 0.0349W_{opt} + 0.0004\gamma_{opt} - 0.5166 \left(\frac{W_s}{W_{opt}} \right) \quad (5.12)$$

- **For coarse-grained sand soils, the K1 – K3 constants are the following:**

$$K_1 = 3.2868 - 0.0412 P_{\frac{3}{8}} + 0.0267 P_4 + 0.0137 (\% \text{ Clay}) + 0.0083 LL - 0.0379W_{opt} - 0.0004\gamma_s \quad (5.13)$$

$$K_2 = 0.5670 + 0.0045 P_{\frac{3}{8}} - 2.98 \times 10^{-5} P_4 - 0.0043(\% \text{ Silt}) - 0.0102(\% \text{ Clay}) - 0.0041 LL + 0.0014W_{opt} - 3.14 \times 10^{-5} \gamma_s - 0.4582 \left(\frac{\gamma_s}{\gamma_{opt}} \right) + 0.1779 \left(\frac{W_s}{W_{opt}} \right) \quad (5.14)$$

$$K_3 = -3.5677 + 0.1142 P_{\frac{3}{8}} - 0.0839 P_4 - 0.1249P_{200} + 0.1030(\% \text{ Silt}) + 0.1191(\% \text{ Clay}) - 0.0069 LL - 0.0103W_{opt} - 0.0017\gamma_s + 4.3177 \left(\frac{\gamma_s}{\gamma_{opt}} \right) - 1.1095 \left(\frac{W_c}{W_{opt}} \right) \quad (5.15)$$

- **For Fine-grained silt soils, the K1 – K3 constants are the following:**

$$K_1 = 1.0480 + 0.0177(\% \text{ Clay}) + 0.0279PI - 0.0370W_s \quad (5.16)$$

$$K_2 = 0.5097 - 0.0286PI \quad (5.17)$$

$$K_3 = -0.2218 + 0.0047(\% \text{ Silt}) + 0.0849PI - 0.1399W_s \quad (5.18)$$

- **For Fine-grained clay soils, the K1 – K3 constants are the following:**

$$K_1 = 1.3577 + 0.0106(\% \text{ Clay}) - 0.0437W_s \quad (5.19)$$

$$K_2 = 0.5193 - 0.0073 P_4 + 0.0095 P_{40} - 0.0027 P_{200} - 0.003 LL - 0.0049W_{opt} \quad (5.20)$$

$$K_3 = 1.4258 - 0.0288 P_4 + 0.0303 P_{40} - 0.0521 P_{200} + 0.0251 (\% \text{ Silt}) + 0.0535 LL - 0.0672 W_{opt} - 0.0026 \gamma_{opt} + 0.0025 \gamma_s - 0.6055 \left(\frac{W_s}{W_{opt}} \right) \quad (5.21)$$

where, $P_{3/8}$ = percentage passing sieve #3/8; P_4 = percentage passing #4 sieve; P_{40} = percentage passing #40 sieve; P_{200} = percentage passing #200 sieve; W_s = moisture content of the specimen, %; W_{opt} = optimum moisture content of the soil, %; γ_s = dry density of the sample, kg/m³; and γ_{opt} = optimum dry density, kg/m³.

5.2.1.2 Empirical Models

The empirical predictive models that are based on strength characteristics of unbound materials can be used to predict the resilient modulus if the material properties or stresses are not provided. California Bearing Ratio (CBR) test provides a good correlation between strength and resilient modulus of unbound materials. NCHRP (2004) proposed the following correlations between M_r and the CBR:

$$M_{r_{opt}} = 2555(CBR)^{0.64} \quad (5.22)$$

where

CBR: California bearing ratio test, %, $M_{r_{opt}}$: Resilient modulus at optimum moisture content, psi

Also, the NCHRP (2004) proposed the following correlations between CBR and soil index if the CBR test is not performed

$$CBR = \frac{75}{1+0.728(wpl)} \quad (5.23)$$

where

WPI: Percent of passing#200 × plasticity index

5.2.1.3 Moisture Dependent Resilient Modulus Models

Resilient modulus of unbound materials is affected by changes in moisture content due to the differences in the stress state. Several researchers developed empirical models to capture the impact of the stress state and the moisture variation (Edris and Lytton 1976, Fredlund and Morgenstern 1977, Fredlund et al. 1977, Drumm et al. 1997). Witczak et al. (2000) proposed a generalized model (presented in Equation 5.24) to adjust the resilient modulus of unbound materials to any given degree of saturation based on the resilient modulus and the degree of saturation at optimum moisture content.

$$\log \frac{M_R}{M_{Ropt}} = a + \frac{b-a}{1+\exp\left[\ln\frac{-b}{a}+k_m(S-S_{opt})\right]} \quad (5.24)$$

where M_R/M_{Ropt} = resilient modulus ratio; M_R = resilient modulus at any degree of saturation; M_{Ropt} = resilient modulus at a reference condition; a = minimum of $\log M_R/M_{Ropt}$, b = maximum of $\log M_R/M_{Ropt}$; k_m = regression parameter; and $S-S_{opt}$ = variation in degree of saturation expressed in decimals. For purposes of this study, the degree of saturation at any given moisture content was computed using Equation 5.25 and 5.26.

$$\gamma_d = \frac{G_s}{1+e} \gamma_w \quad (5.25)$$

$$S_r = G_s \frac{w}{e} \quad (5.26)$$

where: S_r = degree of saturation, G_s = specific gravity, w = moisture content, γ_w = unit weight of water, γ_d = dry unit weight, e = void ratio

It is well known that unbound materials above the groundwater table are in an unsaturated state. The change in the stress state of the unsaturated soil is related to the matric suction which is the difference between pore air pressure and pore water pressure. Several researchers studied the effect of matric suction on the resilient modulus of unbound materials (Khoury et al. 2010, Cary and Zapata 2010 and 2011, Han and Vanapalli 2015, Khoury 2016). The matric suction could be measured in the field or predicted through the hydrostatic or transient pressure distribution given the height above the groundwater table level; as shown for a hydrostatic condition in Equation 5.27.

$$u_a - u_w = -\gamma_w h \quad (5.27)$$

where: u_a is pore air pressure, u_w is pore water pressure, γ_w is unit weight of water, h is the average distance from the point of interest to the water table for a period of time for which the water level has been fairly stable.

Soil Water Characteristics Curve (SWCC) defines the relationship between the soil matric suction and volumetric water content or the degree of saturation. Fredlund and Xing (1994) proposed a SWCC relationship to predict the degree of saturation from matric suction as presented in Equations 5.28 and 5.29. Perera et al. (2005) presented a method to predict the Fredlund and Xing fitting parameters for different soil types based on soil index properties as presented in Equations 5.30-5.36.

$$S = C(h) \times \left[\frac{1}{\left[\ln \left[\exp(1) + \left(\frac{h}{a} \right)^b \right] \right]^c} \right] \quad (5.28)$$

$$C(h) = \left[1 - \frac{\ln \left(1 + \frac{h}{h_r} \right)}{\ln \left(1 + \frac{10^6}{h_r} \right)} \right] \quad (5.29)$$

where

S: Degree of saturation, h : matric suction ($u_a - u_w$), a , b , c , h_r : fitting parameters to the

equation.

- **For soils with plasticity index = 0**

$$a = 0.8627(D_{60})^{-0.751} \quad (5.30)$$

$$\bar{b} = 7.5$$

$$c = 0.1772 \ln(D_{60}) + 0.7734 \quad (5.31)$$

$$\frac{h_r}{a} = \frac{1}{D_{60} + 9.7e^{-4}} \quad (5.32)$$

- **For soils with plasticity index > 0**

$$a = 0.00364(wPI)^{3.35} + 4(wPI) + 11 \quad (5.33)$$

$$\frac{b}{c} = -2.313(wPI)^{0.14} + 5 \quad (5.34)$$

$$c = 0.514(wPI)^{0.465} + 0.5 \quad (5.35)$$

$$\frac{h_r}{a} = 32.44e^{0.0186(wPI)} \quad (5.36)$$

where \bar{b} = Average value of fitting parameter b.

5.2.2 Long Term Pavement Performance (LTPP) Program

The Federal Highway Administration (FHWA) LTPP team released the Seasonal Monitoring Program (SMP) in 64 sections across the U.S. and Canada to study the temporal variation in pavement response due to the changes in the environmental conditions such as temperature and moisture content. Ten Time Domain Reflectometry (TDR) probes were placed in one hole located in the outer wheel path to measure soil moisture content of the unbound materials at depths up to 1.90 m from pavement surface (Zollinger et al. 2008). Falling Weight Deflectometer (FWD) is used in the LTPP protocol to monitor the structural capacity of pavements by measuring the deflection of the pavement surface. These deflections were registered by seven to nine transducer sensors (geophones) installed at -305, 0, 203, 305, 457, 610, 914, and 1524 mm away from the center of the loading plate. Then, 16 drops are applied at each FWD testing point with

different loads (Von Quintus and Simpson 2002). The magnitude and shape of the pavement deflection basin is a function of different parameters such as temperature, moisture variation, traffic loads, etc. It is well known that the shape of the deflection basin provides an overall assessment of the pavement response. The maximum deflection defines the composite modulus which receives about 70% contribution from the subgrade (Horak et al 1989) while the furthest deflections define the stiffness of the subgrade layer (Tonkin et al. 1998).

5.2.3 Layered Elastic Analysis (LEA) of Pavements

The load bearing capacity assessment of pavements under changing loads and climatic conditions is necessary to track the pavement service life. Layered elastic analysis can predict the structural behavior of pavements if all parameters that affect the structural capacity are present (Truss 2004, Elshaer et al. 2017). Parameters such as stiffness of materials, layer thickness, and traffic loads are needed to be deployed into layered elastic analysis to give a reliable assessment of the pavement deflection response to a range of loads. Elshaer et al. (2017) introduced a method using KENLAYER software to predict the FWD deflection basin using the soil moisture profile. The authors proposed that the most accurate method to estimate in-situ pavement deflection method is to divide the subgrade layer into several layers above the groundwater table while the layer below the groundwater table level was considered as one infinite fully saturated layer.

5.3 PAVEMENT SECTIONS

Four LTPP flexible pavement sections in different climatic zones; from Maine, Minnesota, Texas, and Montana with different layer thicknesses, material types, and depths to bedrock were selected for this study. The pavement structure and material

physical properties for the presented sections are shown in Table 5.1. The selection of these sites was based on the variety of the gradation and plasticity index of the material types. The LTPP data evaluated at these sites included the FWD deflection measured in the outer wheel path (at last drop of load 40 kN), thickness of pavement layers, gravimetric moisture content of unbound materials in depth, mid-depth asphalt temperature, and the depth to the groundwater table, while the depth to the bedrock was extracted from the NCHRP (2003) report.

Table 5.1. Selected LTPP sites and subgrade soil characterizations

| LTPP Sites | 1 | 2 | 3 | 4 |
|--|---------------------------|---------------------------|------------------------|-------------------------|
| | 23-1026 | 27-1018 | 48-1077 | 30-8129 |
| Location | Maine (ME) | Minnesota (MN) | Texas (TX) | Montana (MT) |
| Surface type | AC (183 mm) | AC (112 mm) | AC (127 mm) | AC (82 mm) |
| Base Layer properties | | | | |
| Base material type | Uncrushed Gravel (477 mm) | Uncrushed Gravel (132 mm) | Crushed Stone (265 mm) | Crushed Gravel (580 mm) |
| AASHTO Classification | A-1-a | A-1-b | A-1-a | A-1-a |
| Passing # 200, % | 7 | 6.9 | 7 | 7.5 |
| Plasticity Index, PI | NP | NP | NP | NP |
| D60 (mm) | 45.2 | 2.6 | 9 | 8.5 |
| Optimum Moisture % | 7 | 7 | 5 | 6 |
| In situ Dry Density (kg/m ³) | 2270 | 2030 | 2139 | 2217 |
| Specific Gravity (Gs) | 2.65 | 2.675 | 2.60 | 2.71 |
| Void Ratio (e) | 0.17 | 0.34 | 0.22 | 0.22 |
| Max lab Dry Density (kg/m ³) | 2227 | 2195 | 2227 | 2211 |
| Subgrade Layer properties | | | | |

| LTPP Soil type | Coarse-Grained Soil: Silty Sand with Gravel | Coarse-Grained Soils: Poorly Graded Sand with Silt | Fine-Grained Soils: Sandy Silt | Fine-Grained Soils: Gravelly Lean Clay with Sand |
|---|--|---|---------------------------------------|---|
| AASHTO Classification | A-2-4 | A-3 | A-4 | A-6 |
| Percent Passing # 200 | 12.6 | 6.2 | 73.6 | 60.3 |
| D60 (mm) | 4.8 | 0.38 | 0.04 | 0.07 |
| Plasticity index PI | NP | NP | NP | 16 |
| Percent of Coarse Sand | 26 | 42 | 3 | 3 |
| Percent of Fine Sand | 46 | 34 | 20 | 16 |
| Percent of Silt | 11.3 | 4.5 | 61.1 | 39.2 |
| Percent of Clay | 1.3 | 1.5 | 12.5 | 21.1 |
| Optimum Moisture % | 10 | 8 | 11 | 11 |
| In situ Dry Density (kg/m³) | 1960 | 1828 | 1721 | 1810 |
| Specific Gravity (Gs) | 2.782 | 2.65 | 2.685 | 2.65 |
| Void Ratio (e) % | 0.42 | 0.45 | 0.56 | 0.46 |
| Max lab Dry Density (kg/m³) | 1922 | 1970.3 | 1826 | 1874 |
| Porosity | 0.30 | 0.31 | 0.36 | 0.32 |
| Depth to bedrock | Infinite | 2.5 m from top of subgrade layer | Infinite | Infinite |
| Moisture and deflection data year | (1994) 16 September, (1995) 3 April | (1994) 25 April, 10 October | (1997) 16 September | (1997) 11 August |

5.3.1 ANALYSIS PROCEDURES

The KENLAYER multi-layer elastic analysis computer program was used to calculate the deflection basin. The predicted deflection basin was conducted using the given FWD load, FWD plate radius, the thickness of all layers, Poisson's ratio of materials and the modulus of all materials. The unbound material layers were divided into sublayers to the

groundwater table. The sublayers' thickness was determined based on the TDR location depths; TDRs fell in the middle of sublayers. Then, the layer below the groundwater table was determined based on the depth to bedrock. If the depth to the bedrock was shallow, the layer of subgrade below the water table was considered as 2 layers; 1 fully saturated layer and 1 bedrock layer. If the depth to the bedrock was deep, then the subgrade layer below groundwater table was considered as one infinite layer.

For the cases where no direct TDR measurements were implemented, matric suction was considered as an independent stress state and approximately estimated from hydrostatic pressure distribution at the mid-height of each sublayer (Equation 5.27). This assumption represents a system with no evapotranspiration mechanisms. Then, the predicted moisture content was estimated using representative SWCCs (Equations 5.28-5.36) given the matric suction and soil index. Figure 5.1 exhibits the employed SWCCs for subgrade soils in Maine (A-2-4), Minnesota (A-3), Texas (A-4) and Montana (A-6). The soils with more fine materials and more plasticity have higher air entry values where air starts to enter the largest pores in the soil and the soil exhibits unsaturated condition. As expected, increasing the matric suction decreases the degree of saturation.

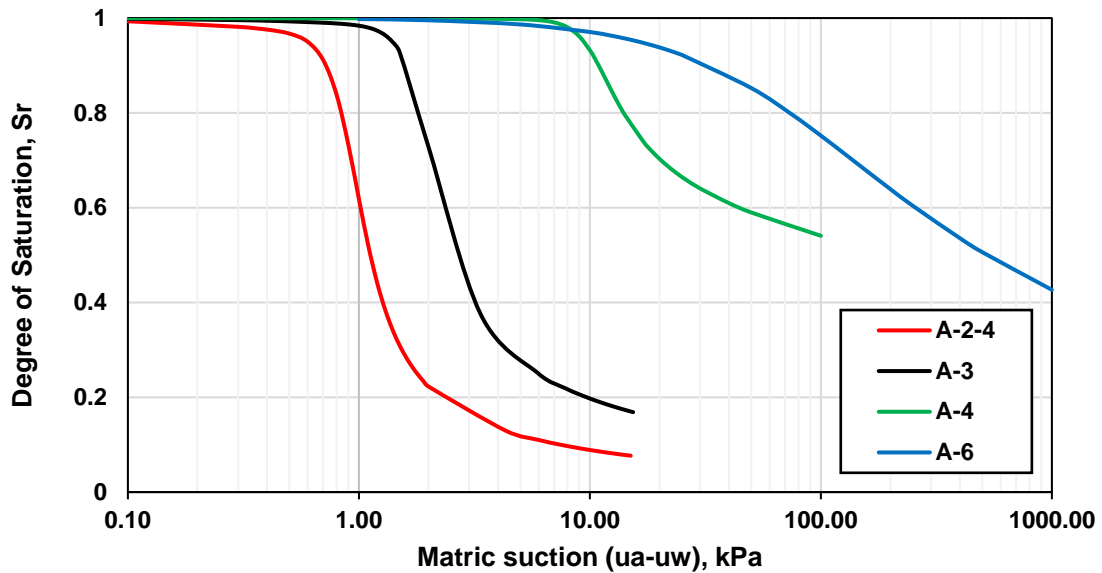


Figure 5.1. Predicted SWRC for the proposed soils

The following five methods as shown in Figure 5.2 were employed to estimate the resilient modulus of each sublayer in the unbound layers to be implemented into the layered elastic analysis and to predict the FWD deflection basin:

Method A ($K-\theta_{opt} + \text{Witczak Measured M.C.}$)

In this method,

- 1- The traffic load on the pavement surface was transmitted into the underlying layers based on a load distribution slope of 0.5:1 (Haung, 2004). The radius of the tire on the pavement surface was computed based on the load of 40 kN and tire pressure of 0.57 MPa. Then, the stresses (θ and τ_{oct}) at the middle of each sublayer were calculated based on Boussinesq's equations under the point of loading.
- 2- The nonlinear regression parameters (K_1 , K_2 and K_3) were estimated at the optimum moisture content from LTPP regression models (Equations 5.4-5.21) based on the material properties

- 3- Then, the resilient modulus at each sublayer was estimated from the nonlinear constitutive ($K-\theta$) model in Equation 5.3 at the optimum moisture content.
- 4- The measured degree of saturation profile from TDRs was implemented in Witczak model (presented in Equation 5.24) to adjust the resilient modulus at each sublayer from optimum moisture condition to the given measured moisture content.

Method B ($K-\theta_{\text{opt}}$ + Witczak Predicted M.C.)

In this method,

- 1- The resilient modulus at optimum moisture content in each sublayer was determined following the same procedure as in Method A from steps 1 – 3.
- 2- The matric suction was estimated from Equation 5.27, then, the degree of saturation at each sublayer was predicted from SWCC (shown in Figure 5.1).
- 3- Finally, the predicted degree of saturation profile was implemented in Witczak model (presented in Equation 5.24) to adjust the resilient modulus at each sublayer from the optimum moisture condition to the given predicted moisture content.

(Note: the difference between this method and Method A was the use of the measured degrees of saturation versus the predicted ones, respectively)

Method C ($K-\theta$)

In this method,

- 1- The stresses (θ and τ_{oct}) at each sublayer was determined following the same procedure as in Method A in step 1.
- 2- The nonlinear regression parameters (K_1 , K_2 and K_3) at each sublayer were estimated at the measured moisture content profile from LTPP regression models (Equations 5.4-5.21) based on the material properties.

- 3- Finally, the resilient modulus at each sublayer was calculated from (K- θ) equation at the measured moisture content for each sublayer. The difference between this method and the previous two methods is that the resilience modulus at each sublayer was independent from its value at optimum moisture content; each sublayer was treated individually based on the applied stresses and moisture content.

Method D (CBR + Witczak Measured M.C.)

In this method,

- 1- CBR value was used to predict the resilient modulus at the optimum moisture content for the whole layer (presented in Equation 5.22).
- 2- Then, the measured degree of saturation profile was implemented in Witczak model (Equation 5.24) to adjust the resilient modulus from optimum moisture condition to the given measured moisture content. The difference between this method and Method A is that the resilient modulus at optimum moisture content in Method A is different at each sublayer while in this method the $M_{r_{opt}}$ is the same value for all sublayers.

Method E (CBR + Witczak Predicted M.C.)

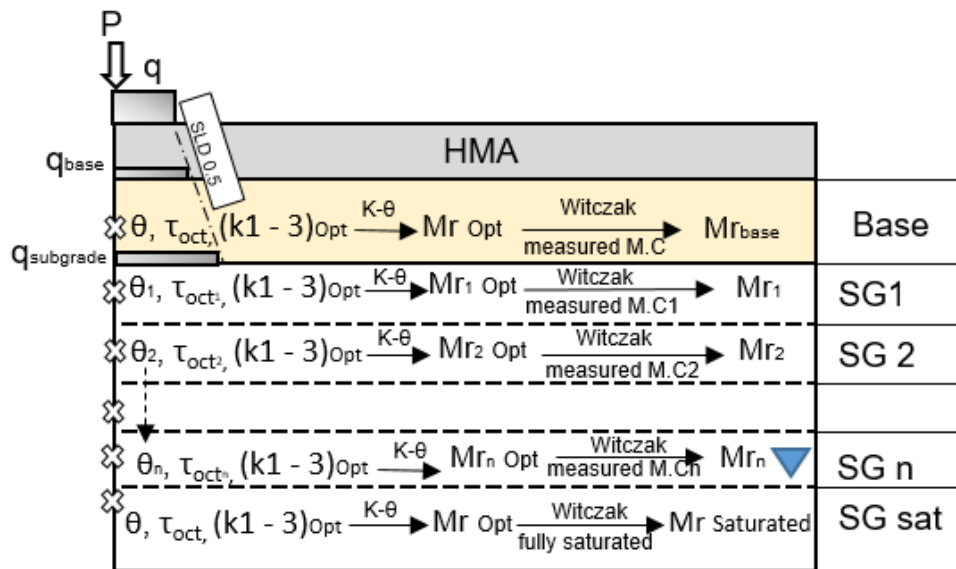
In this method,

- 1- The resilient modulus at optimum moisture content was determined following the same procedure as in Method D.
- 2- The matric suction was estimated from Equation 5.27, then, the degree of saturation at each sublayer was predicted from SWCC (shown in Figure 5.1).
- 3- Finally, the predicted degree of saturation profile was implemented in Witczak model (presented in Equation 5.24) to adjust the resilient modulus from the optimum

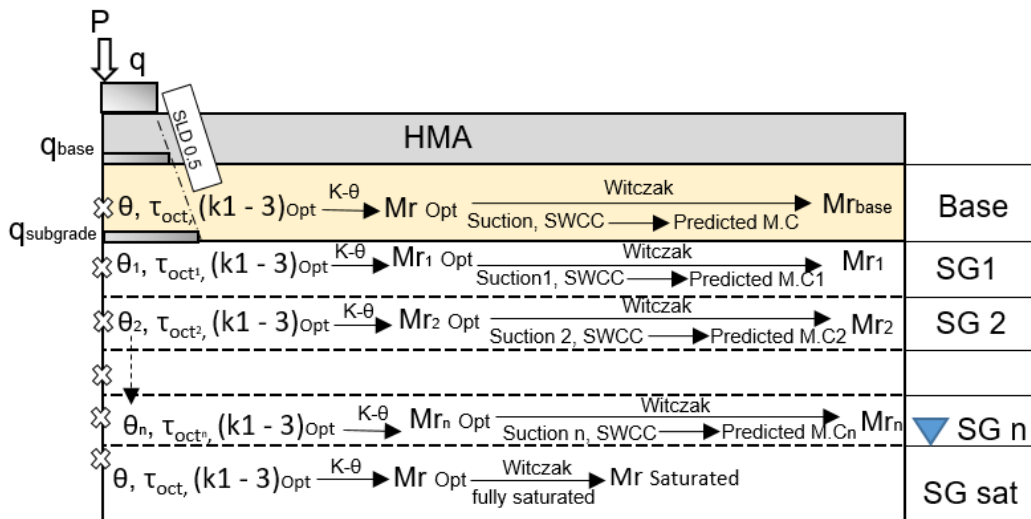
moisture condition to the given predicted moisture content of each sublayer. The difference between this method and Method D is the use of the measured degrees of saturation versus the predicted ones, respectively).

Figure 5.3 shows the flow diagram of the proposed method to predict the deflection basins.

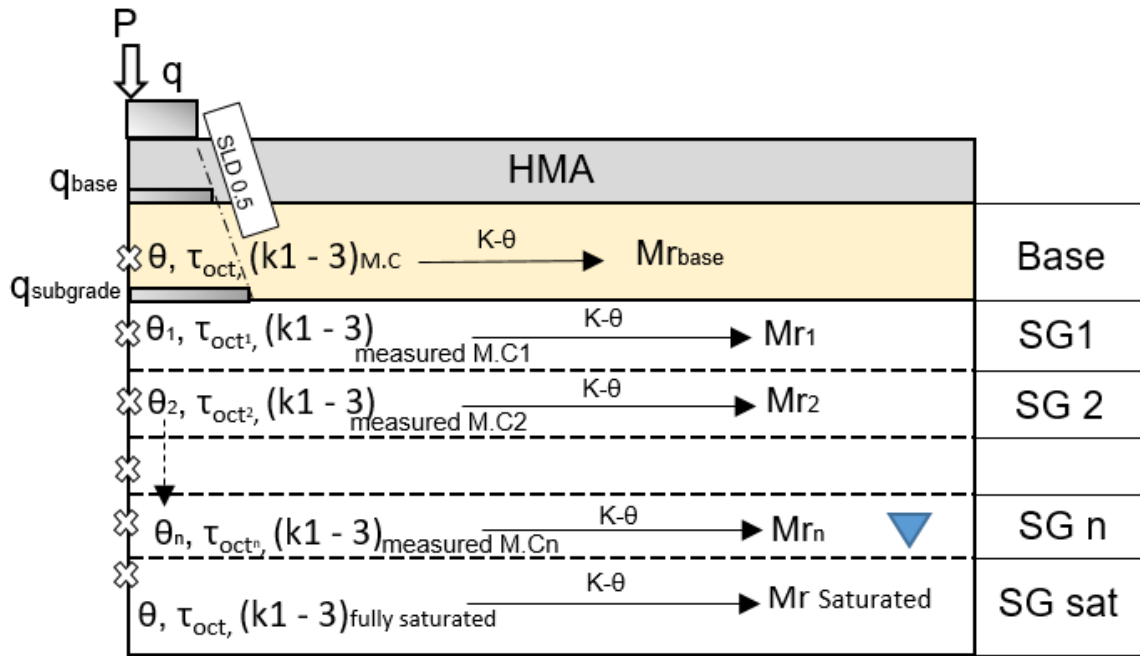
Method A



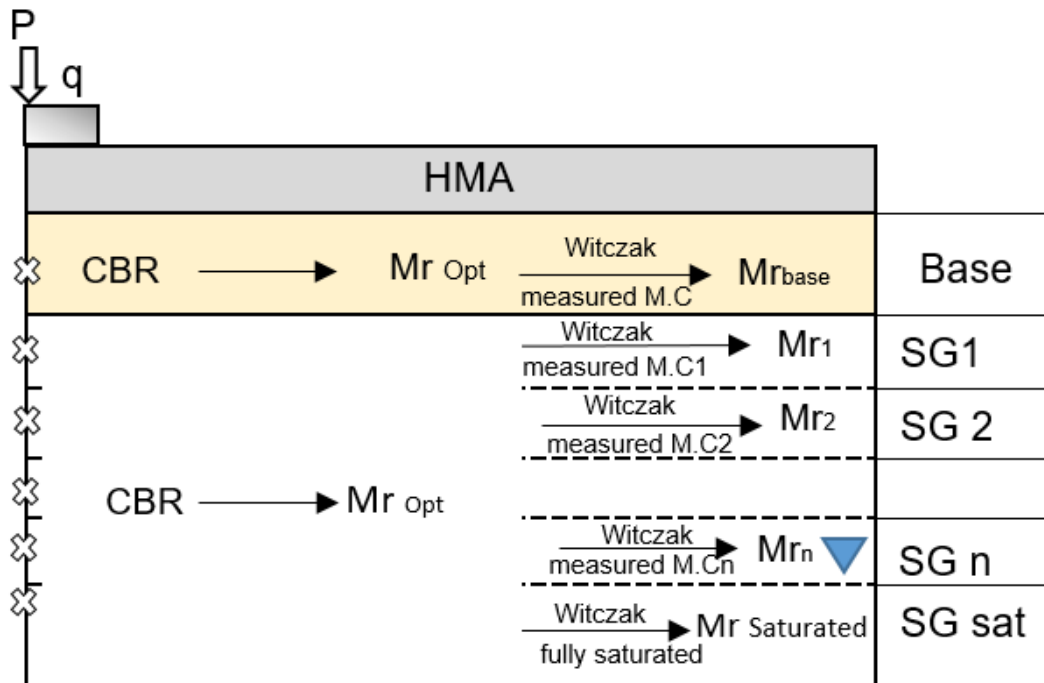
Method B



Method C



Method D



Method E

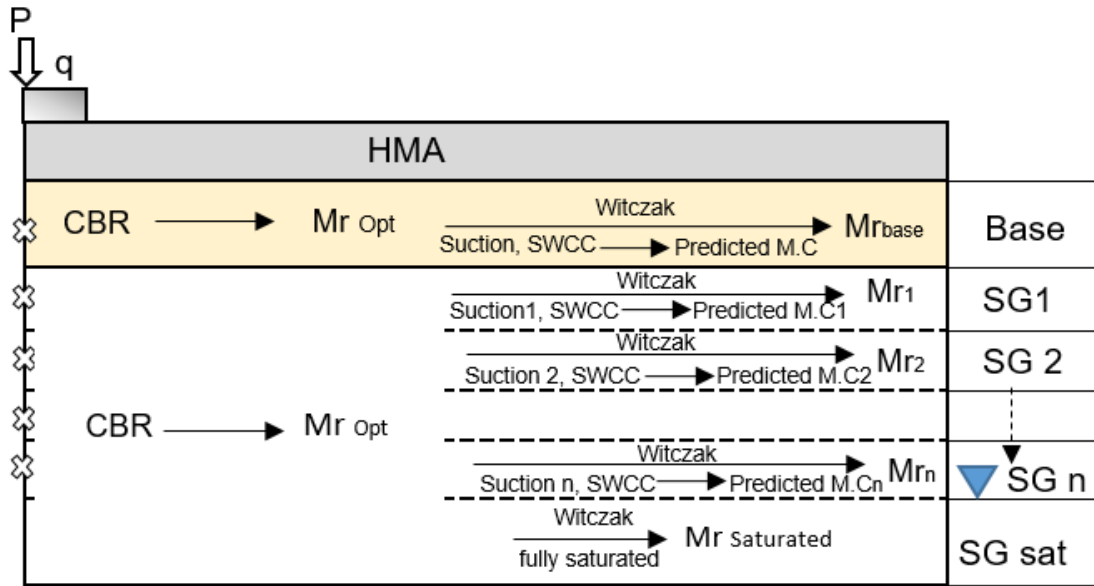


Figure 5.2. Schematic demonstration of the methods used to obtain stress and moisture-dependent resilient modulus

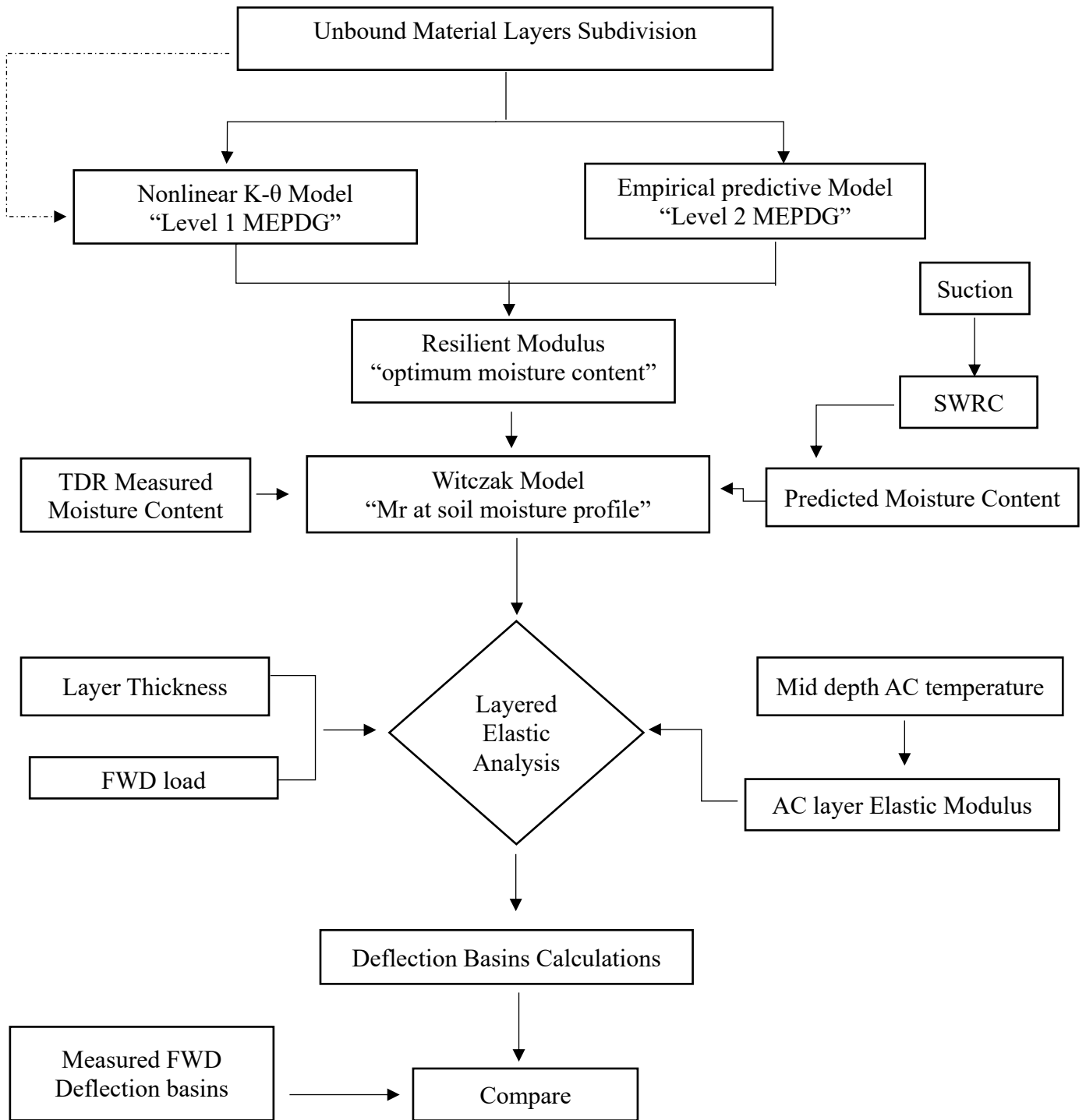
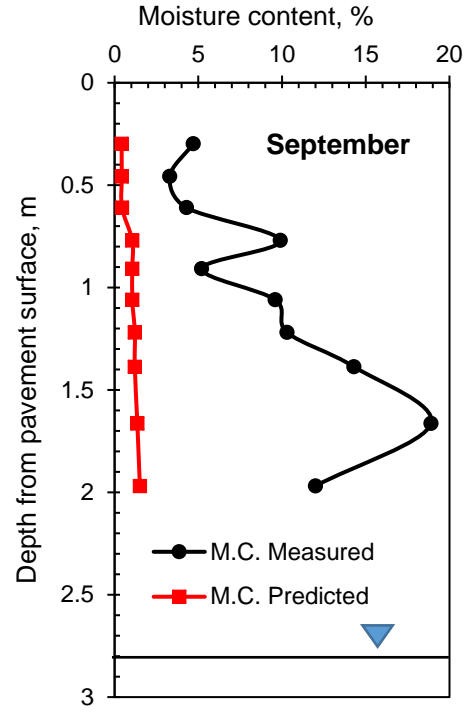
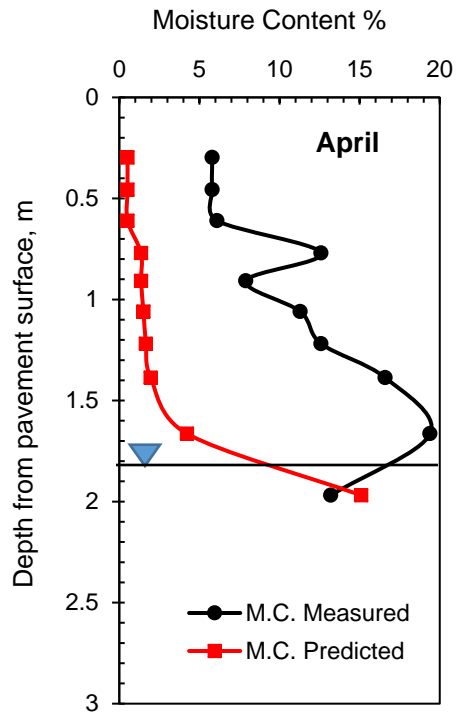


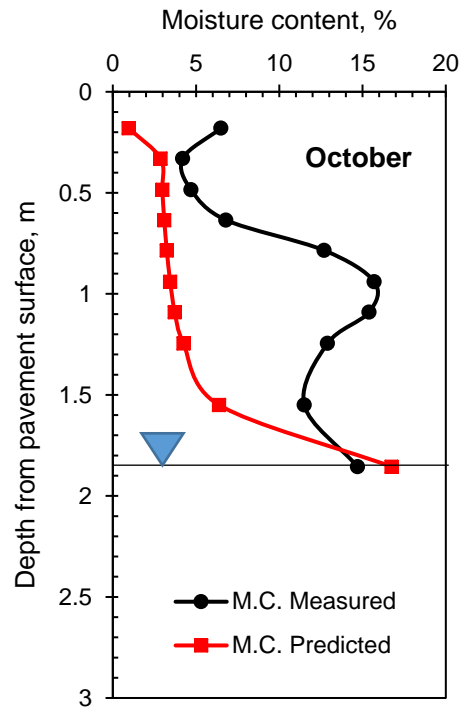
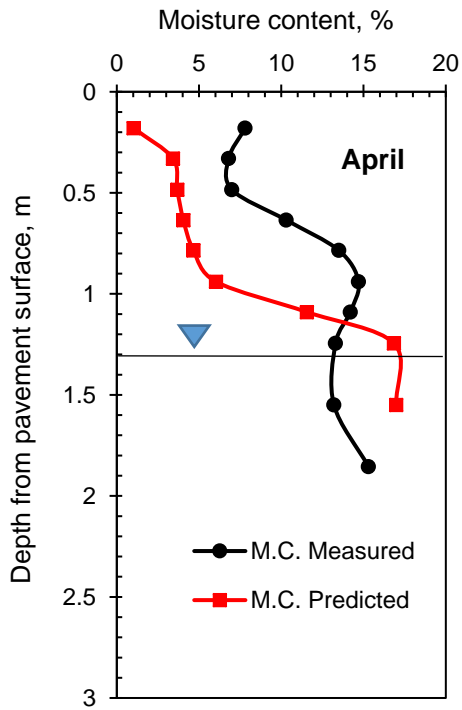
Figure 5.3. Flow Diagram of the procedure

5.4 RESULTS AND DISCUSSIONS

Figures 5.4 (a - d) show the TDR-based measured moisture content profiles and the predicted moisture content profiles (given suction and SWCC) and the depth to the groundwater table on different dates for the presented sections in Maine, Minnesota, Texas and Montana, respectively. The figures depicted that the groundwater table changes seasonally where it rises in the spring and drops in the fall. These figures illustrate that the predicted moisture contents from the hydrostatic pressure distribution method were less than the measured moisture content from TDR at coarse-grained soil (e.g. A-2-4 and A-3). On the other hand, fine-grained soils showed different behavior where the predicted moisture content was greater than the TDR measured moisture content for non-plastic material (A-4) and fluctuated for the plastic material (A-6). In other words, the difference between predicted and measured moisture content was based on how deep the groundwater table was, the potential infiltration system, the gradation, and the plasticity index of the material.



(a)



(b)

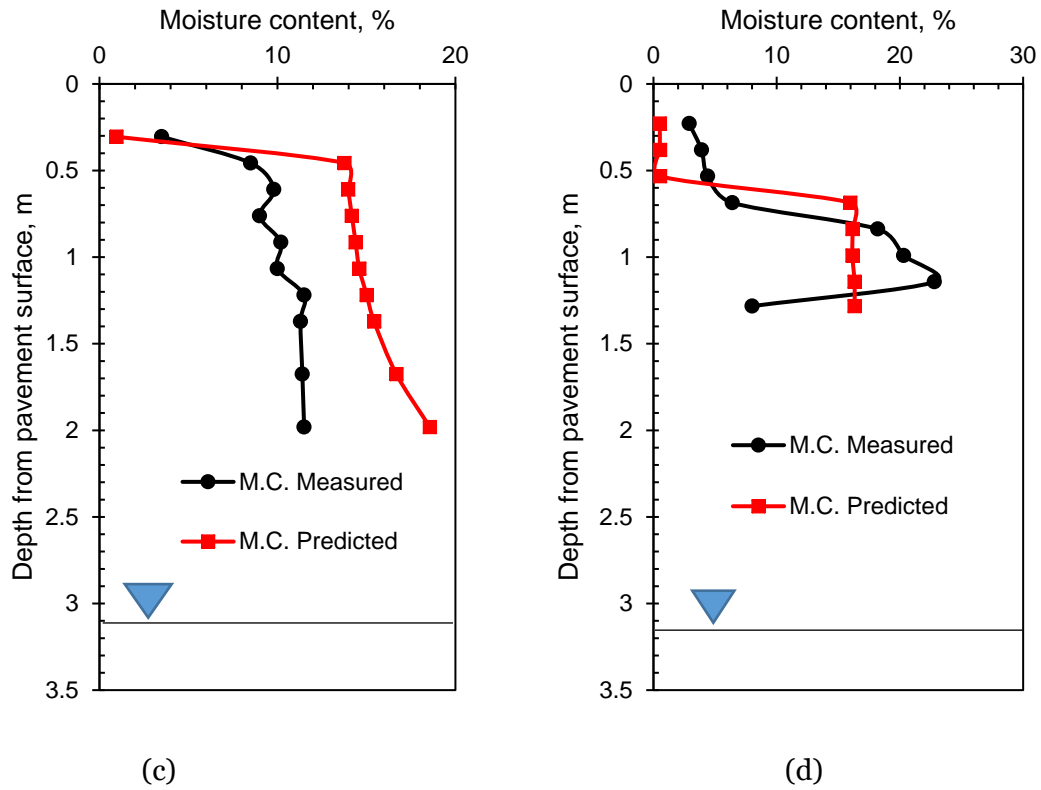


Figure 5.4. TDR Measured and Suction - SWCC predicted moisture content profiles for (a) Maine section; (b) Minnesota section; (c) Texas section; (d) Montana section

Figures 5.5 – 5.8 show the comparison between the average measured FWD deflection basins adjusted to 40 kN load with the associated standard deviation and the calculated deflection from layered elastic analysis using the five methods for the Maine, Minnesota, Texas and Montana sections, respectively. It can be seen that the shape of deflection basins for all the proposed methods was similar to the measured FWD deflection basin. However, the magnitude of the deflection basin varied between the proposed methods. This difference in the magnitude was based on the method that was used to define the resilient modulus at each sublayer.

For the section in Maine, Methods A, B and C which are considered the nonlinear resilient modulus based on the approximate approach to calculate the stresses and moisture variations overestimated the measured FWD deflection basin. On the other hand, the predicted deflection basins using empirical Methods D and E fitted reasonably well with the measured values. However, the differences in the magnitude of both Methods D and E were based on the distribution of the measured and predicted moisture content which resulted in a difference in resilient modulus of each sublayer, and therefore the predicted deflection basin.

It was originally expected that the deflection calculation from stress-dependent methods, i.e. Method A, B and C, would have been close to the FWD measured deflection; while they showed higher deflection. Thus, in order to improve the predicted deflection results, an iterative procedure was examined using KENLAYER non-linear analysis. This iterative method was accomplished by extracting the stresses at the mid-depth of each sublayer after the non-linear analysis. Then, the calculated stresses were used in Equation 5.3 to obtain the resilient modulus at optimum moisture content followed by moisture-dependency adjustment as explained before.

Furthermore, Method F incorporated the calculated stresses from the iterative solution and the adjusted resilient modulus using the TDRs measured moisture profile while Method G incorporated the calculated stresses from the iterative solution and the adjusted resilient modulus using predicted moisture profile. The findings from both Methods F and G, shown in Figure 5.5, still indicated higher deflection magnitude compare to the measured FWD deflection. The reason for this outcome could be due to the different parameters such as the nonlinear regression parameters (K_1 , K_2 , K_3) and the resilient modulus model that used in the KENLAYER software to calculate the stresses

which did not consider the octahedral shear stresses. Thus, it is recommended to perform triaxial lab measurements to obtain the nonlinear regression parameters and, then, deploy it into layer elastic analysis to calculate the stresses and the corresponding resilient modulus. For the rest of the analyses presented in this paper, only the approximate method to calculate the stresses and the corresponding resilient modulus (Methods A, B and C) was performed rather than the iterative method.

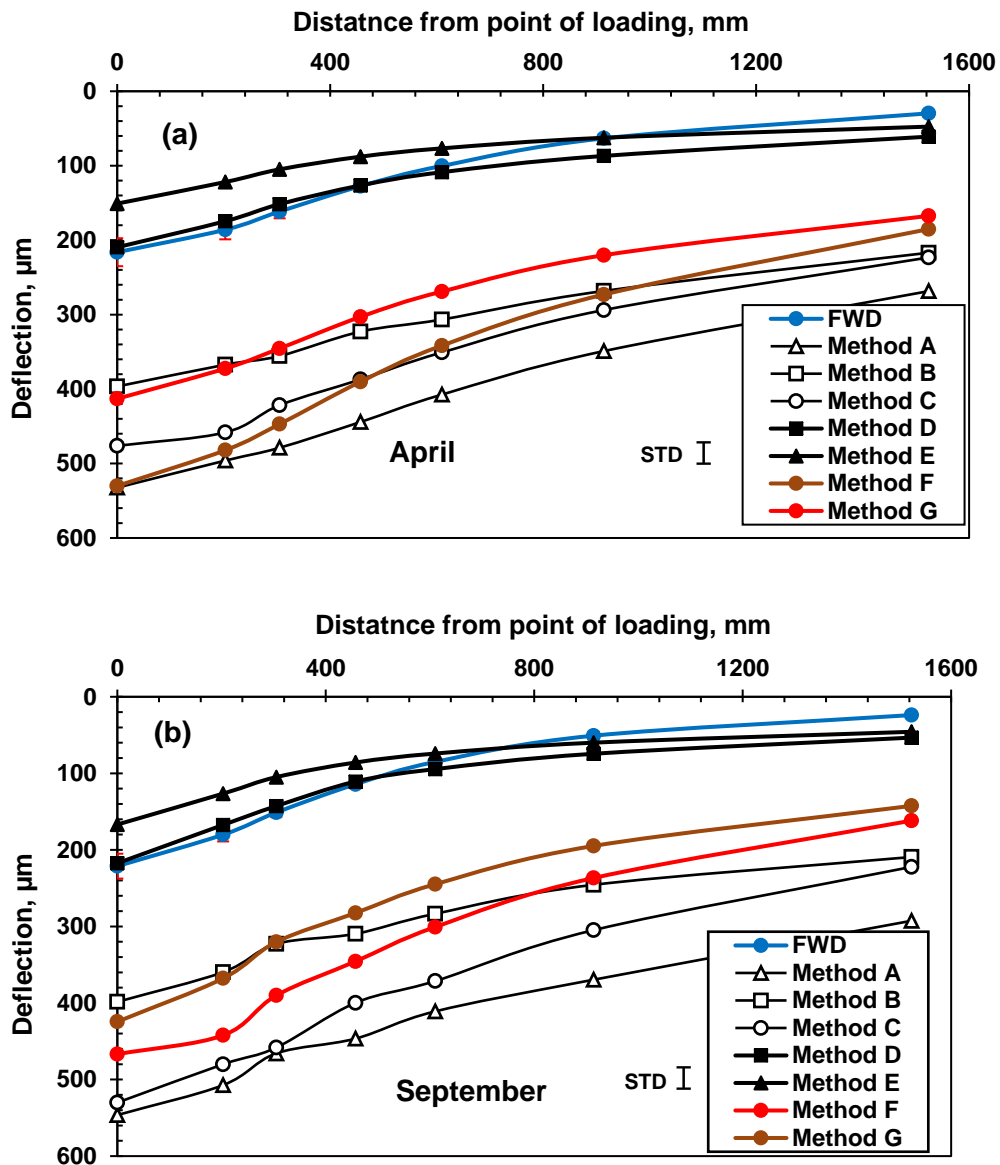
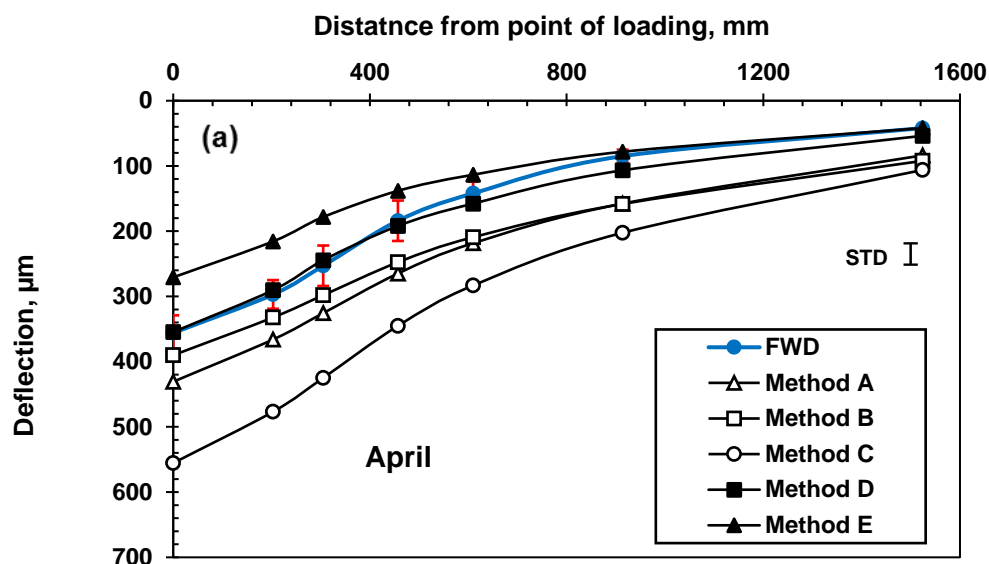


Figure 5.5. Measured and Predicted Deflection Basins for Maine Section (a) April (b)

September

For Minnesota section, the predicted deflection basins based on the TDRs' measured moisture content and using Methods A and C overestimated the FWD measured deflection. However, Method B that considered the nonlinear resilient modulus coupled with the predicted moisture content resulted in a very similar magnitude to the measured FWD deflection basin for the first three points. The differences in the deflection magnitudes could be due to the contribution of the moisture variation to analysis. Furthermore, the method that considered the CBR empirical model coupled with measured moisture content (Method D) matched very well with the measured FWD deflection basin. In contrast, Method E that considered the predicted moisture content profile in the analysis underestimated the measured FWD deflection values at all points except the furthest points; because the lower predicted moisture content resulted in stiffer unbound materials, and therefore, lower deflection values.



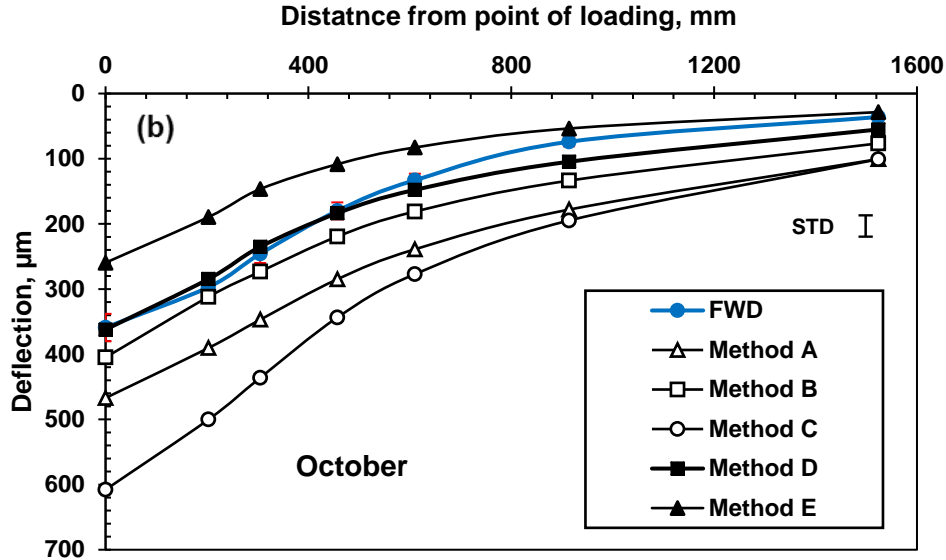


Figure 5.6. Measured and Predicted Deflection Basins for Minnesota Section (a) April (b) October

For Texas section, the predicted deflection basins for all the proposed methods overestimated the measured FWD deflection. Despite the differences in the presented methods to predict the resilient modulus of unbound materials at each sublayer, the predicted deflection basin from Methods A, C and E were very similar. The reason for this similarity is that these methods resulted in similar resilient modulus and therefore similar deflection basin. This means that the predicted resilient modulus for fine-grained soils did not substantially change in sublayers due to incorporating different parameters such as percent of fine materials, the plasticity of the material, bulk and octahedral stresses and moisture variation. Furthermore, Method B that considered the nonlinear analysis at each sublayer coupled with the predicted moisture content resulted in very large predicted deflections compared to the FWD measured deflections. This difference was due to the higher predicted moisture contents, which resulted in lower resilient modulus and therefore higher deflection. Consequently, Method D overestimated the measured values and resulted in the lowest predicted deflection among all other proposed methods.

Thus, Method D could be considered as a good indicator of the maximum deflection as shown in Figure 5.7.

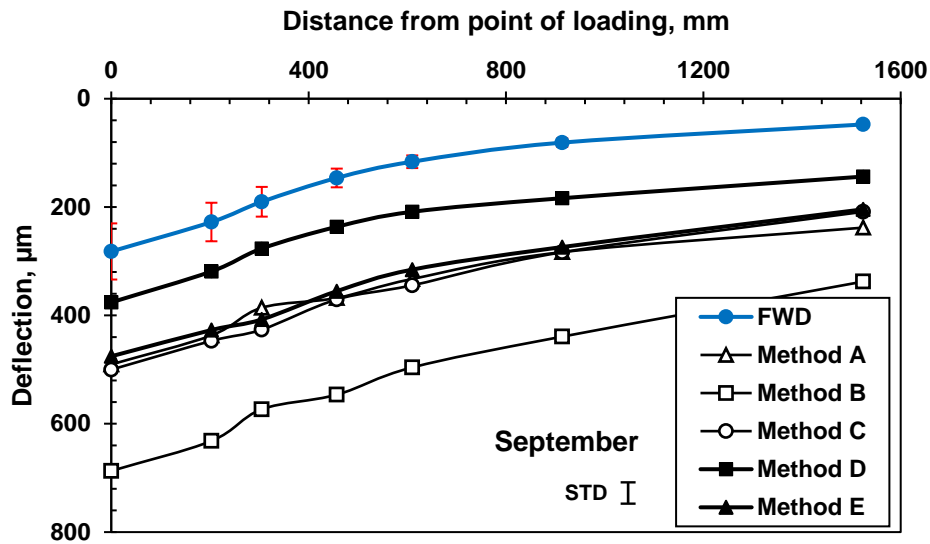


Figure 5.7. Measured and Predicted Deflection Basins for Texas Section

For Montana section, the predicted deflection from Methods A, B and C showed the same shape of as the measured deflection. However, the magnitudes of the predicted deflections from these methods were higher than the measured deflection. In contrast, Methods D and E showed different behavior; they underestimated the measured deflections in the first deflection points and overestimated the deflection basin in the rest of the deflection points. This difference was due to the moisture variation and the plasticity of the material, which resulted in a lower resilient modulus, and therefore, higher deflection. Although the predicted moisture contents at the subgrade sublayers were less than the measured moisture contents, the predicted deflections from Method B were larger than the predicted deflections from Method A. This might have been because of the plasticity of the material, which resulted in minimal differences in the predicted moisture content at different depths, and therefore, minimal difference in resilient

modulus. Despite the differences in the moisture contents of the base and subgrade layers between Methods D and E, they showed the same maximum deflection. The reason was that, in these cases, the stiff base compensated the weak subgrade with low resilient modulus; for example in Method E, the base layer was dry based on the predicted moisture content as shown in Figure 5.4 (d) resulted in higher resilient modulus for the base (stiff base material).

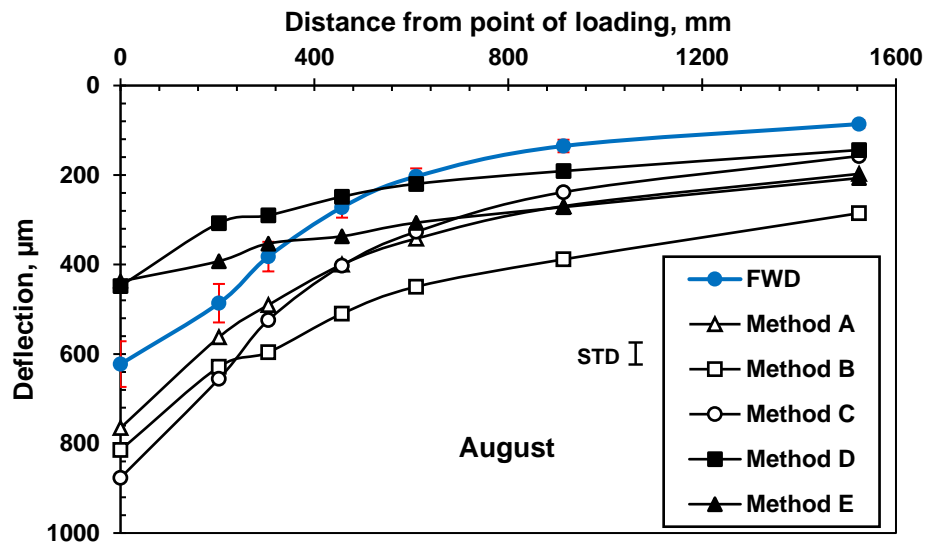


Figure 5.8. Measured and Predicted Deflection Basins for Montana Section

Based on the above analyses from Maine and Minnesota sections with the coarse-grained soils, when considering the stresses and nonlinearity of the unbound material at each sublayer in the analysis (Methods A, B, and C) the deflection can be considered conservative and practically acceptable with regards to mechanical response. However, this conservative prediction may result in uneconomical actions. On the other hand, using the CBR empirical models to obtain the resilient modulus coupled with the measured soil moisture content (Method D) can be a good indicator of the FWD deflection at different

groundwater table elevations for the overall pavement structure and the base layer. Moreover, CBR empirical models coupled with the predicted soil moisture content (Method E) would be only a good indicator of the behavior of subgrade soil.

Based on the above analyses from Texas and Montana sections with the fine-grained soils, the models that considered nonlinear material parameters resulted in larger deflections. On the other hand, Method D can be a good indicator for predicting the maximum FWD deflection in non-plastic materials. In contrast, considering the nonlinear analysis of unbound materials by incorporating the measured moisture content (Method A and C) could be a good predictor for FWD deflection basins in plastic materials, yet conservative and potentially not cost-effective.

5.5 SUMMARY AND CONCLUSIONS

The unbound materials are stress dependent, thus, any changes in the moisture will lead to the changes in the stress levels and consequently in the material properties. Five methods were introduced to estimate the pavement deflection response by incorporating the stress level and moisture variation in the resilient modulus of unbound materials. Four LTPP sections in different climatic zones with different material types were used to investigate the effect of each resilient modulus method on the pavement deflection response. All procedures involved dividing unbound layers into several sublayers in the layered elastic analysis to predict the in situ measured FWD deflection.

In general, there was a good agreement between the predicted deflection shape from layer elastic analysis and the FWD-measured deflection for the presented LTPP sections. However, there were differences in the deflection magnitudes among the modulus prediction methods. For the non-plastic soil materials, using the CBR empirical predictive model to estimate the unbound materials resilient modulus at optimum moisture content,

adjusting for the given moisture content, and implementing Layered elastic analysis (LEA) were shown to be relatively adequate to predict the in-situ FWD deflection basins. In contrast, based on this study, it is difficult to draw a firm conclusion for plastic soil materials since the predicted deflection basins from the approximate stress-dependent methods and CBR empirical models all overestimated the measured FWD deflection basin. If the pavement structural assessment has to be performed based on the furthest deflection points, which define the stiffness of the subgrade layer for coarse-grained soil material types, the approach that involved incorporating the predicted moisture content from the hydrostatic pressure distribution in the empirical predictive relationship between resilient modulus and soil index seems appropriate.

Future work is needed to conduct nonlinear parameters from lab measurements to be implemented in the presented methods and test different nonlinear resilient modulus models at the presented and different pavement sections with different materials to determine the most appropriate model to estimate the actual behavior of pavement response.

5.6 ACKNOWLEDEMENTS

The author would like to thank the Federal Highway Administration for acting as a project sponsor. Thanks, are also extended to the coauthors of this work: Dr. Majid Ghayoomi and Dr. Jo Sias Daniel, both of University of New Hampshire. The author also thanks Dr. Eshan Dave of University of New Hampshire for the feedback.

CHAPTER 6

BEARING CAPACITY ANALYSIS OF PAVEMENT STRUCTURES FOR SHORT TERM FLOODING EVENTS

6.1 INTRODUCTION

The assessment of the load carrying capacity of a flooded pavement structure is complex due to numerous unknown parameters. The necessity of applying load restrictions on pavements that have been flooded mainly depends on the integrity of the pavement structure. This makes it difficult for agencies to decide based on visual inspection alone because of the unknown behavior or conditions of the saturated unbound materials beneath the pavement surface subjected to traffic loads. An incorrect assessment of the bearing capacity of an inundated pavement may lead to severe damage or sudden failure of the pavement structure.

Unbound layers in pavement structure such as base, subbase, and subgrade soil play a critical role in the overall performance of the pavement, particularly when moisture contents are at or near fully saturated conditions. The changes in water content can result in degradation of the stiffness and strength of the pavement materials and consequently reduction of the load bearing capacity of the road. A large portion of pavement damage is attributed to the presence of excess pore water in soils that led to lower effective stress and strength. Heavy traffic loading can potentially cause pavement failure during flooding if no traffic restrictions are enforced. Thus, it is essential to investigate the effect of water saturation on the soil bearing capacity and whether the soil can carry the loads applied on the pavement without experiencing excessive deformation or shear failure.

In pavement engineering practice, load bearing capacity can be obtained using tests such as Falling Weight Deflectometer (FWD), Dynamic Cone Penetrometer (DCP), or California Bearing Ratio test (CBR). In geotechnical engineering, the bearing capacity is controlled by the shear strength mobilized on the failure slip surface. The concept of foundation bearing capacity in saturated soil was developed by Terzaghi (1943) using conventional soil mechanics. Recently, several researchers investigated the bearing capacity of unsaturated soils where the soil layer is above the groundwater table (Broms 1963, Steensen-Bach et al. 1987, Miller and Muraleetharan 1998, Costa et al. 2003). All these studies have shown substantial influence of matric suction on the bearing capacity of unsaturated soils.

The type of pavement failure depends on the factors influencing the pavement structure; including: 1) functional failure that occurs due to the degree of surface roughness 2) Structural failure where the pavement structure is incapable of sustaining the imposed loads on the pavement surface (Christopher et al. 2006). The latter failure might be expected if it occurs due to the repeated loads over time at the end of the pavement design life or unexpected when very small number of cycles of excessive overload are applied or the pavement material is weakened. Soil bearing capacity failure is categorized as a structural failure where the subgrade soil cannot further sustain the required capacity. Therefore, the shear failure in flexible pavements under excessive water and post-flooding loading could be assessed using the concept of shear failure in soils.

The objective of this investigation is to provide a methodology to evaluate the structural capacity of flooded pavements in order to avoid sudden failures due to relatively small number of passes over a severely weakened pavement structure. This is accomplished by

estimating the bearing capacity of pavement systems with saturated and unsaturated soils by incorporating a matric suction profile, the saturated shear strength parameters (i.e. c' and ϕ'), and Soil Water Characteristics Curves (SWCC). The bearing capacity was calculated under different moisture conditions ranging from unsaturated to flooded, fully saturated condition. The flooded condition was achieved by raising the water table from an initial hydrostatic pressure distribution for a generic site. The load distribution in the subgrade soil was estimated assuming a 1:1 slope in depth. Finally, the maximum tire load on the pavement surface was back calculated based on the computed load bearing capacity of the soil layer using layer elastic analysis. Layer elastic analysis was performed by incorporating matric suction in resilient modulus of unsaturated subgrade soil layer divided into sublayers (152.4 mm each) up to the groundwater table to evaluate the nonlinearity of the soil layer. This information can assist agencies and town planners determine when traffic should be allowed considering ultimate failure criteria.

6.2 MATERIALS AND METHODS

6.2.1 Material Characterization

Three different pavement sections (Table 6.1) with three different types of subgrade soil and varying Ground Water Table (GWT) levels were evaluated. The subgrade soils represent a range of common subgrade materials from across the U.S. For this study, the soil physical properties were obtained from Arizona State University soil map application (NCHRP 9-23b, 2012) for sites in New Hampshire, Texas, and Vermont.

Table 6.1. Pavement cross sections and material properties

| Pavement Layer | Surface | Base course | Subgrade |
|-----------------------|-------------------------------------|---|--------------------------------------|
| Properties | Asphalt concrete E = 2000 MPa | Crushed stone (A-1-b) E = 262 MPa | A-2-4 (NH) A-4 (TX) A-7-5 (VT) |
| Section # | Thickness (mm) | | |
| 1 | 76.2 | 152.4 | infinite |
| 2 | 152.4 | 304.8 | |
| 3 | 203.2 | 406.4 | |

Measured laboratory values were not available for all of the soil properties required for the analysis in this project. Therefore, established relationships were used to estimate the water content, degree of saturation, specific unit weight, void ratio, and dry densities from physical soil indices. The Equations from the Enhanced Integrated Climate Model (EICM) in the Mechanistic - Empirical Design guide (MEPDG) developed under NCHRP projects 1-37A were used and are shown in Equations 6.1-6.6 below:

$$S_{opt} (\%) = 6.752(WPI)^{0.147} + 78 \quad (6.1)$$

$$G_s = 0.041(WPI)^{0.29} + 2.65 \quad (6.2)$$

$$S \times e = W \times G_s \quad (6.3)$$

$$\rho_{dry} = \frac{G_s \times \gamma_w}{1+e} \quad (6.4)$$

$$W_{opt} (\%) = 8.6425 D_{60}^{-0.1038} \quad \text{If PI} = \text{zero} \quad (6.5)$$

$$W_{opt} (\%) = 1.3(WPI)^{0.73} + 11 \quad \text{If PI} > \text{zero} \quad (6.6)$$

where:

WPI = Percent of passing#200 × plasticity index, D60: Grain diameter corresponding

to 60% passing by weight or mass (mm), S_{opt} : degree of saturation at the optimum moisture content, W_{opt} : optimum moisture content, e : void ratio, ρ_{dry} : max dry density of the soil, G_s : specific gravity

Table 6.2 shows the estimated soil properties determined from the above Equations and the effective cohesion (c') and effective internal friction angle (ϕ') estimated based on the soil properties from the Swiss Soil Standard.

To begin the analysis, the water table was placed at an elevation equivalent to the top of the subgrade layer to simulate a fully saturated soil. The water table was then lowered in 152.4 mm intervals down to 25 meter below the pavement surface. The matric suction was set to zero for saturated soils while a hydrostatic capillary suction was calculated from Equation 6.7 for soils above the water table. The subgrade soil above the water table was divided into sublayers where the matric suction in each sublayer was calculated at the mid height with an initial hydrostatic capillary pressure distribution.

$$u_a - u_w = \gamma_w h \quad (6.7)$$

where: u_a is pore air pressure = zero in this case, u_w is pore water pressure = $-\gamma_w h$, γ_w is unit weight of water, h is the average distance from the point of interest to the groundwater table for a period of time for which the GWT has been fairly stable.

Table 6.2. Properties of the selected soils

| Soil Type | A-2-4 | A-4 | A-7-5 |
|--|--------------|------------|--------------|
| Percent Passing # 200 | 22.5 | 80 | 92.5 |
| Liquid Limit (L.L) | 17.5 | 26 | 60 |
| Plasticity Index (PI) | 0 | 9 | 30 |
| Specific Gravity (G_s) | 2.650 | 2.723 | 2.757 |

| | | | |
|--|-------|-------|-------|
| Void Ratio (e) | 0.34 | 0.52 | 0.80 |
| Max Dry Density (gm/cm³) | 1.980 | 1.798 | 1.535 |
| W_{opt} % | 10 | 16.50 | 25.71 |
| S_ropt % | 78 | 87 | 89 |
| Cohesion (c') | 0 | 7 | 25 |
| Internal friction angle (φ') | 39 | 41 | 31 |

The Soil-Water Characteristic Curve (SWCC) proposed by Fredlund and Xing (1994) available in the EICM and widely used in the pavement practice was used to predict the degree of saturation from suction at each layer, as shown in Equations 6.8 and 6.9 (NCHRP 1-37 A, 2000).

$$S = C(h) \times \left[\frac{1}{\left[\ln \left[\exp(1) + \left(\frac{h}{a} \right)^b \right] \right]^c} \right] \quad (6.8)$$

$$C(h) = \left[1 - \frac{\ln \left(1 + \frac{h}{h_r} \right)}{\ln \left(1 + \frac{10^6}{h_r} \right)} \right] \quad (6.9)$$

where

S: Degree of saturation, a, b, c, h_r: fitting parameters to the Equation.

Perera et al. (2005) proposed relationships to predict the fitting parameters of the Fredlund and Xing Equation based on soil index properties as follows (NCHRP, 2004):

- Correlations for Soils with PI > 0 (For Plastic materials)

$$a = 0.00364(wPI)^{3.35} + 4(wPI) + 11 \quad (6.10)$$

$$\frac{b}{c} = -2.313(wPI)^{0.14} + 5 \quad (6.11)$$

$$c = 0.514(wPI)^{0.465} + 0.5 \quad (6.12)$$

$$\frac{h_r}{a} = 32.44e^{0.0186(wPI)} \quad (6.13)$$

- Correlations for Soils with PI = 0 (For granular soils with Plasticity Index equal to zero)

$$a = 0.8627(D_{60})^{-0.751} \quad (6.14)$$

$$\bar{b} = 7.5$$

$$c = 0.1772 \ln(D_{60}) + 0.7734 \quad (6.15)$$

$$\frac{h_r}{a} = \frac{1}{D_{60} + 9.7e^{-4}} \quad (6.16)$$

where \bar{b} = Average value of fitting parameter b.

Figure 6.1 depicts the predicted SWRC for New Hampshire soil (A-2-4), Texas soil (A-4) and Vermont soil (A-7-5) plotted as the relationship between the degree of saturation (Sr) and matric suction (ua-uw) using the Fredlund and Xing and Perera's correlation models. The soils with more fine materials and more plasticity have higher air entry values ranging from 2 kPa for A-2-4 to 14 kPa for A-4 and 90 kPa for A-7-5 soils. It means if the matric suction is beyond these specified values, the soil exhibits unsaturated condition rather than fully saturation condition. As expected, increasing the matric suction decreases the degree of saturation.

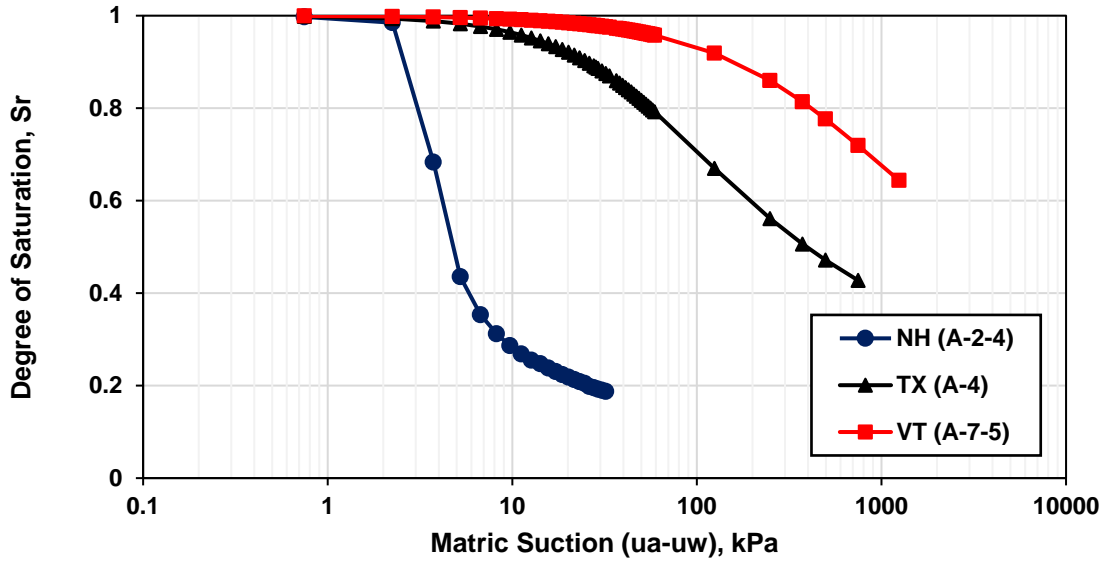


Figure 6.1. Predicted SWRC for the proposed soils

Available correlations between strength and stiffness of unbound materials and physical soil indices were employed to estimate the CBR and resilience modulus (M_r) of the proposed soils at an optimum moisture content as in Equations 6.17 and 6.18, respectively.

$$CBR = \frac{75}{1+0.728(wpl)} \quad (6.17)$$

$$M_r = 2555(CBR)^{0.64} \quad (6.18)$$

Then, the resilience modulus of subgrade soil at different degrees of saturation was estimated using Witczak model in EICM (NCHRP 1-37 A, 2000) as provided in Equation 6.19 given the optimum moisture content and the corresponding degree of saturation.

$$\log \frac{M_R}{M_{Ropt}} = a + \frac{b-a}{1+\exp\left[\ln\frac{-b}{a}+k_m(S-S_{opt})\right]} \quad (6.19)$$

where M_R/M_{Ropt} = resilient modulus ratio; M_R = resilient modulus at any degree of saturation; M_{Ropt} = resilient modulus at a reference condition; a = minimum of log

MR/MR_{opt}, b = maximum of log MR/MR_{opt}; km = regression parameter; and S-S_{opt} = variation in degree of saturation expressed in decimals. Using the available data from the literature and assuming a maximum modulus ratio of 2.5 for fine-grained materials and 2 for coarse-grained materials, the values of a, b, and km for coarse-grained and fine-grained materials are summarized in Table 6.3 (Witczak et al., 2000)

Table 6.3. Regression parameters of Equation 6.19

| Parameter | Coarse-grained materials | Fine-grained materials |
|----------------|--------------------------|------------------------|
| a | -0.3123 | -0.5934 |
| b | 0.3 | 0.4 |
| k _m | 6.8157 | 6.1324 |

6.2.2 Bearing Capacity Calculation Procedure

In a pavement system truck loads are transmitted from the pavement surface to underlying layers including subgrade soil. In this study, the radius of the tire on the pavement surface (r) was computed based on the load of 40 kN and tire pressure of 0.827 MPa. Then, the tire on the soil surface was estimated based on 1:1 pressure distribution as a conservative distribution angle of the stresses on the soil. Then, the load distribution at the top of the subgrade was treated as a circular footing for bearing capacity analysis.

The conventional method to estimate the ultimate bearing capacity in saturated soils for circular footing was proposed by Terzaghi 1943 as in Equation 6.20

$$q_u = 1.3c'N_c + \gamma DN_q + 0.3\gamma BN_\gamma \quad (6.20)$$

where: q_u = ultimate bearing capacity; c' = effective cohesion; γ = unit weight; D = footing base level, m; B = footing width; the diameter in the case of circular footing; N_c, N_q, N_γ = bearing capacity factors.

Vanapalli et al. (1996) proposed a modified form of Terzaghi's Equation for a surface

footing with respect to matric suction using effective shear strength parameters and shape factors proposed by Vesic (1973) in Equation 6.21. This Equation is the same as Equation 6.20 if the matric suction is zero. Therefore, this Equation can capture a smooth transition between saturated and unsaturated soil.

$$q_u = 1.3[C' + (u_a - u_w)_{avg} S^\psi \tan \phi'] N_c \left[1 + \left(\frac{N_q}{N_c} \right) \left(\frac{B}{L} \right) \right] + 0.3\gamma B N_\gamma \left[1 - 0.4 \left(\frac{B}{L} \right) \right] \quad (6.21)$$

$$\psi = 1 + 0.34(I_p) - 0.0031(I_p^2) \quad (6.22)$$

where: $(u_a - u_w)_{avg}$ = average matric suction, ϕ' = effective friction angle ; S = degree of saturation, ψ = bearing capacity fitting parameter proposed by Vanapalli et al. (2007)

The bearing capacity factors for cohesion (N_c) and surcharge (N_q) by Terzaghi were used in this analysis while the bearing capacity factor for the unit weight was utilized from Kumbhokjar (1993). The reason behind the proposed bearing capacity factors were because these show a good correlation between predicted and measured soil bearing capacity according to Vanapalli et al. 2007

The average matric suction values for the selected soils were calculated from the soil surface to the bottom of the influence stress zone; in this study considered to be 1.5B to the depth that there is a significant distribution of stress in soil (Chen 1999). Then, the degree of saturation was estimated from the soil water retention curve (Figure 6.1). Figure 6.2 shows a schematic of the proposed method.

vertical stresses on the pavement layer from the ultimate bearing capacity on the soil was computed as a proportion of the actual vertical stress of 0.827 MPa on the pavement surface and the resultant stresses on the top of soil layer at different degrees of saturation.

6.3 RESULTS AND DISCUSSIONS

The changes in bearing capacity with groundwater table level for the selected subgrade soils and the three different pavement structures are shown in Figure 6.3. For the A-2-4 soil, the pavement structure has a significant impact on the bearing capacity, with the thickest pavement structure showing more than twice the bearing capacity of the thinnest pavement structure. The bearing capacity increases quickly as the water table drops (shallow slope at the top portion of the curve), and then continues to increase, but at a much slower rate once the GWT drops below an effective depth. The effective depth depends on the thickness of the pavement structure: 1 meter for the thinnest pavement structure and 2.30 meter for the thickest pavement structure. The silty (A-4) and clayey (A-7-5) soils show different behavior. There is only a small impact of the pavement thickness on the bearing capacity and the bearing capacity increases at a relatively constant rate as the GWT drops up to an effective depth. The effective depth for A-4 and A-7-5 soils are 6 meter and 12 meter from pavement surface respectively for all pavement structures. Then, below that effective depth the bearing capacity increases at a minimal rate then remains stable. For the A-2-4 soil, there is a discontinuity in the curves for the two thicker pavement structures at a depth of 1.5B where the degree of saturation changes from 85% to 60%.

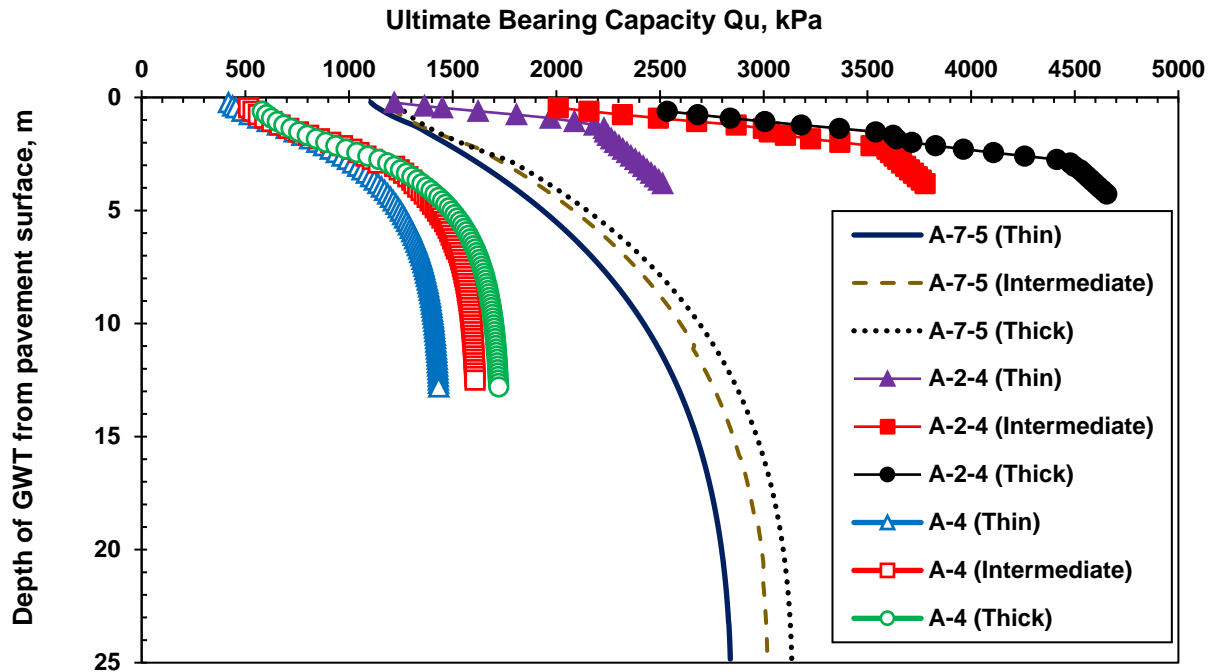


Figure 6.3. Variation of bearing capacity with groundwater table levels for the proposed soils

Figure 6.4 shows the ratio of bearing capacity as the water table drops to the bearing capacity under full saturation conditions. The bearing capacity ratio increases quickly as the GWT drops to the effective depth then below that depth the bearing capacity increases at a slower rate for all soils. The bearing capacity ratio increases to 1.8 for A-2-4 soil and from 2.5 to more than 3 times for A-4 soil as the GWT drops to the effective depth with differences in ratios for the different pavement thicknesses. The pavement thickness does not significantly affect the ratio for the A-7-5 soil. The slope of bearing capacity ratio for the A-7-5 material is steeper than the A-2-4 and A-4 soil types. This is may be because of the gradation, plasticity and the infiltration rate of the material type. It can be seen from both Figures 6.4 and 6.5 that the load bearing capacity of the coarse grain soils is greater than the bearing capacity of the fine grain soils at specific water content due to the gradation and mechanical properties of the materials; i.e. c' and φ'

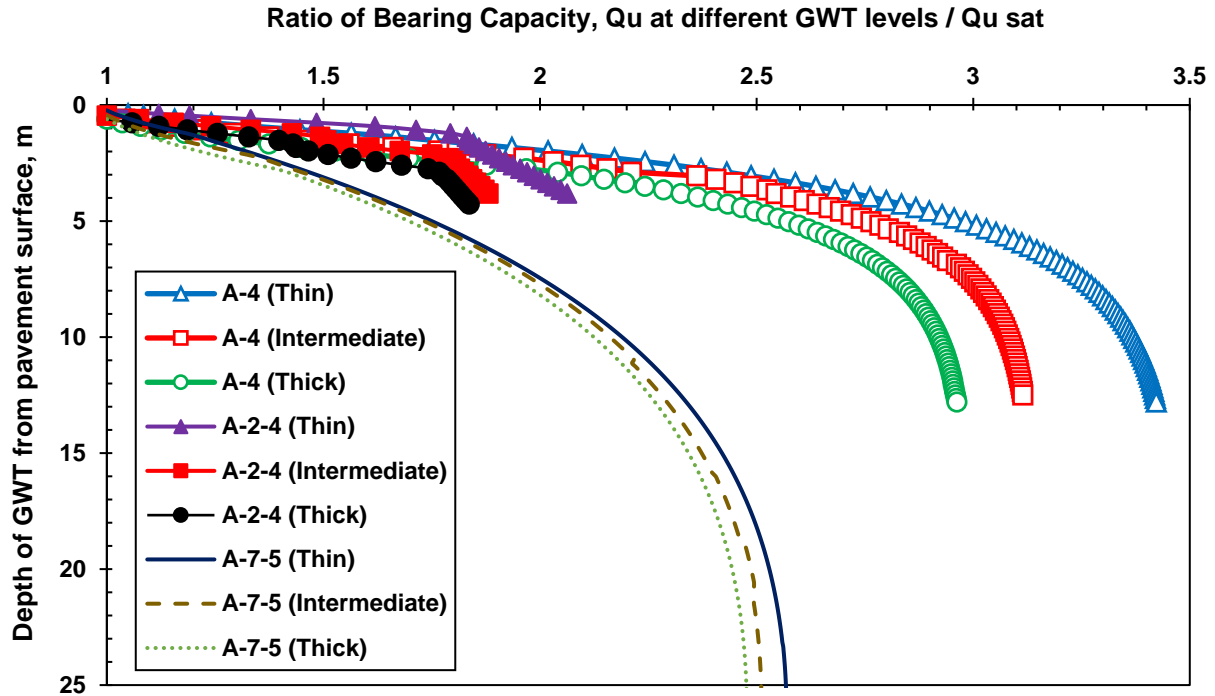


Figure 6.4. Ratio of bearing capacity with groundwater table levels for the proposed soils

Figure 6.5 shows the maximum tire load (assuming a tire pressure of 0.827 MPa for single axle single tire load) that the pavement cross section could withstand without shear failure of the subgrade. Under most conditions evaluated, the pavements will have sufficient capacity to carry most practical tire loads. The trends in the results are still valuable for understanding pavement performance and valuable for the airport applications. It can be seen that for all soil types there is a significant impact from different pavement structures. A-2-4 soil type shows the largest difference between load magnitudes at three pavement cross sections and the lowest difference is for the A-4 soil type. This is may be because of the saturation of the soil and the influence of the stress zone. Despite the difference of the gradation, plasticity and shear strength parameters for A-2-4 and A-7-5 soil types; soil types behave similarly in the thin pavement structure.

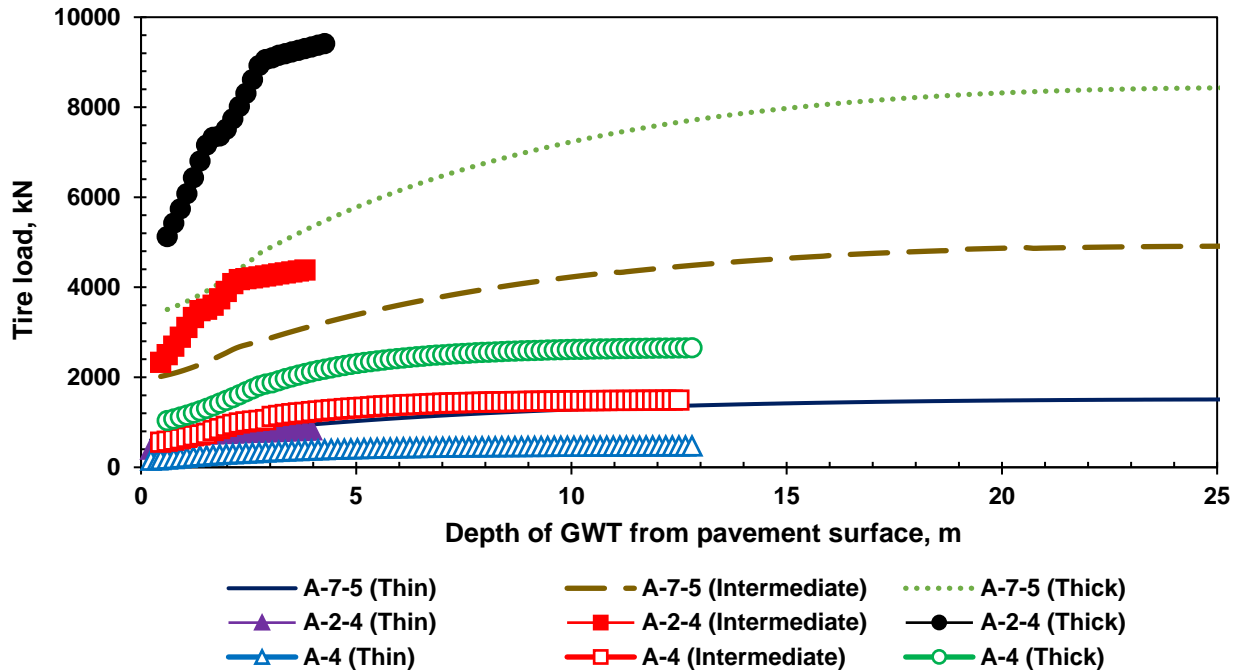


Figure 6.5. Tire loads at ultimate bearing capacity at groundwater table levels for the proposed soils

6.4 SUMMARY AND CONCLUSIONS

With a goal of assessing the load carrying capacity of a flooded pavement structure and assisting agencies in decisions on when to apply traffic restrictions, the bearing capacity of the pavement structure post flooding were evaluated using the theory of shear failure in soils. The bearing capacity of the selected soils was calculated using modified Terzahi's formula including the effect of matric suction and shear strength parameters c' and ϕ' for three different flexible pavement cross sections. Layer elastic analysis was used to back calculate the traffic load that meets the bearing capacity of the pavement system. The following conclusions are drawn based on the observations.

- The theory of shear failure in soils with contribution of matric suction and soil water characteristic curve can be applied to pavement practice to evaluate the potential for sudden failure of a flooded pavement structure. By incorporating the matric suction

in the analysis, bearing capacities are larger than those determined from the fully saturated condition.

- The load bearing capacity of the pavement with coarse grain soil is greater than the ones of fine grain soils due to the higher shear strength.
- For A-2-4 and A-4 soils and thin pavement structures, of the location of the groundwater table does not have a large impact on the pavement bearing capacity. There is a significant impact from different pavement thicknesses and groundwater table variation on pavement bearing for A-7-5 subgrade soils.
- The effective water table zone in which dramatic changes in capacity occur was shown to be dependent on the subgrade material.
- The effective depth was shown to depend on the pavement thickness for A-2-4 soil type but not for A-4 and A-7-5 soil types.
- The pavement structure significantly changes the tire loads as the water table recedes down to the effective depth.
- For the thinnest pavement structure, the tire loads on the pavement surface are shown to be similar for all three subgrades despite the difference in ultimate bearing capacity for each soil.

The use of this information can be adapted to develop more comprehensive engineering-based approach for agencies to evaluate the bearing capacity of the flooded pavements to avoid any sudden failure. This study is limited to the three soil material types, it is essential to investigate more soil material types with different properties to verify and validate this approach. Future work will be investigated more soil material types and validate the approach using sections from SMP-LTPP at different environmental

conditions.

6.5 ACKNOWLEDGEMENTS

The author would like to thank the Federal Highway Administration for acting as a project sponsor. Thanks, are also extended to the coauthors of this work: Dr. Majid Ghayoomi and Dr. Jo Sias Daniel, both of University of New Hampshire. The author also thanks Dr. Eshan Dave of University of New Hampshire for the feedback.

CHAPTER 7

SUMMARY AND CONCLUSIONS

In the aftermath of flood events, the decision to open roads for traffic are based on the assessment of the pavements, which relies on visual inspection and experience. An incorrect assessment of the flooded pavement structural capacity due to unforeseen conditions may lead to unexpected outcomes or failure. Hence, the development of guidance is essential to advance the current knowledge of flooded pavement behavior based on their performance properties and structural capacities.

Throughout this dissertation, five technical chapters were developed to improve understanding of how pavements perform under flooded conditions and how performance changes as the flood waters recede and moisture contents return to normal. The goals of these studies were to identify the important parameters that affect the performance of inundated pavements, present an alternative method to estimate the in-situ measured FWD deflection, identify the critical influence depth of subsurface water level for allowable damage post flood events, and present a method for estimating the bearing capacity of pavements in short term flooding events to avoid any sudden failure. A short summary of each technical chapter is provided below, as well as further remarks relating to future work.

The assessment of the structural capacity of inundated pavements is vital to avoid damage in the pavement structure. Parameters such as traffic loads and environmental factors are not easily obtained during a flooding event; consequently, it is difficult to accurately assess the performance of inundated pavements due to the combination of these

parameters. In Chapter 2, a study has been presented to accurately determine the most critical parameters that affect the performance of inundated pavements and to determine how much the uncertainty in different pavement properties impacts the pavement response. The influence of layer thickness, unbound material types, interlayer bond conditions and traffic loading types was examined for a series of pavement cross sections using two methods; mechanistic approach using layered elastic analysis and empirical approach using 1993 AASHTO design method. The parameters were tested using analysis of variance techniques. The findings show that the most important parameters for the assessment of rutting pavement performance are the base and subgrade material characterization. Accurate information on the base-layer thickness, interlayer bond conditions, and traffic types are required to accurately assess the fatigue performance of inundated pavements. The results presented in this chapter will assist agencies through improvements in understanding of how pavements perform under flooded conditions and identifying the most important parameters to gather for the assessment pavements post flood events.

Chapter 3 presents methods to incorporate the measured soil moisture profile into flexible pavement evaluation and investigates how the change in the groundwater table will affect the pavement deflection. Four methods were developed to estimate a moisture-dependent resilient modulus from field data. Parameters such as moisture content, unbound material types, groundwater table, depth to bedrock, AC temperature and layer thickness were utilized in the layered elastic analysis to estimate in-situ FWD measured deflection. The findings show that the most accurate method of estimating in-situ FWD measured deflection is to divide the subgrade layer above the groundwater table into several layers. This method will assist agencies in assessing the structural capacity of

pavements as an initial estimate of FWD pavement deflection if an appropriate moisture content profile is used and the limitation is considered correctly.

It is well known that post flood events, the floodwaters recede and the subsurface water levels substantially changes in the unbound material layers. Changes in subsurface water level causes variation in saturation within the unbound material layers, resulting in unknown behavior of pavements under these circumstances. In Chapter 4, the variation of the subsurface water levels in the unbound materials was examined to study the impacts on the structural capacity of pavements. This study has been done using the matric suction as an indirect way to obtain the resilient modulus of unsaturated layers divided into sublayers. The estimated in-situ FWD deflection, the horizontal strain at the bottom of asphalt layer and the vertical strain at the top of subgrade layer were evaluated at different subsurface water levels. When the base and subgrade layers are fully saturated, the pavement structure will significantly lose its strength. Strength begins to recover when the subsurface water level drops below the base course layer. Gradation and plasticity of unbound materials are one of the most critical parameters involving in determining the structural capacity of pavements. This study will enable agencies to determine the influence subsurface water level at which the road can withstand traffic with minimum deterioration.

The pavement unbound materials are stress dependent. Changes in the moisture content, density, traffic, etc. will change the stress level and, therefore, the material behavior. In Chapter 5, the effect of stress dependency coupled with moisture sensitivity of unbound materials on the deflection response was examined. Several methods for estimating stress and moisture dependent resilient modulus have been developed to estimate the in-situ measured FWD deflection using four LTPP sections with different material types. The in-

situ FWD deflection was estimated using the method of dividing unbound layers into several layers in layered elastic analysis. The findings show that for the presented plastic soil material, the approximate and iterative methods considering stress-dependent resilient modulus each sublayer overestimated the in-situ pavement surface deflection. Thus, future work including different plastic materials needed to investigate the most appropriate method to estimate resilient modulus for predicting the in-situ FWD deflection. For non-plastic soil materials, the empirical predictive relationship is suitable to predict the resilient modulus used in the layered elastic analysis to predict the in-situ FWD deflection. The predicted moisture content profile shows a good prediction of the stiffness of coarse-grained subgrade layer.

The final technical chapter of the dissertation investigates the catastrophic failure of pavement structure under flooding events. The bearing capacity of the pavements post-flooding using the theory of shear failure in soils was evaluated to avoid sudden failures due to relatively small number of passes over severely weakened pavements. Layered elastic analysis was used to determining the traffic load on the pavement surface. The findings show that the bearing capacity of pavements can be estimated from shear failure theory with the contribution of matric suction. Agencies can use this study to develop a more comprehensive engineering-based approach to assess the bearing capacity of the flooded pavements to avoid sudden failure.

The research efforts presented in this document are aimed to serve as pieces in the progression toward how to assess pavements post-flood events based on their performance and structural capacities. This dissertation evaluates data obtained under a range of soil types from non-plastic to plastic materials with different pavement

structures.

Opportunities for future work exist by expanding the dataset and could accomplish the following:

- Validate the method of estimating the in-situ FWD deflection using different soil material gradations and pavement structures using the resilient modulus models presented in this dissertation.
- Identify and test different resilient modulus models for fine-grained soils considering the stress effect and suction levels to estimate the in-situ measured deflection basin.
- Verify and validate the method of estimating the in-situ deflection at different FWD loads. This will provide a platform for a future cost-effective tool to evaluate the structural capacity of pavements.
- Perform physical model testing to validate the methodologies in this dissertation.
- The findings of the pavement response data (e.g. deflection, horizontal and vertical strains) from Chapter 4 need to be correlated with the subsurface water recessions time in the unbound material layers through a hydraulic analysis to better understanding the behavior of flooded pavements. By accomplishing such a correlation, the agencies will be able to determine the optimum time to reopen the road for traffic based on performance properties and structural capacities.
- Develop a comprehensive performance model as a function of water recession time. This would be valuable to agencies and could save money from the road investigating post-flood events. This model could be applicable for any other state of the road. In other words, the performance of pavements could be predicted anytime if the limitation is considered correctly. To develop such a model, different material properties and pavement structures should be analyzed from across the country. The

proposed model can be broken down according to road classification (i.e. low volumes roads and interstate highways).

CHAPTER 8

REFERENCES

AASHTO. Mechanistic-Empirical Pavement Design Guide (MEPDG). (2008). A Manual of Practice Interim Edition, Washington, D.C., pp 124-128.

Arizona State University (ASU) Soil Map Application, <http://nchrp923b.lab.asu.edu/>

Broms BB (1963) “The Effect of Degree of Saturation on the Bearing Capacity of Flexible Pavements”, Highway Research Record 71:1–14

Chen, X. and Zhang, Z., (2014). “Effects of Hurricanes Katrina and Rita Flooding on Louisiana Pavement Performance.” In Pavement Materials, Structures, and Performance, American Society of Civil Engineers, Reston, Va., pp. 212-221.

Carmichael, R.F. III and Stuart, E. (1985). “Predicting Resilient Modulus: A Study to Determine the Mechanical Properties of Subgrade Soils.” *Transportation Research Record* TRR 1043, Transportation Research Board, National Research Council, Washington, DC, pp. 145-148.

Cary, C. E., and C. E. Zapata. (2010) “Enhanced Model for Resilient Response of Soils Resulting from Seasonal Changes as Implemented in Mechanistic–Empirical Pavement Design Guide”. In *Transportation Research Record: Journal of the Transportation Research Board*, No. 2170, Transportation Research Board of the National Academies, Washington, D.C., 2010, pp. 36–44.

Cary, C. E., & Zapata, C. E. (2011). Resilient modulus for unsaturated unbound materials. *Road Materials and Pavement Design*, 12(3), 615-638.

Ceratti, A., Gehling, W., and Nunez, W. P. (2004). “Seasonal variations of a subgrade soil resilient modulus in southern Brazil.” *Transportation Research Record*. 1874, Transportation Research Board, Washington, D.C., 165–173.

Chen, X. and Zhang, Z., (2014). “Effects of Hurricanes Katrina and Rita Flooding on Louisiana Pavement Performance.” In *Pavement Materials, Structures, and Performance*, American Society of Civil Engineers, Reston, Va., pp. 212-221.

Chen FH (1999) “Soil Engineering, Testing, Design and Remediation.” CRC Press LLC, N.W., Boca Raton, Florida, USA

Christopher, B. R., Schwartz, C., & Boudreau, R. (2006). *Geotechnical Aspects of Pavements: Reference Manual*. US Department of Transportation, Federal Highway Administration

Clarke, C. R., & Cosby, S. (2007). Flood effect evaluation on SH24–North of Washington, Oklahoma in McClain County. In a meeting held by the USGS Oklahoma Water Science Center, National Weather Center, Norman, Oklahoma

Costa YD, Cintra JC, Zornberg JG (2003) “Influence of Matric Suction on the Results of Plate Load Tests Performed on a Lateritic Soil Deposit”. *Geotechnical Testing Journal*, 26(2):219–226

Dai Shongtao, and John Zollars, “Resilient Modulus of Minnesota Road Research Project Subgrade Soil”, *Transportation Research Record* 1786, TRB, National Research Council, Washington, D.C., 2002, pp 20-28.

Daniel, J.S., Jacobs, J.M., Douglas, E., Mallick, R.B. and Hayhoe, K., (2014). “Impact of Climate Change on Pavement Performance: Preliminary Lessons Learned Through the Infrastructure and Climate Network (ICNet).” In *Climatic Effects on Pavement and Geotechnical Infrastructure*, American Society of Civil Engineers, Reston, Va., pp. 1–9.

Drumm, E. C., Reeves, J. S., Madgett, M. R., and Trolinger, W. D. (1997). “Subgrade resilient modulus correction for saturation effects.” *J. Geotech. Geoenviron. Eng.*, 123(7), 663–670.

Drumm, E. C., Boateng-Poku, Y., & Johnson Pierce, T. (1990). Estimation of subgrade resilient modulus from standard tests. *Journal of Geotechnical Engineering*, 116(5), 774-789.

Edris, Earl V. Jr., and Lytton, Robert L., (1976) “*Dynamic Properties of Subgrade Soils Including Environmental Effects*”, Texas Transportation Institute Report No. TTI-2-18-74-164-3, Texas A&M University, College Station, TX, May 1976.

Elkins, G. E., Schmalzer, P., Thompson, T. and Simpson A. (2003) “Introduction to the LTPP Information Management System (IMS)” Rep. No. FHWA-RD-03-088, Federal Highway Administration, U.S. Department of Transportation, Washington, D.C.

Elshaer, M., Ghayoomi, M., and Daniel, J. S. (2017). “Methodology to evaluate performance of pavement structure using soil moisture profile”. Road Materials and Pavement Design, in press, DOI: 10.1080/14680629.2017.1283356

Erlingsson, S., (2010). Modelling of Rutting Performance – Comparison with LTPP Road Sections. NordFoU PPM, Nordic Cooperation Program report no. 2.4.1.

Fredlund, D. G., Bergan, A. T., and Wong, P. K. (1977). “Relation between resilient modulus and stress research conditions for cohesive subgrade soils.” Transportation Research Record. 642, Transportation Research Board, Washington, D.C., 73–81.

Fredlund, D. G., & Morgenstern, N. R. (1977). Stress state variables for unsaturated soils. Journal of Geotechnical and Geoenvironmental Engineering, 103(ASCE 12919).

Fredlund, D. G., & Xing, A. (1994). Equations for the soil-water characteristic curve. Canadian geotechnical journal, 31(4), 521-532.

Gaspard, K., Martinez, M., Zhang, Z. and Wu, Z., (2007). “Impact of Hurricane Katrina on roadways in the New Orleans Area.” Technical Assistance Report No. 07-2TA, LTRC Pavement Research Group, Louisiana Department of Transportation and Development, Louisiana.

Goel, A. and Das, A., (2008) “Non-destructive testing of asphalt pavements for structural condition evaluation: a state of the art, Nondestructive Testing and Evaluation”, Vol. 23(2), 2008, pp.121-140.

George, K. P. (2004). Prediction of resilient modulus from soil index properties. Final

Report, MS-DOT-RD-04-172

Han, Z., & Vanapalli, S. K. (2015). Model for predicting resilient modulus of unsaturated subgrade soil using soil-water characteristic curve. *Canadian Geotechnical Journal*, 52(10), 1605-1619.

Hanek G. L., Truebe M. A., and Kestler M. A. (2001) "Using Time Domain Reflectometry (TDR) and Radio Frequency (RF) Devices to Monitor Seasonal Moisture Variation in Forest Road Subgrade and Base Materials" United States Department of Agriculture, Federal Highway Administration, United States Department of Transportation DC.

Helali, K., Robson, M., Nicholson, R. and Bekheet, W., (2008) "Importance of A Pavement Management System in Assessing Pavement Damage from Natural Disasters: A Case Study to Assess the Damage from Hurricanes Katrina and Rita in Jefferson Parish, Louisiana." In 7th International Conference on Managing Pavement Assets, Preserving What We Have, investing in the Future, and Finding the Balance, Transportation Research Board, Washington, DC., 2008

Hicks, R.G., and Monismith, C.L., (1971) "*Factors Influencing the Resilient Response of Granular Materials*", in Highway Research Record 345, Highway Research Board, National Academy of Sciences, Washington, DC, 1971.

Hodges, J. W., Rolt, J., and Jones, T. E. (1975). "The Kenya road transport cost study: research on road deterioration."

Horak E, Maree JH and van Wijk AJ (1989) Procedures for using Impulse Deflectometer (IDM) measurements in the structural evaluation of pavements. Proceedings of the Annual Transportation Convention Vol 5A, Pretoria, South Africa.

Huang, Y. H. (1993). Pavement analysis and design.

Janoo, V. C.; Eaton, R.; and Barna, L., (1997). Evaluation of Airport Subsurface Materials. Special Report 97-13, US. Army Cold Regions Research and Engineering Laboratory, USA.

Khalili, N., Geiser, F., & Blight, G. E. (2004). Effective stress in unsaturated soils: review with new evidence. *International Journal of Geomechanics*, 4(2), 115-126.

Khan, M.U., Mesbah, M., Ferreira, L. and Williams, D.J., (2015) “Development of A Post-Flood Road Maintenance Strategy: Case Study Queensland, Australia.” *International Journal of Pavement Engineering*, pp.1-12.

Khosravifar, S., Afsharikia, Z., & Schwartz, C. W. (2015, June). Evaluation of Resilient Modulus Prediction Models for Cohesive and Non cohesive Soils. In *Airfield and Highway Pavements 2015* (pp. 778-788).

Khoury, C. K., and Khoury, N. K. (2009) “The effect of moisture hysteresis on resilient modulus of subgrade soils.” 8th Int. Conf. Bearing Capacity Roads, Railways, and Airfields, Univ. of Illinois–Urbana- Champaign, Champaign, IL, 71–78.

Khoury, C., Khoury, N., and Miller, G. (2010) “Effect of suction hysteresis on resilient modulus of fine-grained soil.” *Transportation Research Board 89th Annual Meeting Compendium Papers (CD-ROM)*, Transportation Research Board, Washington, DC, 10–14.

Khoury, N. N., and Zaman, M. (2004). “Correlation among resilient modulus, moisture variation, and soil suction for subgrade soils.” *Transportation Research Record 1874*, Transportation Research Board, Washington, DC, 99–107.

Khoury, N. (2016). Resilient modulus–moisture content relationships for pavement engineering applications.

Khoury, C., Khoury, N., & Miller, G. (2011). Effect of cyclic suction history (hydraulic hysteresis) on resilient modulus of unsaturated fine-grained soil. *Transportation Research Record: Journal of the Transportation Research Board*, (2232), 68-75.

Knott, J. F., Elshaer, M., Daniel, J. S., Jacobs, J. M., & Kirshen, P. (2017). Assessing the Effects of Rising Groundwater from Sea Level Rise on the Service Life of Pavements in Coastal Road Infrastructure. *Transportation Research Record: Journal of the Transportation Research Board*, (2639), 1-10.

Kumbhokjar AS (1993) “Numerical Evaluation of Terzaghi’s N_v .” *Journal of Geotechnical Engineering*, American Society of Civil Engineers 1999(3):598–607

Lary, J.A. and Mahoney, J.P. (1984). “Seasonal Effects on the Strength of Pavement Structures.” *Transportation Research Record*, TRR 954, Transportation Research Board, National Research Council, Washington, DC, pp. 88–94.

Li, Y., 2004. Pavement testing and evaluation. In: M. Kutz, (2004). “Handbook of Transportation Engineering”. New York, NY, USA: McGraw-Hill Professional Publishing. Ch. 15. 1000 p.

Liang, R., Rabab’ab, S., and Khasawneh, M. (2008). “Predicting moisture dependent resilient modulus of cohesive soils using soil suction concept.” *J. Transp. Eng.*, 134(1), 34–40.

Mallick, R. and T. El-Korchi. (2013). *Pavement Engineering Principles and Practice*, Second Edition. CRC Press, Taylor and Francis Group, LLC: Boca Raton.

Mallick, R.B., Tao, M., Daniel, J.S., Jacobs, J. and Veeraragavan, A. (2015). “Development of A Methodology and A Tool for The Assessment of Vulnerability of Roadways to Flood Induced Damage.” *Journal of Flood Risk Management*, 2015, in press

Martin, T., and Crank, S. (2001). “Use of Pavement Strength Information in Network Asset Management.” Austroads Project No: BS.A.C.025, RC1702.

Miller GA, Muraleetharan KK (1998) “In Situ Testing in Unsaturated Soil”. *Proceedings of the Second International Conference on Unsaturated Soils*, Beijing, China, Vol. 1:416–421

Mohammad L. N., B. Huang, A J. Puppala, and A. Allen, “Regression Model for Resilient Modulus of Subgrade Soils”, *Transportation Research Record* 1442, TRB, National Research Council, Washington, D.C., pp 47-54.

Moosazadeh, J., and Witczak, M. W. (1981). “Prediction of subgrade moduli for soil that exhibits nonlinear behavior.” *Transportation Research Record*. 810, Transportation

Research Board, Washington, D.C., 9–17.

Mndawe, M.B., Ndambuki, J.M., Kupolati, W.K. and Badejo, A.A., (2015). “Assessment of The Effects of Climate Change on the Performance of Pavement Subgrade.” *African Journal of Science, Technology, Innovation and Development*, Vol 7(2), 2015, pp.111-115.

NCHRP. 2004b. (2004). Laboratory Determination of Resilient Modulus for Flexible Pavement Design. National Cooperative Highway Research Program Research Results Digest, No. 285. Washington, DC: Transportation Research Board, National Research Council.

Noureldin, A. S. (1994) “Influence of Stress Levels and Seasonal Variations on In Situ Pavement Layer Properties”. In *Transportation Research Record 1448*, TRB, National Research Council, Washington, D.C., 1994, pp. 16-24.

Ng, C. W. W., & Zhou, C. (2014). Cyclic behaviour of an unsaturated silt at various suctions and temperatures. *Géotechnique*, 64(9), 709-720.

Orr D. (2014). “Overview of Backcalculation.” Presented at Falling-Weight Deflectometer User Group (FWDUG) Annual Meeting, Indianapolis, Indiana.

Ovik, J.M., Siekmeier, J.A. and Van Deusen, D.A., (2000). “Improved spring load restrictions guidelines using mechanistic analysis”. Minnesota Department of Transportation.

Perera, Y. Y., Zapata, C. E., Houston, W. N., & Houston, S. L. (2005). Prediction of the soil-water characteristic curve based on grain-size-distribution and index properties. In *Advances in Pavement Engineering* (pp. 1-12).

Rada, G., and Witczak, M.W., (1981) “Comprehensive Evaluation of Laboratory Resilient Moduli Results for Granular Material”, in *Transportation Research Record 810*, Layered Pavement Systems, Transportation Research Board, National Research Council, National Academy of Sciences, Washington, DC, 1981.

Richter, C. A. (2006). “Seasonal Variations in the Moduli of Unbound Pavement Layers”

Rep. No. FHWA-HRT-04-079, Federal Highway Administration, U.S. Department of Transportation, Washington, D.C.

Rohde, Gustav T. (1994). "Determining pavement structural number from FWD testing." Transportation Research Record 1448.

Salour, F., S. Erlingsson, and C. E. Zapata. (2015) "Model for Seasonal Variation of Resilient Modulus in Silty Sand Subgrade Soil Evaluation with Falling Weight Deflectometer". Transportation Research Record: Journal of the Transportation Research Board, No. 2510, Transportation Research Board, Washington, D.C., 2015, pp. 65–73.

Santero, N.J., Masanet, E. and Horvath, A., (2011). "Life-Cycle Assessment of Pavements. Part I: Critical Review." Resources, Conservation and Recycling, Vol. 55(9), pp. 801–809.

Santha, B.L "Resilient Modulus of Subgrade Soils: Comparison of Two Constitutive Equations", Transportation Research Record 1462, TRB, National Research Council, Washington, D.C., pp 79-90.

Sauer, E. K., & Monismith, C. L. (1968). Influence of soil suction on behavior of a glacial till subjected to repeated loading. Highway Research Record, (215).

Sawangsuriya, A., Edil, T. B., and Benson, C. H. (2009). "Effect of suction on resilient modulus of compacted fine-grained subgrade soils." Transportation Research Record 2101, Transportation Research Board, Washington, DC.

Seed, H.B. Chan, C.K., and Lee, C.E. (1962). "Resilience Characteristics of Subgrade Soils and Their Relation to Fatigue Failures in Asphalt Pavements." *Proceedings, International Conference on the Structural Design of Asphalt Pavements*, University of Michigan, Ann Arbor, MI, pp. 611 636.

Seed, H. B., Mitry, F. G., Monismith, C. L., and Chan, C. K. (1967). "Prediction of pavement deflection from laboratory repeated load tests." NCHRP Rep. No. 35, Washington, D.C.

Sivakumar, V., Kodikara, J., O'hagan, R., Hughes, D., Cairns, P., & McKinley, J. D. (2013). Effects of confining pressure and water content on performance of unsaturated compacted clay under repeated loading. *Géotechnique*, 63(8), 628-640.

Steensen-Bach JO, Foged N, Steenfelt JS (1987) "Capillary Induced Stresses – Fact or Fiction?" Ninth ECSMFE, Groundwater Effects in Geotechnical Engineering, Dublin 83–89

Sultana, M., Chai, G., Martin, T. and Chowdhury, S., (2016). "Modeling the Postflood Short-Term Behavior of Flexible Pavements." *Journal of Transportation Engineering*, American Society of Civil Engineers, Reston, Va., p.04016042.

Terzaghi K (1943) "Theoretical Soil Mechanics". John Wiley and Sons, New York

Tonkin and Taylor (1998) "Pavement deflection measurement & interpretation for the design of rehabilitation treatments", Transfund New Zealand Research Report, Issue 117, 1998

Topp, G.C., J.L. Davis, and A.P. Annan. (1980). "Electromagnetic determination of soil water content: Measurement in coaxial transmission lines". *Water Resour. Res.* 16:574-582.

Truss, Daner Patrise, (2004) "Pavement Deflection Data as a Tool for the Prediction of Freeze/Thaw Response. " Master's Thesis, University of Tennessee, 2004.

Uzan, J. (1992). "Resilient characterization of pavement materials." *International Journal of Numerical and Analytical Methods in Geomechanics*, Vol. 16, No. 6, pp. 435–459.

Vanapalli SK, Fredlund DG, Pufahal DE, Clifton AW (1996) "Model for the Prediction of Shear Strength with respect to Soil Suction". *Canadian Geotechnical Journal* 33:379–392

Vanapalli SK and Mohamed FMO, (2007) "Bearing capacity of model footings in unsaturated soils," In *Experimental Unsaturated Soil Mechanics*, Springer Proc. in Physics. Springer, 2007, 112, 483–493.

Vennapusa, P., White, D.J. and Miller, D.K., (2013). "Western Iowa Missouri River

Flooding - Geo-Infrastructure Damage Assessment, Repair and Mitigation Strategies.” Iowa DOT Project TR-638, Federal Highway Administration.

Vesić AS (1973) “Analysis of Ultimate Loads of Shallow Foundations”. Journal of the Soil Mechanics and Foundation Division, ASCE 99(SM1):45–73

Vokas, C. A. and Stoll D. S. (1985) Reinforced Elastic Layered System, Transportation Research Record, Issue No. 1153, pp. 1-7.,

Von Quintus, H., Simpson, A. 2002. Back-Calculation of Layer Parameters for LTPP Test Sections, Volume II: Layered Elastic Analysis for Flexible and Rigid Pavements. FHWA Report No. FHWA-RD-01-113.

Watanatada, T., Harral, C., Paterson, W. D. O., Dhareshwar, A. M., Bhandari, A., and Tsunokawa, K. (1987). “The Highway Design and Maintenance Standards Model— Volume 1. Description of the HDM-III Model.” The Highway Design and Maintenance Standards Series (The World Bank).

Wang J. (2001) “Three-dimensional Finite Element Analysis of Flexible Pavements”, Master of Science, University of Maine.

Witczak M.W., Andrei D. and Houston W.N. (2000) “Resilient Modulus as Function of Soil Moisture – Summary of Predictive Models”. Development of the 2002 Guide for the Development of New and Rehabilitated Pavement Structures, NCHRP 1-37 A, Inter Team Technical Report (Seasonal 1), June 2000.

Witczak M.W., Houston W.N. and Andrei D. (2000) “Resilient Modulus as Function of Soil Moisture – A Study of the Expected Changes in Resilient Modulus of the Unbound Layers with Changes in Moisture for 10 LTPP Sites”. Development of the 2002 Guide DD-3.35 for the Development of New and Rehabilitated Pavement Structures, NCHRP 1-37 A, Inter Team Technical Report (Seasonal 2), June 2000.

Witczak M.W., Houston W.N. and Andrei D. (2000) “Selection of Resilient Moduli for Frozen/Thawed Unbound Materials”. Development of the 2002 Guide for the Development of New and Rehabilitated Pavement Structures, NCHRP 1-37 A, Inter Team

Technical Report (Seasonal 3), June 2000.

Witczak M.W., Houston W.N., Zapata C.E., Richter C., Larson G. and Walsh K. (2000) “Improvement of the Integrated Climatic Model for Moisture Content Predictions”. Development of the 2002 Guide for the Development of New and Rehabilitated Pavement Structures, NCHRP 1-37 A, Inter Team Technical Report (Seasonal 4), June 2000.

Witczak, M., and Uzan, J. (1988). “The universal airport design system, Report I of IV. Granular material characterization.” Rep. to Department of Civil Engineering, Univ. of Maryland, College Park, Md.

Yang, R. R., Huang, W. H., and Tai, Y. T. (2005). “Variation of resilient modulus with soil suction for compacted subgrade soils.” Transportation Research Record. 1913, Transportation Research Board, Washington, D.C., 99–106.

Yang, S. R., Lin, H. D., Kung, J. H. S., and Huang, W. H. (2008). “Suction controlled laboratory test on resilient modulus of unsaturated compacted subgrade soils.” J. Geotech. Geoenviron. Eng., 134(9), 1375–1384.

Yau A., and H. L. Von Quintus., “Study of LTPP Laboratory Resilient Modulus Test Data and Response Characteristics”, Final Report, October 2002 (FHWA-RD-02-051), USDOT, FHWA, October 2002.

Zapata, C., & Cary, C. E. (2012). “Integrating the national database of subgrade soil-water characteristic curves and soil index properties with the MEPDG.” National Cooperative Highway Research Program Project.

Zhang, Z., Wu, Z., Martinez, M. and Gaspard, K., (2008). “Pavement Structures Damage Caused by Hurricane Katrina Flooding.” In Journal of geotechnical and geoenvironmental engineering, Vol. 134(5), pp. 633-643

Zollinger D., Lee S., Puccinelli J., and Jackson N. (2008) “Long Term Pavement Performance Computed Parameter: Moisture Content” Rep. No. FHWA-HRT-08-035, Federal Highway Administration, U.S. Department of Transportation, Washington, D.C